Doctoral Thesis

A study of the mechanism that facilitates eukaryotic DNA mismatch repair to function on chromatin

Riki Terui

Department of Biological Science

Graduate School of Science

Osaka university

November 2018

Table of Contents

Abbreviations

MMR: mismatch repair

NPE: nucleoplasmic extract

Exo1: exonuclease 1

Smarcad1: SWI/SNF-related matrix-associated actin-dependent regulator of chromatin subfamily A containing DEAD/H box 1

CAF-1: chromatin assembly factor-1

IDL: insertion/deletion loop

DSB: double-strand break

PCNA: Proliferating Cell Nuclear Antigen

RFC: Replication factor C

SV40: simian virus 40

FACT: facilitates chromatin transcription

MNase: micrococcal nuclease

PCR: polymerase chain reaction

qPCR: quantitative polymerase chain reaction

cDNA: complementary DNA

HDR: homology-directed repair

SDS: sodium dodecyl sulfate

PAGE: polyacrylamide gel electrophoresis

EDTA: ethylenediaminetetraacetic acid

Abstract

Precise replication of genomic DNA is critical to maintaining genetic information. Although the fidelity of replication depends largely on the accuracy of DNA polymerases, the post-replicative mismatch repair (MMR) system, which corrects misincorporated bases left behind DNA polymerases, functions as a last resort to prevent mutations. The importance of MMR is reinforced by the fact that defects in the MMR genes in humans greatly elevate the risk of tumorigenesis. In eukaryotes, replication errors are recognized by two MutS complexes, MutSα (Msh2-Msh6) and MutSβ (Msh2-Msh3), each of which is a ring-shaped heterodimer that encircles double-stranded DNA. Upon recognition of a mispaired base, a MutS complex changes its conformation to a sliding clamp and recruits MutLα, a latent nicking-endonuclease. MutLα is activated through the interaction with replication clamp Proliferating cell nuclear antigen (PCNA) that functions as a strand-discrimination signal for eukaryotic MMR. Strand-specific nicking by MutLα leads to the degradation of the error-carrying strand.

A key reaction in MMR is 1D-communication between the MMR proteins and a strand discrimination signal. Since PCNA encircles double-stranded DNA, PCNA and MutLα that is recruited onto DNA by MutS complexes most likely need to travel along DNA to interact with each other. On the other hand, eukaryotic DNA is wrapped around histone octamers to be assembled into nucleosomes. Recent studies have shown that the sliding of MutSα along DNA is impeded by the presence of nucleosomes. Although chromatin remodelers and histone chaperones handle nucleosomes to facilitate reactions on chromatin such as replication, transcription, and recombination in eukaryotes, such factors for MMR have not been identified, and how the MMR system deals with nucleosomes to carry out the repair reaction remains highly ambiguous.

The nucleoplasmic extract of *Xenopus* eggs (NPE) is a physiological model system for DNA replication and repair, and recapitulates both MMR and chromatin assembly *in vitro*. To understand how the MMR reaction occurs in the context of chromatin, I took advantage of this system. Based on a preliminary finding in our lab that supercoiling of DNA, an indirect readout of chromatin assembly, is inhibited on a mismatch-carrying DNA in NPE, I first tested how nucleosomes around a mispaired base behave. Interestingly, the sensitivity to micrococcus nuclease (MNase) was significantly increased around a mispaired base, and the number of histones on mismatch-carrying

DNA in NPE was also reduced, indicating that nucleosomes are excluded from the region surrounding a mismatch. A fine mapping of the MNase sensitivity revealed that nucleosomes within approximately a 1-kb region flanking a mismatch are most strongly reduced. A series of immunodepletion experiments showed that this reaction, termed nucleosome exclusion, is dependent on the Msh2-containing complexes but independent of MutLα. To identify factors that facilitate nucleosome exclusion, I sought for proteins that preferentially bind to mismatch-carrying DNA in an Msh2-dependent manner. Mass-spectrometry identification of the mismatch-carrying DNA binding proteins showed that a chromatin remodeling enzyme Smarcad1 is preferentially accumulated on mismatch-carrying DNA. Immunoblotting analysis revealed that Smarcad1 is recruited to mismatch-carrying DNA in an Msh2-dependent manner. Depletion of Smarcad1 from NPE weakened nucleosome exclusion, and this was restored by recombinant Smarcad1, indicating that Smarcad1 facilitates nucleosome exclusion. To investigate the impact of Smarcad1 on the cellular replication fidelity, I switched the model system from NPE to the budding yeast *Saccharomyces cerevisiae*. Although single deletion of *FUN30*, the homolog of Smarcad1, only modestly increased the rate of mutations, I found that double deletion of *FUN30* and either *msh6Δ* or *msh3Δ* synergistically increases the rate of mutations, suggesting that Fun30 cooperates with MutS complexes to suppress mutations. Furthermore, deletion of Cac1, the largest subunit of Chromatin assembly factor-1 (CAF-1), suppressed synergistic increase of the mutation rates caused by *fun30Δ* and either *msh6Δ* or *msh3Δ*, suggesting that Fun30 counteracts CAF-1 mediated chromatin assembly to suppress mutations. These results demonstrate that the MMR system involves exclusion of nucleosomes around mispaired bases and engages Smarcad1/Fun30 to promote nucleosome exclusion. Smarcad1/Fun30 probably assists MutS complexes by excluding nucleosomes to facilitate MMR.

General Introduction

1. Overview

Precise replication of genomic DNA is vital for all living organisms. Errors in DNA replication result in the accumulation of mutations in genomes, leading to malfunction of genes. Although mutations are critical driving force for evolution, the level of mutations must be kept low such that the identity of species is maintained. The fidelity of replication depends largely on extremely precise base discrimination by DNA polymerases. Replicative DNA polymerases from both prokaryotes and eukaryotes misincorporate incorrect nucleotides only once in the synthesis of ten million bases. However, this level of accuracy does not suffice for faithful replication of genomic DNA, as in some cases genomic DNA is composed of more than a billion bases. For instance, nearly a thousand replication errors are expected when a human diploid genome, which is approximately six billion base long, is replicated. To avoid accumulation of mutations, most, if not all, cellular organisms are equipped with mismatch repair systems that correct replication errors.

The most prevalent mismatch repair pathway is the one that is catalyzed by MutS and MutL homologs. The MutS/MutL-dependent mismatch repair system, which I simply call the mismatch repair system or MMR hereafter, is essentially conserved from bacteria and archaea to eukaryotes. In this system, the repair reaction involves recognition of mispaired bases, discrimination of the newly synthesized DNA, resection of the error-containinig strand, and re-synthesis of the correct strand. I will summarize recent advances in the understanding of the molecular mechanism of MMR in section 2.

In eukaryotes, DNA is packaged into chromatin immediately after the replication fork via wrapping around histone octamers 1.65 turns. DNA therefore must be transiently unwound from nucleosomes when a naked DNA segment is required for a DNA transaction such as replication, recombination, and repair. Eukaryotic cells have thus evolved specialized families of proteins that handle histones and nucleosomes; histone chaperones facilitate the assembly and disassembly of nucleosomes by dealing with strong electrostatic interaction between DNA and histones, and chromatin remodeling enzymes utilize the energy of ATP hydrolysis to mobilize nucleosomes. I will discuss what is known for the mechanism that handles nucleosome barriers in section 3.

While virtually nothing had been understood for the relationship between

chromatin and MMR until recently, this research field has suddenly become an area of intense interest for these ten years. Yet, the models are still somewhat contradictory between each report, and a comprehensive view on the mechanism of how the MMR system handles nucleosomes has not been fermented. In section 4, I will summarize what has been understood and what remains uncertain for MMR on chromatin. Finally, I will clarify open questions in this research field, set up the aim of this research, and describe the approach and organization of this thesis in section 5.

2. ***Molecular mechanism of MMR***

2-1. Recognition of mispaired bases

The starting point of replication error correction is the recognition of mispaired bases. The product of the *E. coli mutS* gene was the first-identified mismatch sensor protein (Su and Modrich 1986). MutS binds to all type of base-base mismatches and insertion/deletion loops (IDLs) of one to four unpaired nucleotides (Su et al. 1988). Higher organisms also have MutS homologs (MSHs) (Jiricny 2013). In eukaryotes, Msh2, Msh6, and Msh3 are mainly involved in somatic MMR. Msh2 and Msh6 form a ring-shaped heterodimer, MutSα (Drummond et al. 1995; Palombo et al. 1995). MutSα binds to base-base mismatches and insertion/deletion loops (IDL) of one or two unpaired bases, and it also binds to IDLs of more than two unpaired bases (Marsischky and Kolodner 1999). Msh2 and Msh3 also form a ring-shaped heterodimer, MutSβ (Marsischky et al. 1996). MutSβ binds to IDLs of one to 14 unpaired nucleotides (Acharya et al. 1996; Habraken et al. 1996; Palombo et al. 1996). Consistent with these DNA binding properties, mutation spectra of *msh6Δ* or *msh3Δ* strains of yeast suggested that MutSα mainly contributes to the repair of base-base mismatches and small IDLs, and MutSβ contributes to the repair of IDLs (Marsischky et al. 1996). MutS complexes bind to heteroduplex DNA by encircling double-stranded DNA (Lamers et al. 2000; Obmolova et al. 2000; Warren et al. 2007; Gupta et al. 2012). MutS complexes form ADP-bound open ring forms before binding to a mispaired base. After binding to a mispaired base, MutS complexes undergo conformational change to mobile clamps via exchange of ADP to ATP. ATP-bound MutS complexes slide along DNA (Gradia et al. 1997; Acharya et al. 2003; Mazur et al. 2006; Heinen et al. 2011). Sliding of MutS complexes is conserved from prokaryotes to eukaryotes, suggesting the importance of this feature for MMR. As described below, the sliding of MutS complexes may be important for searching for

strand-discrimination signals and resection of the error-containing DNA strand.

2-2. Strand discrimination

To suppress mutations, MMR must remove misincorporated bases. To distinguish the misincorporated base in a mismatched base pair, MMR must recognize not only mispaired bases but also strand-discrimination signals.

Removal of the error-containing segment depends on helicase-mediated unwinding in bacteria and exonucleic degradation in eukaryotes, both of which initiate from a strand discontinuity such as a nick or gap, or a terminus of DNA. Therefore, a strand discontinuity naturally determines the strand to be repaired if it is present sufficiently close to a mismatch. In fact, it has been demonstrated that strand discontinuities, such as nicks or gaps, can direct strand-specific correction of mispaired bases *in vitro* (Langle-Rouault et al. 1987; Lahue et al. 1989; Holmes et al. 1990; Thomas et al. 1991; Genschel and Modrich 2003; Dzantiev et al. 2004; Constantin et al. 2005; Zhang et al. 2005). Such a DNA terminus is necessarily present at the site of DNA replication, and it is a widely accepted idea that MMR can be directed to the nascent DNA due to the presence of DNA termini when a mismatch is recognized immediately after its synthesis. Nevertheless, studies of bacterial MMR have clearly proven that this mode of MMR contributes only to a minor fraction of replication error correction, and the majority of MMR events depends on the post-replicative discrimination of the newly-synthesized DNA.

In *E. coli*, the adenine base in d(GATC) sequences are methylated by a DNA adenine methylase, encoded by the *dam* gene (Marinus and Morris 1973; Lacks and Greenberg 1977; Geier and Modrich 1979). Since synthesized DNA is temporally hemi-methylated until the newly-synthesized DNA is fully methylated by the Dam methylase, it has been speculated that the methylation directs strand-specific mismatch repair (Wagner and Meselson 1976). In fact, when hemimethylated heteroduplex DNA was introduced into *E. coli*, mispaired bases on the unmethylated DNA strand was preferentially repaired (Pukkila et al. 1983). Not only deletion but also overexpression of the DNA adenine methylase greatly elevated mutation rates in *E. coli*, supporting the idea that kinetics of methylation of d(GATC) sequences contribute to ensuring sufficient time for strand discrimination (Marinus and Morris 1974; Herman and Modrich 1981). 5′ to the dG of unmodified d(GATC) sequence is incised by MutH (Welsh et al. 1987). The

endonuclease activity of MutH is activated by MutL. MutL forms a homodimer and it is recruited to the mismatch-carrying DNA in a MutS-dependent manner (Grilley et al. 1989; Au et al. 1992; Galio et al. 1999; Schofield et al. 2001; Acharya et al. 2003; Selmane et al. 2003; Liu et al. 2016). In the presence of MutS, MutL, ATP, and a mispaired base, the latent endonuclease activity of MutH is activated, and it preferentially incise the unmethylated strand of hemimethylated heteroduplex DNA (Au et al. 1992).

Eukaryotes have different systems to discriminate the newly-synthesized DNA. In eukaryotes, d(GATC) sites are not methylated and no eukaryotic homolog of MutH has been identified. Instead of MutH, MutLα, a MutL homolog heterodimer which consists of Mlh1 and Pms2 in human and Mlh1 and Pms2 in yeast, has latent endonuclease activity (Kadyrov et al. 2006). Instead of hemimethylated d(GATC), PCNA (*P*roliferating *C*ell *N*uclear *A*ntigen) functions as a strand-discrimination signal in eukaryotes. PCNA is a sliding clamp that supports various DNA transactions including DNA replication and repair (Boehm et al. 2016). Since PCNA is loaded onto DNA in a precise orientation with the ring facing the direction of DNA synthesis, it has information for the newly synthesized DNA strand. The latent endonuclease activity of MutLα is activated by MutSα or MutSβ, a mispaired base, and DNA-bound PCNA, and it induces nicking of either strand (Kadyrov et al. 2006; Pluciennik et al. 2010; Pluciennik et al. 2013). Importantly, DNA-bound PCNA also induces strand-specific MMR in the absence of pre-existing strand-discontinuities (Kawasoe et al. 2016).

Recent studies also showed that a ribonucleotide embedded in a DNA can direct strand-specific MMR (Ghodgaonkar et al. 2013; Lujan et al. 2013). A ribonucleotide embedded in DNA is removed by RNase H2 and converted to a gap (Rydberg and Game 2002; Sparks et al. 2012). Since ribonucleotides are retained in the genomic DNA until they are removed by RNase H2, misincorporated ribonucleotides possibly function to keep the strand-discrimination signals on DNA. Consistent with this idea, RNase H2 promotes MMR preferentially on the leading strand (Ghodgaonkar et al. 2013; Lujan et al. 2013) where strand-discrimination signals need to be kept for more time than the lagging strand due to the limitation of the amount of DNA-bound PCNA.

Although it has been suggested that functional interaction between MutS complexes, MutLα, and PCNA is important to activate the endonuclease activity of MutLα, how MutS complexes, MutLα, and PCNA interact with each other remains elusive. Since MutS complexes and MutLα slides along DNA after the recognition of

mispaired bases, one model proposes that MutLα interacts with PCNA by sliding along DNA (reviewed in Iyer et al. 2006; Jiricny 2013; Kunkel and Erie 2015). Another model is a transactivation model, in which MutS complexes and strand-discrimination signals interact with each other by DNA bending. This model is based on the observations that MutS complexes could induce the incision of DNA which is directed by strand-discrimination signals by trans-interaction (Junop et al. 2001; Schofield et al. 2001; Wang and Hays 2004). Although it is not clear which model is true, the sliding model explains the features of the following resection step.

2-3. Resection

As mentioned above, eukaryotic MMR depends on degradation of error-carrying segments by exonucleases. Exo1 is the only genuine exonuclease whose involvement in eukaryotic MMR has been demonstrated (Tishkoff et al. 1997; Amin et al. 2001; Genschel et al. 2002). Exo1-dependent MMR resects DNA both with a 5′ -to-3′ and a 3′ -to-5′ direction (Genschel et al. 2002; Genschel and Modrich 2003; Dzantiev et al. 2004; Constantin et al. 2005; Zhang et al. 2005). However, Exo1 can hydrolyze DNA only with a 5′ -to-3′ direction at least *in vitro* (Szankasi and Smith 1992). Thus, the exonuclease activity of Exo1 does not account for all of the mechanism of the bidirectional resection of MMR.

In vitro analyses of gap-directed MMR showed that mispaired bases are efficiently repaired when a gap is located at either 3′ or 5′ to a mispaired base (Lahue et al. 1989; Dzantiev et al. 2004; Constantin et al. 2005; Zhang et al. 2005). Moreover, the resection preferentially proceeds to a mispaired base, implying that the resection is directed to a mispaired base. Human cell extracts and reconstituted systems showed that the 5′ -to-3′ resection does not require MutLα, RFC, and PCNA but the 3′ -to-5′ resection requires MutLα, RFC, and PCNA (Genschel and Modrich 2003; Zhang et al. 2005). Furthermore, *in vivo* mutation rates analyses showed that the deletion of MutLα elevates mutation rates to the level similar to the deletion of Msh2 (Strand et al. 1993). These results suggest that MutLα has important roles that are not able to be bypassed by the pre-existing strand discontinuity.

Since MutLα is recruited onto DNA by MutSα which binds to a mispaired base and slides along DNA, MutLα is preferentially localized to a mispaired base surrounding region. Thus, MutLα probably encounters PCNA and incises the newly-synthesized DNA

in the vicinity of a mispaired base. Since PCNA is loaded at nicks, MutLα is iteratively activated by PCNA and the incision gradually approaches a mispaired base. Finally, MutLα incises 5′ to a mispaired base even if strand-discrimination signals are initially localized at 3′ to a mispaired base. If this is the case, the MMR system removes a mispaired base regardless of the directionality of an exonuclease.

Since deletion of *EXO1* increases mutation rates much less than deletion of *MSH2* or *MLH1* in yeast (Tishkoff et al. 1997; Amin et al. 2001) and *exo1*$^{-/-}$ mouse models shows only a modest increase in cancer susceptibility compared to deletion of the genes that are absolutely required for MMR (Wei et al. 2003), it has been suggested that there is an Exo1-independent MMR pathway. Multiple mutations in the *MLH1*, *PMS1*, and *POL30* gene encoding PCNA in *S. cerevisiae*, synergistically increase mutation rates when combined with *exo1Δ* (Amin et al. 2001; Lau et al. 2002; Smith et al. 2013; Goellner et al. 2014), suggesting that MutLα and PCNA have important roles in Exo1-independent MMR. One possible mechanism of Exo1-independent resection in MMR is that an Mlh1-Pms1 dependent nick located on the 5′ side to a mispair initiates strand displacement synthesis by DNA polymerase δ to a position past the mispair (Kadyrov et al. 2009). After the resection step, the gap is filled by DNA polymerases and ligase.

3. Chromatin assembly and disassembly

Since the region after replication fork where MMR occurs is the region where nucleosome assembly occurs, it is important for understanding eukaryotic MMR to consider chromatin structure after the replication fork. A nucleosome is composed of two copies each of Histone H2A, H2B, H3, and H4, and 146-bp DNA. Since all core histones are highly positively charged, they interact to negatively charged phosphate backbone of DNA with high affinity. A heterotetramer of H3/H4 interacts with the central 80 bp of nucleosomal DNA and two H2A/H2B dimers interacts with peripheral nucleosomal DNA (Luger et al. 1997). To establish this well-ordered structure, a H3/H4 tetramer is deposited on DNA before two H2A/H2B dimers in nucleosome assembly. However, due to its high affinity to DNA, histones form only amorphous aggregate when just mixed with DNA under a physiological salt concentration. Thus, histone chaperones neutralize charges on histones and assist the assembly of nucleosomes by preventing unwanted interactions in cells.

Histone chaperone CAF-1 co-localizes with replication forks, presumably

through its interaction with PCNA (Shibahara and Stillman 1999), and it mediates chromatin assembly in a DNA synthesis-dependent manner (Smith and Stillman 1989; Gaillard et al. 1996). Since CAF-1 binds to newly synthesized histone H3 and H4, it probably deposits de novo H3 and H4 onto newly synthesized DNA (Verreault et al. 1996; Tagami et al. 2004). Not only CAF-1 but also HIRA mediates de novo incorporation of histone H3 and H4 (Tagami et al. 2004). In contrast to CAF-1, HIRA mediates chromatin assembly in the absence of DNA synthesis (Ray-Gallet et al. 2002). Although how parental H3 and H4 are transferred onto newly replicated DNA remains elusive, since it has been reported that histone chaperone Asf1 binds to parental H3 and H4 (Groth et al. 2007), it is possible that Asf1 contributes to deposition of parental H3 and H4 onto the replicated DNA. Moreover, histone chaperone FACT (facilitates chromatin transcription), which is a heterodimer of Spt16 and Ssrp1 in humans (Orphanides et al. 1999), reassembled nucleosomes after the replication fork in the reconstituted chromatin replication with purified proteins (Kurat et al. 2017). Thus, FACT is a candidate for the histone chaperone, which deposits both a H3/H4 tetramer and H2A/H2B dimers.

Due to these histone chaperones, eukaryotic DNA is rapidly packaged into chromatin immediately after replication forks. Observations of intermediates of chromatin replication products of *Drosophila melanogaster* embryos, SV40 minichromosomes, and *Saccharomyces cerevisiae* by electron microscopes showed that nucleosomes are reassembled from approximately 230-bp behind replication forks (McKnight and Miller 1977; Sogo et al. 1986; Lucchini and Sogo 1995). In addition, Reijns et al. showed that the genomic localization of Okazaki fragments junctions is influenced by nucleosome positioning, implying that nucleosome assembly precedes maturation of the lagging strand (Reijns et al. 2015). Thus, most of transactions on eukaryotic DNA face nucleosomes, which have potential to barrier DNA against DNA-binding proteins. To overcome the inhibitory effect of nucleosome and promote DNA transactions on chromatin, eukaryotes have gained histone chaperones and chromatin remodelers, both of which has activities to handle nucleosomes.

The most representative histone chaperone that has activity to displace nucleosomes is FACT. Although FACT has activity to deposit nucleosomes as described above, it also has activity to displace nucleosomes. FACT was first identified as a factor that is required for transcription through nucleosomes by RNA polymerase II (Orphanides

et al. 1998). FACT facilitates the displacement of H2A/H2B dimer from nucleosome to promote chromatin transcription (Belotserkovskaya et al. 2003). Not only transcription, FACT also promotes DNA unwinding by the MCM helicase on nucleosomal DNA (Tan et al. 2006) and chromatin replication in vitro (Kurat et al. 2017), implying that FACT is used as a temporal carrier that receives histones when proteins, such as an RNA polymerase II or a replication machinery, pass through nucleosomes.

Chromatin remodelers use energy from ATP hydrolysis to slide, evict, or exchange histones in nucleosomes (Ransom et al. 2010; Narlikar et al. 2013; Polo and Almouzni 2015). For example, INO80, a nucleosome remodeling complex, evicts nucleosomes at the DSB ends and promotes recruitment of Rad51 (Tsukuda et al. 2005; Chen et al. 2012). One of the chromatin remodeling enzyme whose functions in cells have recently been emerged is Smarcad1. Smarcad1 was identified as Etl1 in mice (Soininen et al. 1992). Etl1 localizes in nuclei since two-cell embryos (Schoor et al. 1993). Knockdown of Etl1 in mouse ES cells causes defects of pluripotency, and Etl1-knockout mice show developmental defects, suggesting that it has important roles in development (Schoor et al. 1999; Hong et al. 2009). Although it has not been clarified whether Smarcad1 contributes to control of gene expression during development, at least, knockdown of Smarcad1 in human cells causes the reduction of histone H3K9 methylation which is characteristic of heterochromatin (Rowbotham et al. 2011), suggesting that Smarcad1 contributes to maintenance of heterochromatin. The yeast counterpart of human Smarcad1, Fun30, contributes to silencing in the heterochromatin at the HMR and HML loci, telomeres, and rDNA repeats (Neves-Costa et al. 2009; Yu et al. 2011). *fun30Δ* alters chromatin condensation at the HML locus, suggesting that it controls nucleosome positioning there (Yu et al. 2011). It has also been suggested that the maintenance of the chromatin structure at centromere is supported by Fun30 (Stralfors et al. 2011; Durand-Dubief et al. 2012). In addition to functions in keeping specific chromatin structures, it has also been suggested that Smarcad1 and Fun30 promote the long-range resection of DNA double-strand breaks (DSBs). Fun30 is recruited to DSB ends immediately after the occurrence of DSBs, and it gradually spreads to 30-kb away from the DSB ends (Chen et al. 2012). This behavior is similar to resection machineries such as Exo1, Sgs1, and Dna2, resection tracks, and reduction of the histones around the DSB sites (Chen et al. 2012; Costelloe et al. 2012; Eapen et al. 2012). These results shows the possibility that Smarcad1 and Fun30 travel along DNA from DSB ends with resection

machineries and promote eviction of nucleosomes to facilitate long-range resection of the DSB ends. It has been also suggested that Smarcad1 localizes replication forks (Rowbotham et al. 2011; Sirbu et al. 2013), and interacts with Msh2-containing complexes (Okazaki et al. 2008; Rowbotham et al. 2011; Chen et al. 2016b). However, the significance of this localization and interaction in the cellular function has been elusive yet.

4. MMR and chromatin

As described in section 1, interactions between DNA-bound MutS complexes, MutLα, and PCNA on DNA, and resection of DNA by exonucleases are essential for the MMR reaction. Since nucleosomes limit the access of DNA-binding factors to DNA, it is probably major constraint for the MMR reaction. In fact, a biochemical study demonstrated that a nucleosome on a mismatch reduces the affinity of the human MutSα to a mismatch, and nucleosomes flanking a mismatch inhibit sliding of human MutSα along DNA (Li et al. 2009). Single-molecule studies also demonstrated that nucleosome arrays inhibit sliding of yeast MutSα along DNA (Gorman et al. 2010; Brown et al. 2016). Consistent with these findings, it was demonstrated that gap-directed MMR in HeLa nuclear extracts is inhibited when nucleosomes were assembled on mismatch-carrying DNA before gap-directed MMR (Schopf et al. 2012; Li et al. 2013). Not only MutSα-mediated steps, the resection step is also probably inhibited by nucleosomes because nucleosomes inhibit resection of Exo1 *in vitro* (Adkins et al. 2013).

In contrast to these *in vitro* findings, the whole-genome study of the mutation landscape in yeast suggests that positions of nucleosomes do not affect the efficiency of MMR *in vivo* (Lujan et al. 2014). These observations give rise to the hypothesis that there is an important mechanism for efficient MMR regardless of the presence of nucleosomes *in vivo*. Several mechanisms of MMR that possibly contribute to overcoming nucleosomes has been proposed. MutSα localizes to chromatin and replication forks by using PWWP domain of Msh6, which interacts with trimethylated Lys36 in histone H3, and PCNA interacting peptide (PIP)-motif of Msh6 (Kleczkowska et al. 2001; Hombauer et al. 2011; Li et al. 2013; Haye and Gammie 2015). These localizations likely help MutSα to recognize mispaired bases before chromatin assembly. In addition, human MutSα counteracts CAF-1-mediated chromatin assembly *in vitro* (Kadyrova et al. 2011; Schopf et al. 2012; Rodriges Blanko et al. 2016). These mechanisms may help the MMR

system to occur before chromatin assembly. Moreover, human MutSα has the chromatin remodeling activity (Javaid et al. 2009). It is possible that this activity makes MMR take place after chromatin assembly. Single molecule studies showed that MutSβ and MutLα can hop over nucleosomes (Gorman et al. 2010; Brown et al. 2016). Thus, it is possible that a MutSβ- or a MutLα-mediated step are resistant to nucleosomes.

5. Open questions and the goal of the research

Since the frequency of replication errors is very low, it is difficult to analyze what happens on nucleosomes exactly when MMR occurs *in vivo*. As described in the previous part, the relationship between MMR and nucleosomes has been mainly investigated *in vitro*. However, behavior of MMR factors on nucleosomes and effects of MMR factors on nucleosomes were investigated without nucleosome assembly activities (Javaid et al. 2009; Li et al. 2009; Gorman et al. 2010; Brown et al. 2016), or with low chromatin assembly activity, which takes more than 10 minutes to assemble nucleosomes on approximately 50% of DNA in the reaction (Kadyrova et al. 2011; Schopf et al. 2012; Rodriges Blanko et al. 2016). Thus, mechanisms that are critical to promoting MMR on the chromatin are possibly overlooked. Moreover, whether the activities described in the previous part are used to handle nucleosomes to facilitate the MMR reaction *in vivo* has not been examined.

To solve these problems, I investigated the relationship between MMR and chromatin assembly by using the nucleoplasmic extract of *Xenopus* eggs (NPE) (Walter et al. 1998). Previous members in our lab have found that NPE recapitulates both the gap-directed mismatch repair reaction (Kawasoe et al. 2016) and the chromatin assembly reaction (Taki Master's thesis 2012) most efficiently in existing *in vitro* systems. Using NPE, a preliminary finding in our lab has suggested that supercoiling of DNA, an indirect readout of chromatin assembly, is inhibited on a mismatch-carrying DNA. These findings indicate the possibility that the existence of the mechanisms that exclude nucleosomes around a mismatch. In *part I* in this thesis, I experimentally demonstrated that nucleosomes are excluded from the region surrounding a mismatch. To further investigate the molecular mechanisms of this reaction, referred to as nucleosome exclusion, mismatch-carrying DNA binding factors were identified in *part II* in this thesis, and chromatin remodeler Smarcad1 and histone chaperone FACT were gained. Immunological experiments suggest that Smarcad1 and FACT promote nucleosome

exclusion. To examine whether Smarcad1 and FACT contribute to MMR in *vivo*, a model system was switched to the budding yeast *Saccharomyces cerevisiae* in *part III* in this thesis. The genetics suggested that Fun30, the counterpart of Smarcad1 in yeast, cooperates with MutS complexes to suppress mutations. Based on these data, I propose the molecular mechanism that handles nucleosomes to facilitate MMR in the presence of the chromatin assembly reaction.

Part I: The MMR system induces exclusion of nucleosomes around a mispaired base

I-1. Introduction

The system that recapitulates nucleosome assembly and MMR *in vitro* is useful to understand how the MMR reaction occurs in the presence of nucleosomes. Since the nucleoplasmic extract of *Xenopus* eggs (NPE) is prepared by extraction of nucleoplasm of nuclei with minimum dilution (Walter et al. 1998), it recapitulates various nuclear reactions *in vitro* (reviewed in Hoogenboom et al. 2017). Importantly NPE supports gap-directed mismatch repair most efficiently among currently available *in vitro* systems (Olivera Harris et al. 2015; Kawasoe et al. 2016). Dr. Takahashi and a previous member in our lab, Ms. Taki, tried to investigate the relationship between MMR and nucleosome assembly by using NPE. Since their preliminary data is an essential background of this thesis, I introduce their findings below.

They prepared mismatch-carrying DNA to examine whether a mispaired base affects nucleosome assembly (Kawasoe et al. 2016). An oligonucleotide DNA was annealed on single-stranded circular DNA, the complementary DNA strand was synthesized *in vitro*, and remaining nicks were ligated. The 3,011-bp closed circular DNA carrying no mispaired base is referred to as $pMM1^{homo}$, and that carrying an A:C mismatch was referred to as $pMM1^{AC}$ (Fig. 1A). They incubated the closed circular DNA in NPE. Deposition of a nucleosome induces approximately one compensatory positive supercoil in closed circular duplexes, and by relaxing this torsional strain, topoisomerase I reduces the linking number of a plasmid by one for each nucleosome assembled in NPE. Agarose gel electrophoresis separates these topoisomers (Fig. 1B). $pMM1^{homo}$ became highly supercoiled within 3 min in NPE (Fig. 1C, lanes 2–6). In contrast to $pMM1^{homo}$, most of $pMM1^{AC}$ were not highly supercoiled in NPE, even at 30 min, and this pattern was kept for 60 min (Fig. 1C, lanes 9–15). This result suggests that nucleosome assembly is inhibited in mismatch-carrying DNA. Ms. Taki also demonstrated that depletion of Msh2 from NPE impaired the inhibition of supercoiling of mismatch-carrying DNA, suggesting that the MMR pathway is involved in the inhibition of supercoiling (Taki, Master's thesis 2012). These preliminary data indicate the probable presence of the mechanism that counteracts nucleosome assembly in the MMR pathway. I assumed that this mechanism is probably a key to understand eukaryotic MMR.

Here, I performed the supercoiling assay using various types of mispaired bases

and confirmed the inhibition of supercoiling of mismatch-carrying DNA. To demonstrate that nucleosomes are excluded around a mispaired base, a micrococcus nuclease digestion assay and quantification of the histones on mismatch-carrying DNA were performed. These experiments demonstrated that nucleosomes around a mispaired base are excluded. Additionally, immunological experiments suggested that both CAF-1- and HIRA-mediated chromatin assembly were inhibited on mismatch-carrying DNA. These observations revealed the existence of an active mechanism in MMR to counteract chromatin assembly.

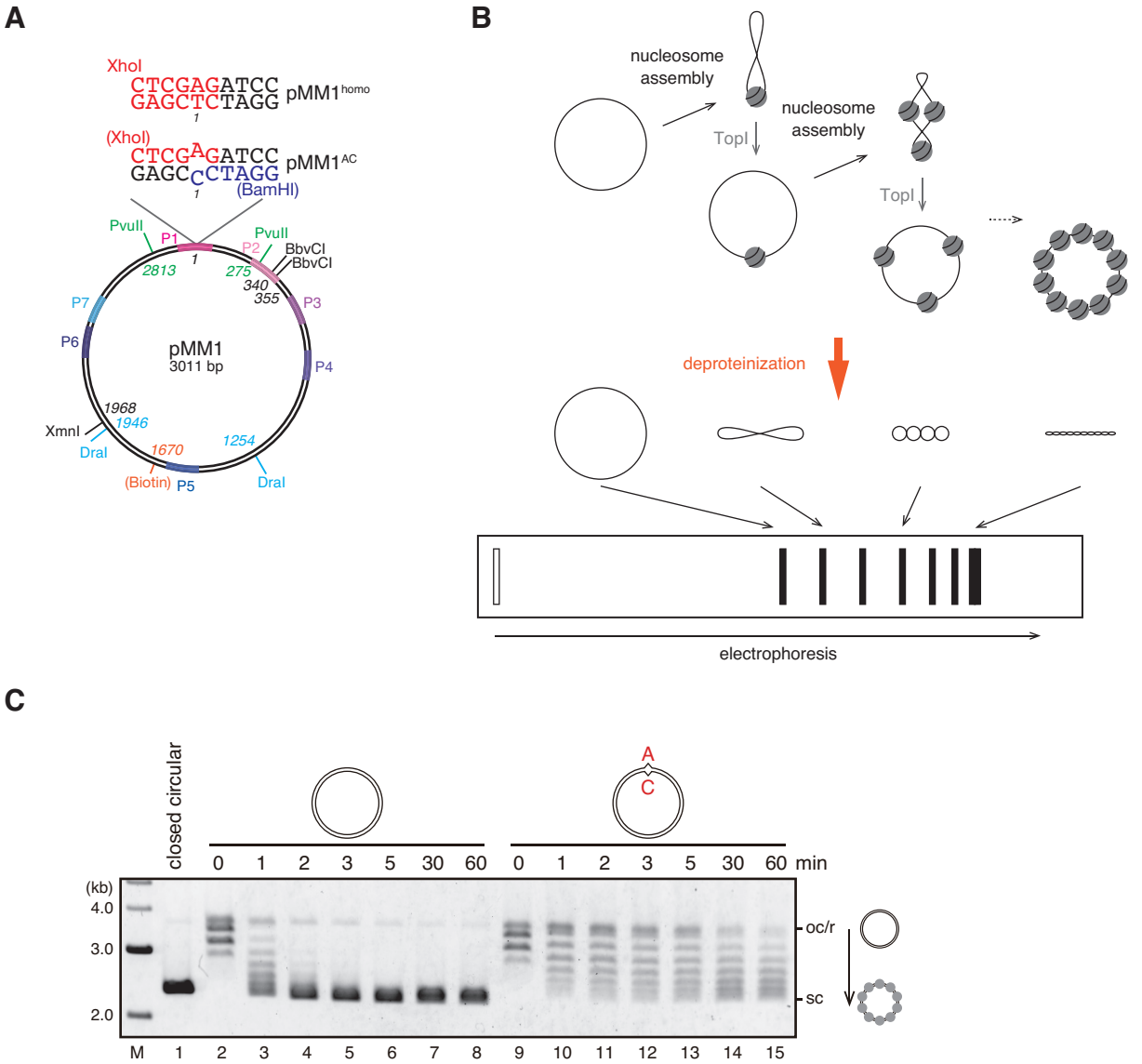

Figure 1. Supercoiling of mismatch-carrying DNA is inhibited in NPE (performed by Dr. Takahashi)
(A) DNA substrate used in this study. The 3,011-bp DNA carries an A:T base pair (pMM1^{homo}), or an A:C mispair (pMM1^{AC}) at position 1. Positions of restriction enzyme sites used in this study, the site of biotin modification, and amplicons for qPCR (P1: 2950–61, P2: 253–383, P3: 476–602, P4: 728–860, P5: 1498–1628, P6: 2266–2397, and P7: 2413–2537) are indicated.
(B) Schematic diagram of the supercoiling assay. Nucleosoeme formation induces torsional stress to the closed circular DNA, and topoisomerase I (TopI) reduces the linking number of the DNA to relax this torsional stress. Thus, a nucleosome induces approximately one compensatory positive supercoil in closed circular DNA in NPE. Agarose gel electrophoresis separates these topoisomers.
(C) Supercoiling assay in NPE. Covalently closed pMM1^{homo} (lanes 2–8) or pMM1^{AC} (lanes 9–15) were incubated in NPE, and sampled at the indicated times. Since closed circular DNA purified from E. coli is highly supercoiled, pMM1 purified from E. coli was used as marker of highly supercoiled pMM1 (lane 1). oc/r: open circular or relaxed DNA, sc: supercoiled DNA. Supercoiling of mismatch-carrying DNA was significantly inhibited.

I-2. Results

Various mispaired bases and an insertion/deletion loop inhibit supercoiling of a plasmid in NPE

I first repeated the supercoiling assay to confirm that supercoiling of mismatch-carrying DNA is inhibited in NPE. An A:C, T:C, G:G, C:C mismatch, 1-IDL, or a 5-IDL carrying pMM1 were constructed. They are referred to as $pMM1^{AC}$, $pMM1^{TC}$, $pMM1^{GG}$, $pMM1^{CC}$, $pMM1^{1IDL}$, $pMM1^{5IDL}$, respectively (Fig. 2). Upon incubation in NPE, $pMM1^{AC}$, $pMM1^{TC}$, $pMM1^{GG}$, and $pMM1^{1IDL}$ were not efficiently supercoiled, indicating that these mispaired bases cause the inhibition of supercoiling (Fig. 2, top). In contrast, $pMM1^{CC}$ and $pMM1^{5IDL}$ did not show any detectable inhibition of supercoiling (Fig. 2, bottom). Although I have not clarified the reason why C:C mismatch and 5IDL did not cause inhibition of supercoiling, it is possible that they are not recognized as substrates for MMR in NPE (see discussion).

Mismatch-carrying DNA is more sensitive to micrococcal nuclease digestion than homoduplex DNA in NPE

If a mismatch prevents nucleosomes to be assembled on DNA in NPE, the sensitivity of $pMM1^{AC}$ to micrococcal nuclease (MNase) should increase. To examine whether the number of nucleosomes is decreased on mismatch-carrying DNA, I next digested mismatch-carrying DNA by MNase. To identify roughly the region where nucleosome density is decreased, two probes for Southern blotting, the PvuII–PvuII probe that anneals to the mismatch-carrying region and the DraI–DraI probe that anneals to the region most distal to the mismatch, were prepared (see Figs. 1A and 4). MNase-digested DNA fragments were separated by agarose gel electrophoresis, stained with SYBR-Gold, and transferred onto nitrocellulose membrane. When $pMM1^{homo}$ was digested by MNase for 15 sec, a smear pattern was generated. As MNase-digestion time was increased, the smear pattern was decreased and a ~150-bp band corresponding roughly to a nucleosome was increased (Fig. 3, top, lanes 1–4). This pattern was also seen by Southern blotting with both the PvuII-PvuII and DraI-DraI probes. These results confirm that nucleosomes are assembled evenly on both regions of $pMM1^{homo}$. In contrast, when $pMM1^{AC}$ was digested by MNase, intensities of all bands were weakened compared to the $pMM1^{homo}$. The mismatch-surrounding region became markedly sensitive to MNase (Fig. 3, middle), suggesting that nucleosome density was decreased especially on a mismatch-surrounding

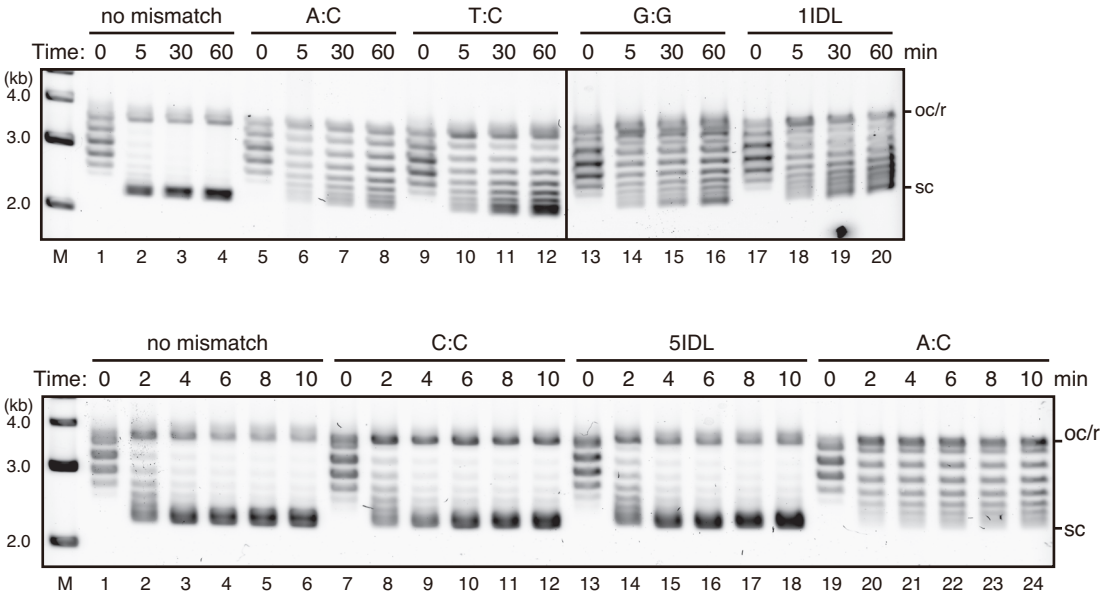

Figure 2. Various mispaired bases inhibit supercoiling of a plasmid in NPE
pMM1 carrying no mismatch, an A:C, T:C, G:G mismatch, an insertion/deletion loop (IDL) of 1 extrahelical nucleotide (1IDL) (top), a C:C mismatch, or an IDL of 5 extrahelical nucleotide (5IDL) (bottom) was incubated in NPE and sampled at the indicated times. The A:C, T:C, G:G mismatches and 1IDL strongly inhibited supercoiling. In contrast, the C:C mismatches and 5IDL did not show inhibition of supercoiling even at early time points.

region. Although the MNase sensitivity was increased on the mismatch-distal region, the effect is milder than the mismatch-surrounding region. I hereafter refer to this reaction as nucleosome exclusion.

Approximately a 1-kb region surrounding a mispaired base is highly sensitive to MNase

To map the region where the MNase sensitivity is increased, I repeated the MNase digestion assay and quantified DNA fragments by quantitative PCR (qPCR) (Fig. 4). Primers were designed to amplify approximately 130-bp DNA fragments (Fig. 1A). If the target region is escaped from MNase-digestion, a positive signal should be detected. Thus, the more nucleosomes are formed, the more positive signal is detected by qPCR. In this assay, an unrelated 'control' plasmid (pControl) was added to the reaction as an internal control to compare the MNase sensitivity between $pMM1^{homo}$ and $pMM1^{AC}$.

Before MNase digestion, a small aliquot of the reaction was sampled and the supercoiling state of the plasmids was analyzed. Since pControl was purified from *E. coli*, it was supercoiled before incubation in NPE (Fig. 4A, lanes 1 and 2). Supercoiling of $pMM1^{AC}$ was inhibited in NPE consistent with Figures 1 and 2 (Fig. 4A, lane 4). When $pMM1^{homo}$ was digested by MNase for 30 sec, approximately 15% of DNA fragments relative to the initial amount of DNA were detected at the mismatch site-spanning region, P1 (Fig. 4B, 'P1', see also Fig. 1A). Increasing the time of MNase treatment to 60 sec and 120 sec, undigested DNA fragments were gradually decreased. In contrast, when $pMM1^{AC}$ was digested by MNase for 30 sec, less than 1% of DNA fragments relative to the initial amount of DNA in reaction were detected at P1 (Fig. 4B, 'P1'), indicating that a mismatch proximal region is strikingly sensitive to MNase compared to $pMM1^{homo}$.

To know the relationship between the MNase sensitivity and distance from a mispaired base, I quantified DNA fragments at additional six regions (Fig. 4B, P2–7, see also Fig. 1A). Although undigested DNA fragments of $pMM1^{AC}$ were decreased compared to those of $pMM1^{homo}$ at all regions, undigested DNA of $pMM1^{AC}$ increased as the distance from a mispaired base becomes farther. In contrast, even if pControl was incubated with $pMM1^{homo}$ or $pMM1^{AC}$, the amount of undigested DNA fragments of pControl was almost the same (Fig. 4B, 'pControl'). This result suggests that a mismatched base affects only *in cis*, but not *in trans*.

To compare MNase sensitivities between $pMM1^{homo}$ and $pMM1^{AC}$ along the distance from the mispaired base, the amounts of undigested DNA fragments of P1–P7

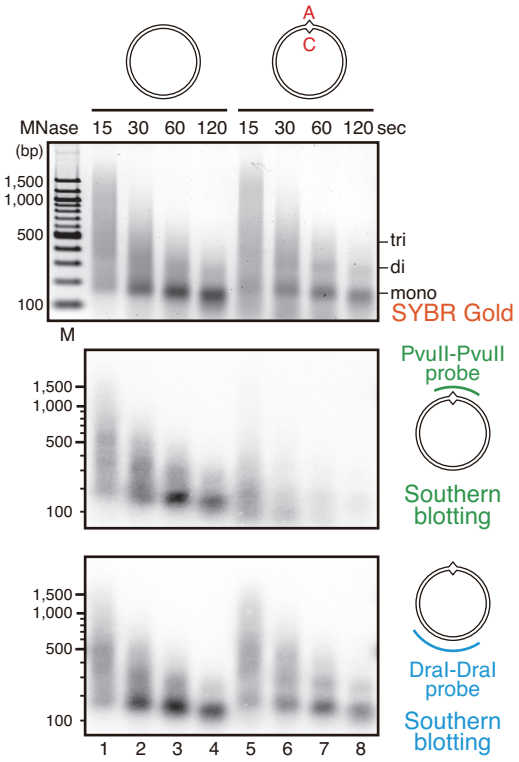

Figure 3. Mismatch-carrying DNA is higly sensitive to MNase digestion
pMM1^{homo} (lanes 1–4) or pMM1^{AC} (lanes 5–8) were incubated in NPE for 60 min and digested by micrococcal nuclease. DNA samples stained with SYBR-Gold (top), Southern blotting with the PvuII-PvuII probe (middle), and with the DraI-DraI probe (bottom) are shown.

were normalized by that of pControl (Fig. 4C). As seen in Fig. 4C, MNase sensitivities of P1–P7 varies even on $pMM1^{homo}$. This is probably because the MNase sensitivity varies depending on sequence context. To see the effect of a mismatch, the amount of undigested DNA of $pMM1^{AC}$ was normalized by that of $pMM1^{homo}$ and relative values were plotted (Fig. 4D). Relative undigested DNA values were particularly decreased within a ~500-bp region from the mismatch (a ~1-kb region toward both sides). Even if the larger 4,571-bp DNA was used, relative undigested DNA values were markedly decreased within a ~500-bp region from the mismatch (Fig. 5). These results suggest that the density of nucleosomes at approximately a 1-kb region surrounding a mismatch is significantly lower than homoduplex.

Msh2-containing complexes are required for nucleosome exclusion

To examine whether the MMR pathway contributes to nucleosome exclusion, the supercoiling assay was performed in NPE depleted of MMR factors. MutSα and MutSβ, both contain Msh2, bind to a mismatched base to initiate the MMR reaction. To immunodeplete both Msh2-containing complexes from NPE, anti-Msh2 antibodies were used for immunodepletion. Anti-Msh6 antibodies were also used to enhance the immunodepletion efficiency. It has been shown that immunodepletion of Msh2-containing complexes from NPE by using these Msh2- and Msh6-antibodies impairs the ability of gap-directed MMR (Kawasoe et al. 2016). As shown in Figure 6A, ~99% of Msh2 was depleted from NPE. In the Msh2-depleted NPE, $pMM1^{AC}$ was supercoiled similarly to $pMM1^{homo}$ (Fig. 6B, compare lanes 2–4 and 5–7), suggesting that the inhibition of supercoiling on mismatch-carrying DNA depends on the Msh2-containing complexes. However, the inhibition of supercoiling was not restored by the addition of recombinant MutSα to the Msh2-depleted NPE (Fig. 6B, lanes 8–10). To clarify whether Msh2-containing complexes are required for nucleosome exclusion, I performed immunodepletion by using other Msh2-antibodies (Fig. 6C). In Figure 6A, I used antibodies against residues 914–932 of Msh2 (referred to as α-Msh2). In addition to α-Msh2, two antibodies, both raised against full-length Msh2 but bled from different rabbits, were used in Figure 6C (referred to as α-Msh2R1 or α-Msh2R2). Immunodepletion by these antibodies depleted more than 95% of Msh2 from NPE. $pMM1^{AC}$ was supercoiled to a similar extent as $pMM1^{homo}$ in these Msh2-depleted NPE (Fig. 6D), strongly suggesting that Msh2 is required for nucleosome exclusion. Although the reason why the

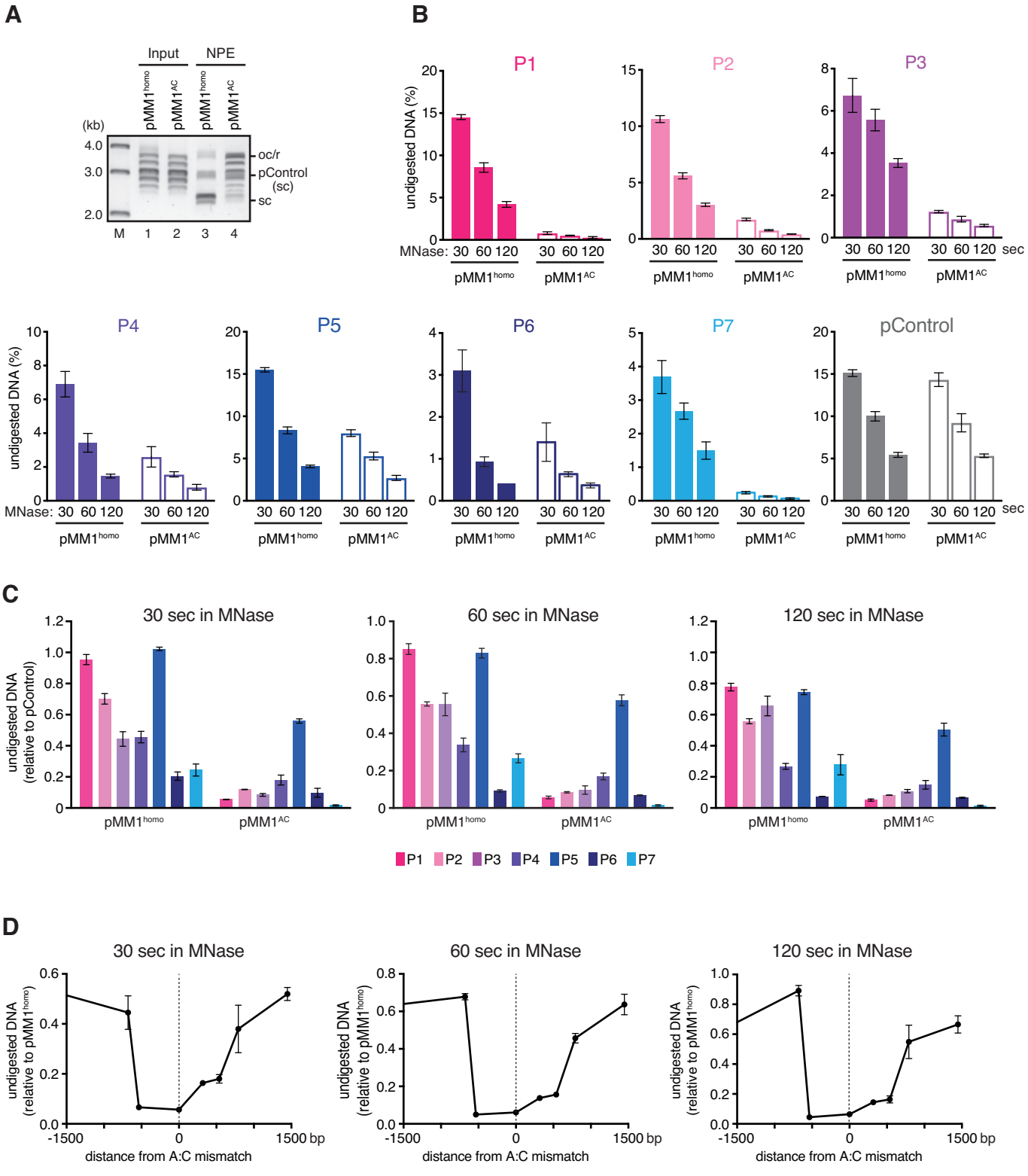

Figure 4. More than 1-kb region surrounding a mismatch is highly sensitive to MNase
(A) Supercoiling assay in NPE. The small aliquot of the reaction was sampled immediately before addition of MNase. The DNA samples were separated by agarose gel electrophoresis and stained with SYBR-Gold. pControl (sc): a supercoiled control plasmid.
(B–D) The MNase assay described in Fig. 2 was repeated in the presence of a control plasmid (pControl), and undigested DNA was quantified by qPCR. The amount of DNA relative to the input (B), normalized to pControl (C), and to pMM1homo (D) are presented. Mean ±1SD (n = 3 biological replicates).

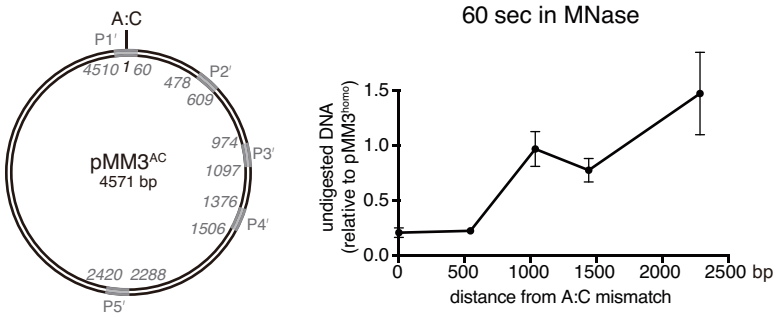

Figure 5. More than 1-kb region surrounding a mismatch is highly sensitive to MNase
The MNase digestion assay was performed with a larger plasmid substrate (pMM3^{AC}). Positions of primers for qPCR are presented on a map of pMM3^{AC}. The DNA amount normalized to the homoduplex DNA (pMM3^{homo}) is presented as a graph. Mean ±1 SD (n = 3). The area with strong nucleosome exclusion was not significantly extended on a larger plasmid compared to the 3-kb substrate.

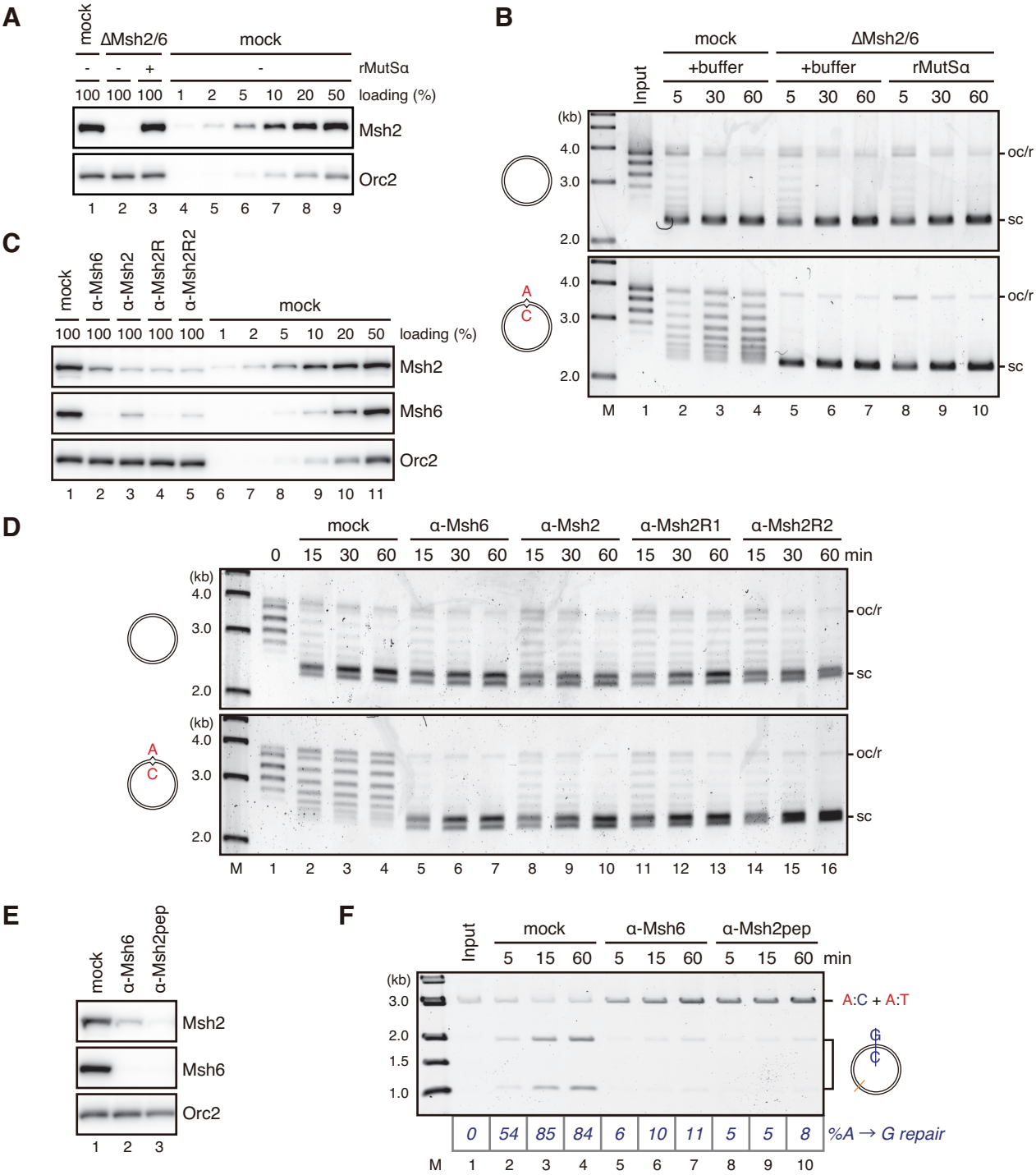

Figure 6. Effects of depletion of Msh2-containing complexes on MMR and supercoiling in NPE.
(A) The immunodepletion efficiency of Msh2. Mock-treated (lanes 1, 4–9, mock) or Msh2- (and Msh6-) depleted NPE (lanes 2, 3, ΔMsh2/6) supplemented either buffer (lanes 1, 2, 4–9) or 900 nM recombinant MutSα (lane 3) was separated by SDS-PAGE and probed with the indicated antibodies. 100% corresponds to 0.25 μL of NPE. Depletion efficiency for Msh2 is estimated as 99% since Msh2 in the ΔMsh2/6 NPE is less than 1% of the mock-treated NPE. Orc2 served as a loading control.
(B) Supercoiling activity of Msh2-depleted NPE described in A. Nucleosome exclusion was impaired by Msh2-depletion. However, addition of recombinant MutSα to the Msh2-depleted NPE did not rescue nucleosome exclusion.
(C) Immunodepletion of NPE with different Msh2/6 antibodies. Following antibodies were used for depletion: Msh6 (against residues 1324–1340 of xMsh6), Msh2pep (against residues 914–932 of xMsh2), and Msh2R1 and Msh2R2 (against full-length xMsh2, from different rabbit). α-Msh2R1 was exclusively used for Msh2 depletion throughout the paper, and therefore it was simply referred to as Msh2 antibodies in other experiments. 100% corresponds to 0.25 μL of NPE.
(D) Supercoiling activity of Msh2- or Msh6-depleted NPE described in C. All Msh2/6 antibodies consistently inhibited supercoiling of pMM1^{AC}, suggesting that the inhibition of pMM1^{AC} supercoiling depends on the Msh2-Msh6 complex.
(E) Depletion efficiencies of Msh6 and Msh2. NPE was depleted using pre-immune (lanes 1, mock), Msh6 (lane 2, α-Msh6), or Msh2pep (lane 3, α-Msh2pep) antibodies. 0.25 μL of NPE was separated by SDS-PAGE and probed with the indicated antibodies.
(F) Gap-directed MMR in Msh2/6-depleted NPE described in E. pMM1^{AC} carrying a 15-nt gap on the A-strand was incubated in NPE for the indicated times. DNA was purified and digested with XmnI and BamHI. The specific A to G repair was mostly inhibited by depletion of Msh6.

recombinant MutSα does not restore nucleosome exclusion has not been clarified, it is possible that immunodepletion by the Msh2- and the Msh6-antibodies depleted not only Msh2-containing complexes but also other factors that is required for nucleosome exclusion. It is noteworthy that the recombinant MutSα complex restores gap-directed MMR of Msh2-depleted NPE (Kawasoe et al. 2016), suggesting that nucleosome exclusion is not required for gap-directed MMR in NPE (see discussion).

Mlh1-containing complexes are not required for nucleosome exclusion

Since MutSα and MutSβ recruits MutLα after recognition of a mismatch, it is possible that not only MutS complexes but also MutLα contributes to nucleosome exclusion. Thus, supercoiling of mismatch-carrying DNA was also examined wih NPE depleted MutL complexes (Fig. 7). Since MutLα consists of Mlh1 and Pms2 in vertebrates, anti-Mlh1 antibodies were used to deplete MutLα from NPE. Although approximately 98% of Mlh1 was depleted from NPE (Fig 7A, compare lane 2 and lanes 3–8), supercoiling of $pMM1^{AC}$ was inhibited in the Mlh1-depleted NPE (Fig. 7B), suggesting that MutLα is not required for nucleosome exclusion. To rule out the possibility that depletion of Mlh1 is insufficient, the efficiency of gap-directed MMR (Kawasoe et al. 2016) was also tested. In NPE, when a gap is introduced on one strand of mismatch-carrying closed circular DNA, a mispaired base on the gap-carrying strand is corrected in Msh2- and Mlh1-dependent manner. Thus, $pMM1^{AC}$ containing a 15-nt gap 340 nucleotides 3′ from the A:C mispaired A (see Fig. 1A) was used as a substrate. Since the A:C mismatch is prepared by annealing of BamHI and XhoI restriction enzyme sites, $pMM1^{AC}$ is refractory to their digestion and correction of the A:C mispair to G:C regenerates a BamHI site. In mock-treated NPE, approximately 80% of $pMM1^{AC}$ was converted into BamHI sensitive molecules (Fig. 7C, bottom, lanes 2–4). In contrast, BamHI sensitive molecules were not detected after incubation in Mlh1-depleted NPE (Fig. 7C, bottom, lanes 5–7), indicating that Mlh1-depletion was sufficient to prevent gap-directed MMR. This result supports the conclusion that MutLα is not required for nucleosome exclusion.

Nucleosome exclusion involves displacement of nucleosomes

Nucleosome exclusion possibly involves inhibition of deposition of *de novo* histones, eviction of pre-deposited histones, and alterations in the kinetics of histone exchange. If nucleosome exclusion involves only inhibition of deposition of *de novo* histones, it could

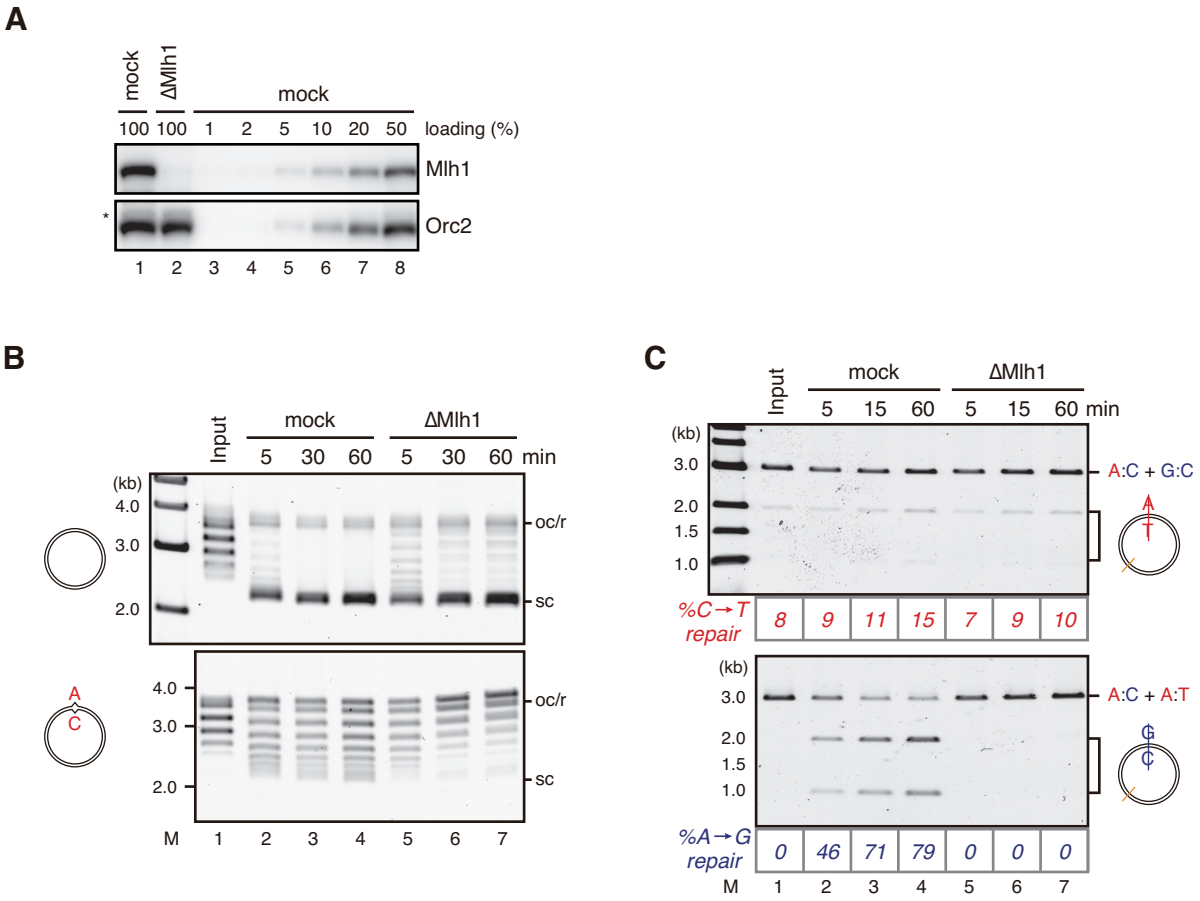

Figure 7. Effects of depletion of Mlh1-containing complexes on supercoiling and gap-directed MMR in NPE.
(A) The immunodepletion efficiency of Mlh1. Mock-treated (lanes 1, 3–8, mock) or Mlh1-depleted NPE (lanes 2, ΔMlh1) was separated by SDS-PAGE and probed with the indicated antibodies. 100% corresponds to 0.25 µL of NPE. Depletion efficiency for Mlh1 is estimated as 98% since Mlh1 in the ΔMlh1 NPE corresponds to 2% of the mock-treated NPE. Orc2 served as a loading control. (*) Cross-reacting band.
(B) Supercoiling activity of Mlh1-depleted NPE.
(C) Gap-directed MMR in Mlh1-depleted NPE. pMM1^{AC} carrying a 15-nt gap on the A-strand was incubated in NPE for the indicated times. DNA was purified and digested with XmnI, or BamHI and XmnI. The specific A to G repair was mostly inhibited by depletion of Mlh1.

not displace nucleosomes that are assembled on mismatch-carrying DNA. To examine this possibility, I next performed stepwise incubation assay (Fig. 8A). To transfer plasmids from 1st NPE to 2nd NPE, pMM1 carrying a biotinylated thymine at position 1670 (Fig. 1A) was immobilized on biotin Sepharose beads via streptavidin. Immobilized $pMM1^{AC}$ was supercoiled in Msh2-depleted NPE (Figs. 8B and C, lane 5), suggesting that it was chromatinized. Even after transfer to the second Msh2-containig NPE, the chromatinized $pMM1^{AC}$ maintained its supercoiled state (Fig. 8C, lane 6). However, because plasmids having the relative linking number less than -8 were not separated by agarose gel electrophoresis in our experimental condition, it is possible that the change of linking number of $pMM1^{AC}$ was not detected even though nucleosomes were displaced. Thus, I next performed the nucleosome displacement assay using pMM1 carrying three mismatches at position 1 (A:C), 803 (A:C), and 2271 (T:C) ($pMM1^{3MM}$) as a substrate to enhance the nucleosome exclusion reaction (Figs. 8D and E). The $pMM1^{3MM}$ was fully supercoiled in an Msh2-depleted NPE (Fig. 8E, lane 10). Upon transfer to the second Msh2-containing NPE, plasmids having relative linking numbers of less than -6 was detectably decreased and that of more than -5 was increased (Fig. 8E, compare lanes 10 and 11), suggesting that pre-assembled nucleosomes are displaced from mismatch-carrying DNA. In contrast, upon transfer into Msh2-depleted NPE, chromatinized $pMM1^{3MM}$ maintained its supercoiled state, suggesting that nucleosome displacement requires Msh2-containing complexes (Fig. 8E, lane 12). The MNase sensitivity of $pMM1^{3MM}$ was also examined in the nucleosome displacement assay to confirm that pre-assembled nucleosomes are displaced after incubation in Msh2-containing NPE (Fig. 8F). In Figure 8F, pControl was added as an internal control and instead of transferring plasmids, the second NPE was directly added to the first NPE to supply Msh2. The amount of undigested DNA of $pMM1^{homo}$ was not altered by incubation in the second NPE (Fig. 8F). After incubation in the Msh2-depleted NPE, the amount of undigested DNA of mismatch site-spanning regions of $pMM1^{3MM}$ was comparable to that of $pMM1^{homo}$, suggesting that nucleosomes were assembled on these mismatch site-spanning regions (Fig. 8F, P1 and P4). The amounts of undigested DNA of these mismatch site-spanning regions (P1 and P4) were decreased after addition of Msh2-containing NPE. These results suggest that pre-assembled nucleosomes are indeed decreased after incubation in Msh2-containing NPE. The amount of undigested DNA of mismatch distal region (P5) of $pMM1^{3MM}$ was not altered after incubation in Msh2-containing NPE,

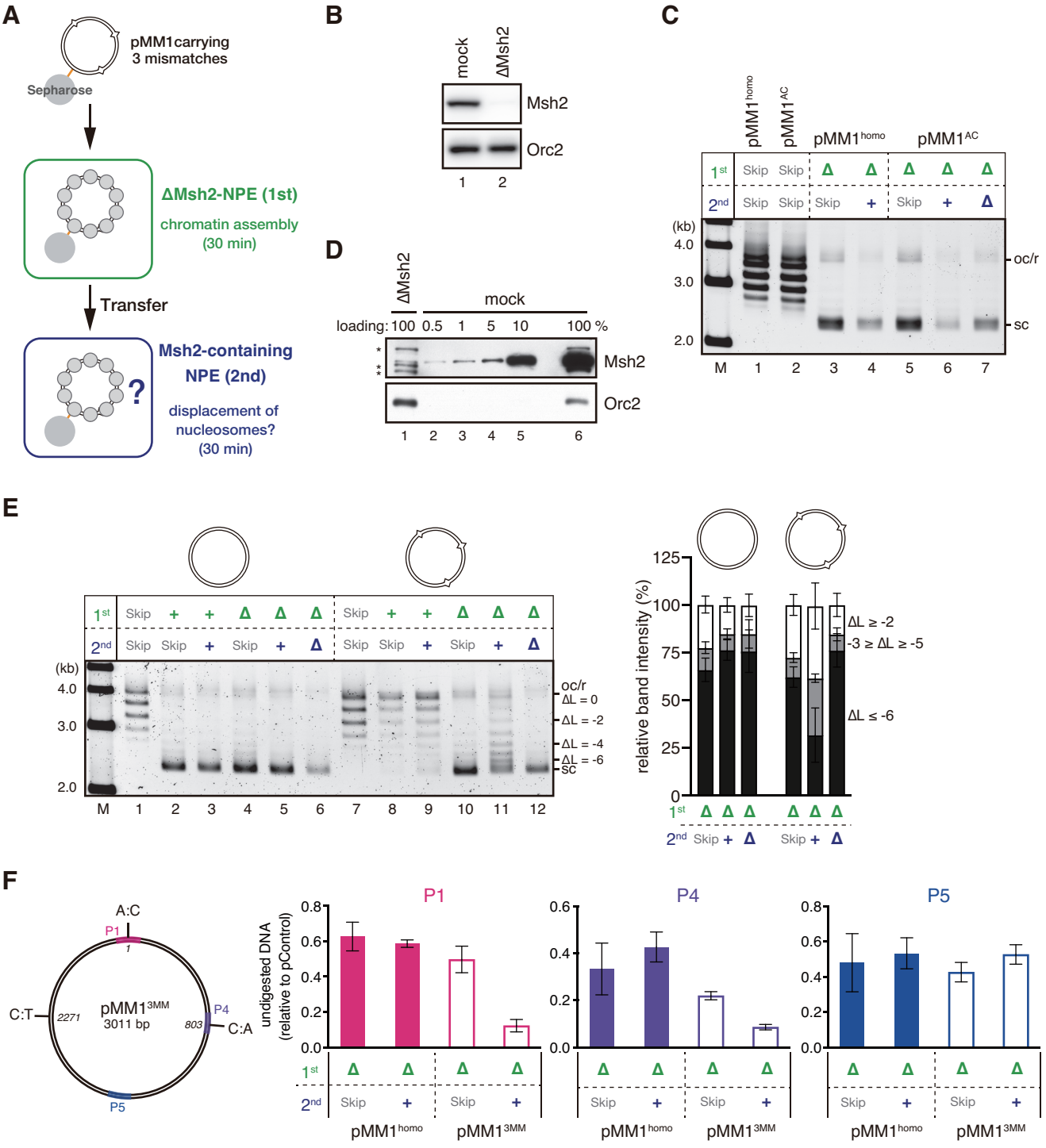

Figure 8. Pre-assembled nucleosomes are displaced around a mismatch in an Msh2-dependent manner.
(A) Schematic diagram of the nucleosome displacement assay. pMM1 was immobilized on Sepharose beads and incubated in an Msh2-depleted NPE for 30 min. The plasmid was then transferred into the second NPE containing Msh2, incubated for additional 30 min, and recovered.
(B) Immunodepletion of NPE with Msh2 antibodies. 0.25 µL of NPE was separated by SDS-PAGE and probed with indicated antibodies. Orc2 served as a loading control.
(C) Nucleosome displacement assay. pMM1^{homo} (lanes 1, 3, and 4) or pMM1^{AC} (lanes 2, 5, 6) was sequentially incubated in the indicated extracts. (+) indicates mock-treated NPE, (Δ) indicates Msh2-depleted NPE, and (Skip) indicates no incubation.
(D) Immunodepletion efficiency of Msh2. Mock-treated (lanes 2–6, mock) or Msh2-depleted NPE (lanes 1, ΔMsh2) was separated by SDS-PAGE and probed with the indicated antibodies. 100% corresponds to 0.25 µL of NPE. The depletion efficiency was estimated as 99% since Msh2 in the ΔMsh2 NPE is less than 1% of the mock-treated NPE. (*) Cross-reacting band. Orc2 served as a loading control.
(E) The nucleosome displacement assay was repeated using pMM1 carrying three mismatches (pMM1^{3MM}, see also panel F). The linking number of each band relative to the oc/r position (ΔL) is indicated on the right of the gel. The ratio of the plasmids of indicated ΔL is quantified and presented as a graph. Mean ± 1SD (n = 5).
(F) The nucleosome displacement assay was repeated without plasmid immobilization and in the presence of pControl. Instead of transferring plasmids, the second NPE was directly added to the first NPE to supply Msh2. The amount of DNA fragments relative to pControl after 60-second MNase digestion was quantified by qPCR. Mean ± 1SD (n = 3).

suggesting that the alteration of nucleosome density is specific to the mismatch site-spanning region.

Supercoiling of primer-extension products depends on both HIRA and CAF-1

The relationship between nucleosome assembly activities and nucleosome exclusion is important to understand the chromatin state where MMR occurs. In the above assays, closed circular double-stranded DNA was used as a substrate. When a closed circular plasmid is directly incubated in *Xenopus* egg extracts, nucleosomes are assembled by HIRA, which is responsible for DNA-synthesis-independent chromatin assembly (Ray-Gallet et al. 2002). It has been confirmed that depletion of HIRA from NPE inhibits supercoiling of $pMM1^{homo}$ (Fig. 9A–C, top, lanes 5–7), suggesting that nucleosome assembly on pMM1 in NPE is mainly mediated by HIRA. Thus the above results suggest that, at least, HIRA-mediated chromatin assembly was counteracted by nucleosome exclusion.

Since mismatch repair occurs immediately behind the replication fork, eukaryotic mismatch repair occurs under the circumstance where DNA-synthesis-coupled chromatin assembly that is mediated by the histone chaperone CAF-1 (Smith and Stillman 1989; Gaillard et al. 1996) occurs. To investigate the relationship between CAF-1-mediated chromatin assembly and nucleosome exclusion, a DNA-synthesis coupled system is needed. The primer-extension assay in NPE meets this need. NPE efficiently converts a primed single-stranded plasmid to the double-stranded form (Fig. 9A). Because unregulated priming is suppressed in NPE (Walter and Newport 2000), DNA synthesis initiates from the 3′ -terminus of the primer. As shown in Figure 9C, when a primed single-stranded plasmid was incubated in NPE and separated by agarose gel, it gradually banded as supercoiled double-stranded DNA (Fig. 9C, bottom, lanes 1–4). A smeared pattern that is estimated as intermediates of the primer-extension reaction appeared at an early time point, and it was gradually decreased as incubation time was increased (Fig. 9C, bottom, lanes 2–4). When HIRA was depleted from NPE, supercoiling of closed circular double-stranded DNA was significantly inhibited, and CAF-1-depletion did not affect supercoiling of closed circular double-stranded DNA (Figs. 9B and C, top, compare lanes 2–4, 5–7, and 8–10). In contrast, as expected, HIRA- or CAF-1-depletion did not alter the supercoiling of the primer-extension products, but simultaneous depletion of HIRA and CAF-1 significantly inhibited supercoiling of the primer-

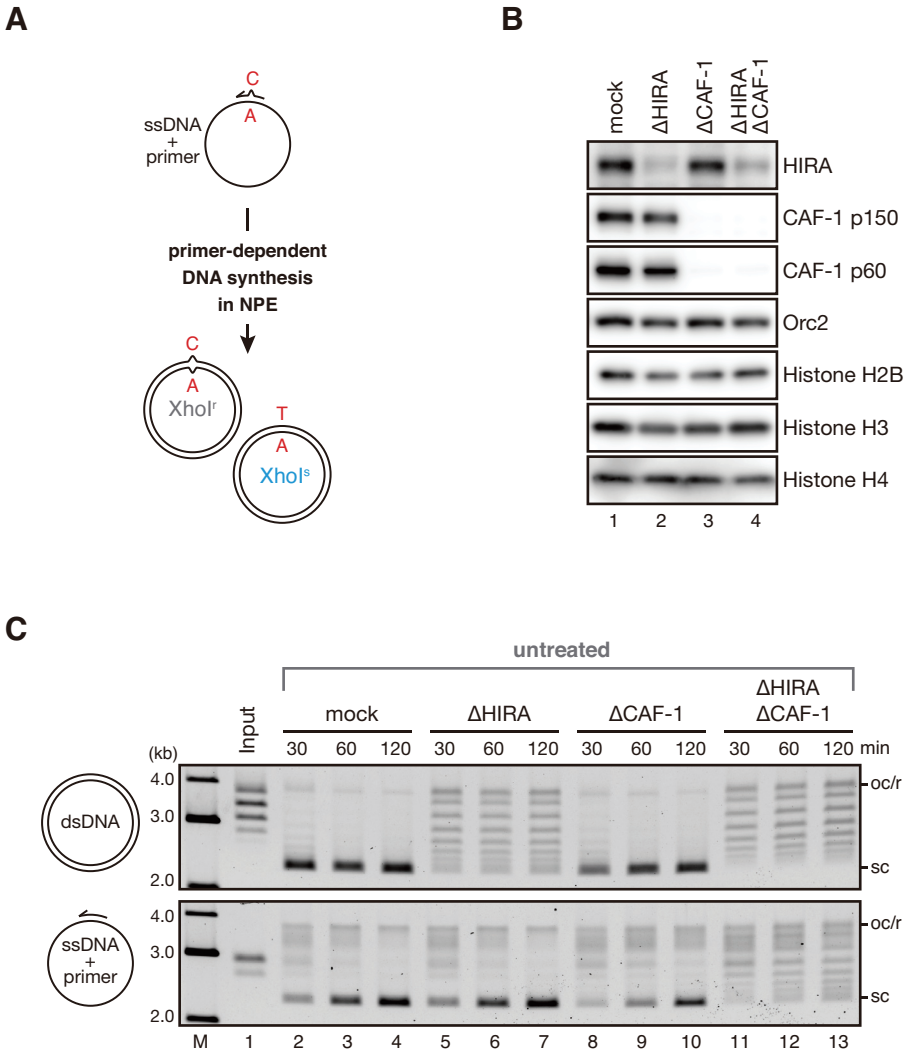

Figure 9. Supercoiling of primer-extension products depends on both HIRA and CAF-1.
(A) Schematic diagram of the primer-extension assay. A 92-nucleotide (nt) primer carrying either no mismatch or an A:C mismatch is annealed on a single-stranded pMM1. Upon incubation in NPE, complementary DNA is synthesized depending on the primer, converting the substrate into covalently closed circular DNA.
(B) The immunodepletion efficiencies of HIRA or CAF-1. NPE was depleted using non-immune (lane 1, mock), HIRA (lane 2, Δ HIRA), CAF-1 (lane 3, ΔCAF-1), or a mixture of HIRA and CAF-1 antibodies (lane 4, ΔHIRA ΔCAF-1). 0.2 μL each of depleted NPE was separated by SDS-PAGE and probed with the indicated antibodies. Approximately 80% of HIRA was depleted from NPE.
(C) Covalently closed pMM1^{homo} (top) or single-stranded pMM1 with a 92-nt primer (bottom) was incubated in the NPE described in (B), sampled at the indicated times, and separated by agarose gel. Although depletion was partial, HIRA-depletion significantly attenuated supercoiling of pMM1^{homo}. In contrast, supercoiling of the primer-extension products was inhibited only when both CAF-1 and HIRA were depleted (lanes 11–13).
This experiment was performed by Dr. Tatsuro Takahashi.

extension products (Figs. 9B and C, bottom, compare lanes 2–4, 5–7, 8–10, and 11–13). These results suggest that nucleosome assembly of the primer-extension products are mediated by both HIRA and CAF-1.

A mispaired base on a primer is efficiently corrected in the primer-extension reaction

Since the primer-extension reaction coincide with both HIRA- and CAF-1-mediated chromatin assembly, the primer-extension assay is a good model system to investigate the relationship between nucleosome exclusion and chromatin assembly. A mismatch is easily induced by using mismatch carrying primer. However, the primer-extension assay has a problem. Since the primer bears strand discontinuities at its 5′ terminus and 3′ terminus, the mismatch should be efficiently corrected by MMR. Thus, I first checked whether the mismatch was retained after the primer-extension reaction.

A 92-nt primer carrying either no mismatch or an A:C mismatch was annealed on a single-stranded pMM1. To examine whether the mismatch is retained on the primer-extension product, the A:C mismatch was located in the recognition site of XhoI (at position 1 on pMM1, see Fig. 1A). If the C on the primer was corrected to T, the primer-extension product became sensitive to XhoI. The primed ssDNA was incubated in NPE and the ratio of the XhoI-sensitive product was calculated as a repair efficiency (Figs. 10A–C). Even when a primer carrying no mismatch was used, a few percentages of the primer-extension products became resistant to XhoI (Fig 10B, top and Fig. 10C). It is possible that a small fraction of the primer was resected from 5′ to the recognition site of XhoI. If this resected recognition site of XhoI was not filled by DNA synthesis, the gap-retaining product should be resistant to XhoI. When a mismatch-carrying primer was used, more than 90% of the mismatch was repaired in mock-treated NPE (Fig 10B, bottom and Fig. 10C). To examine whether the correction of a mismatch in this system depends on the MMR system, the same assay was performed with Mlh1-depleted NPE (Figs. 10A–C). Mlh1 depletion reduced the repair efficiency to approximately 70%. Since 5′ -terminus directed MMR is independent of Mlh1 in human cell extracts and purified reconstituted systems, the effect of Msh2 depletion was also examined. Even in Msh2-depleted NPE, the repair efficiency was approximately 70%, suggesting that the majority of the mismatch was corrected by the MMR-independent pathway. Mismatch correction seen in Msh2- or Mlh1-depleted NPE is possibly mediated by proofreading by DNA polymerases, resection of the primer by exonuclease activities, or flap processing during

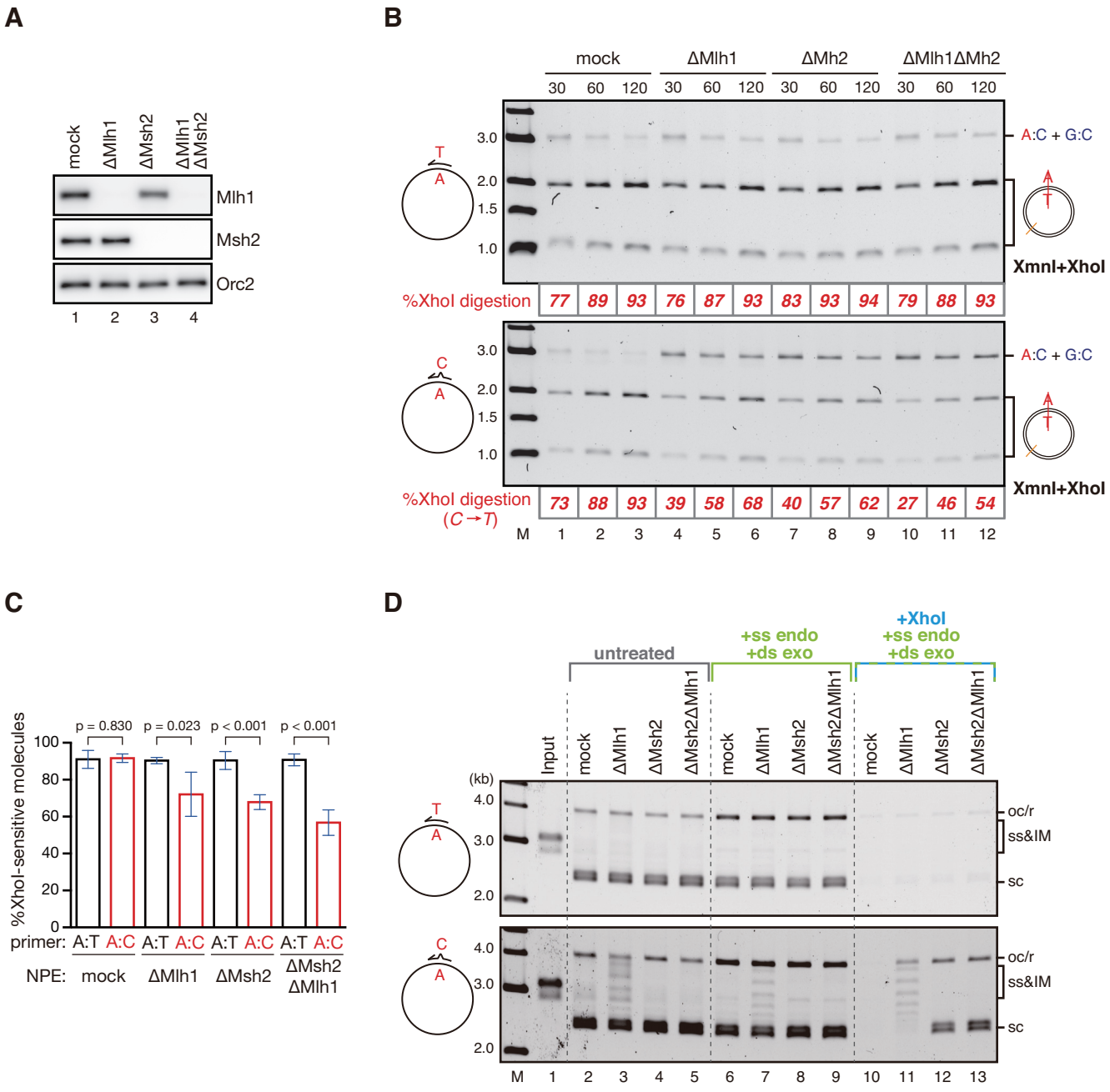

Figure 10. Supercoiling of the mismatch-carrying products of the primer-extension reaction is inhibited in an Msh2-dependent manner.

(A) Immunodepletion of Msh2 and Mlh1. NPE was depleted using non-immune (lane 1, mock), Mlh1 (lane 2, ΔMlh1), Msh2 (lane 3, ΔMsh2), or a mixture of Mlh1 and Msh2 antibodies (lane 4, ΔMlh1 ΔMsh2). 0.25 μL each of depleted NPE was separated by SDS-PAGE and probed with the indicated antibodies.

(B) Single-stranded pMM1 with a 92-nt homoduplex (top) or A:C-mismatch (bottom) carrying primer was incubated in NPE described in A, and sampled at indicated times. The C to T repair efficiency was estimated by digesting the products with XhoI and XmnI. An image of agarose gel electrophoresis of XhoI and XmnI digested DNA products are presented.

(C) A statistical analysis of the primer-extension based mismatch repair. The primer extension assay described in B was repeated three times. Mean of the C to T repair efficiency and one standard deviation (SD) was plotted as a graph.

(D) Supercoiling assay of the primer extension products. The products described in B were separated by agarose gel without any treatment (lanes 2–5), after digestion of intermediates by S1 nuclease and Exo V (lanes 6–9) or after digestion of C to T repair products and intermediates by XhoI, S1 nuclease, and λ exonuclease (lanes 10–13).

the completion of synthesis.

Supercoiling of mismatch-carrying products of the primer-extension reaction is inhibited in an Msh2-dependent manner

To detect the effect of a mismatch on nucleosome assembly in the primer extension assay, a mismatch must be retained on the primer-extension products. In the Mlh1-depleted NPE, approximately 30% of primer-extension products retain the mismatch. Thus, the supercoiling state of the primer-extension product in the Mlh1-depleted NPE was next examined (Fig. 10D). In mock-treated NPE, even when the mismatch-carrying primer was used, most of the products were supercoiled (Fig. 10D, bottom, lane 2), probably because most of the mismatch was corrected. In Mlh1-depleted NPE, primer-extension products showed a ladder pattern when the mismatch-carrying primer was annealed (Fig. 10D, bottom, lane 3). These bands were not digested by S1 nuclease, which is the single-stranded DNA specific endonuclease (Fig. 10D, bottom, lane 7), suggesting that they are not the intermediate of the primer-extension reaction. Additionally, they were resistant to XhoI (Fig. 10D, bottom, lane 11), indicating that they had a mismatch at the XhoI site. These results suggest that primer-extension products escaped from mismatch correction were not supercoiled. To examine whether inhibition of supercoiling of mismatch-carrying DNA in this system depends on the Msh2-containing complexes, the primer-extension assay was also performed with Mlh1- and Msh2-doubly-depleted NPE (Figs. 10A–D). Although approximately 40% of the primer-extension products retained the mismatch (Fig. 10B and C), they were supercoiled in the Mlh1- and Msh2-doubly-depleted NPE (Fig. 10D, bottom, lanes 5, 9, and 13), suggesting that inhibition of supercoiling of mismatch-carrying DNA in the primer-extension system requires the MutS complexes. Since supercoiling of the primer-extension products is mediated by both CAF-1 and HIRA, these results suggest that nucleosome exclusion can counteract both HIRA- and CAF-1-mediated chromatin assembly.

I-3. Discussion

In this part, I investigated chromatin assembly reactions on mismatch-carrying DNA, and found that mispaired bases cause exclusion of nucleosomes. The immunodepletion experiments showed that nucleosome exclusion depends on MutSα, suggesting that nucleosome exclusion occurs at the downstream of the MMR pathway. Thus, nucleosome exclusion is possibly the key to understand eukaryotic MMR on chromatin.

Why don't C:C mismatch and 5IDL cause nucleosome exclusion

Although pMM1$^{A:C}$, pMM1$^{T:C}$, pMM1$^{G:G}$, pMM1^{1IDL} showed inhibition of supercoiling, pMM1^{CC} and pMM1^{5IDL} did not show any detectable inhibition of supercoiling (Fig. 2). It has been reported that affinity of MutSα to a C:C mismatch or large IDLs is lower than that to other mispaired bases (Marsischky and Kolodner 1999). Also, MutSβ is much less concentrated in mammalian cells than MutSα (Drummond et al. 1997; Genschel et al. 1998; Marra et al. 1998). The concentration of Msh3 and Msh2 in NPE has been estimated by quantitative western blotting in our lab, and Msh3 is shown to be approximately 100 times less concentrated than Msh2 (Fig. 11). Consistently, immunodepletion of Msh6 from NPE co-depletes most of Msh2 (Fig. 6E). It is possible that since MutSα poorly binds to C:C mismatch and 5IDL, pMM1^{CC} and pMM1^{5IDL} did not show any detectable inhibition of supercoiling. However, I did not confirm the affinity of MutSα to C:C mismatch and 5IDL. This point needs further investigation.

How does MutSα cause nucleosome exclusion?

My results indicate that MutSα functions as a central factor of nucleosome exclusion. It has been reported that human MutSα has an activity to counteract CAF-1-mediated chromatin assembly *in vitro* (Kadyrova et al. 2011; Schopf et al. 2012; Rodriges Blanko et al. 2016). Nucleosome exclusion also counteracted CAF-1 (Figs. 10B, C, and 11D). It is possible that *Xenopus* MutSα retains the activity that counteracts CAF-1-mediated chromatin assembly, and this activity contributes to nucleosome exclusion. In addition to the inhibition of CAF-1, results in *part I-2* demonstrated that nucleosome exclusion involves inhibition of HIRA. Although I don't have any supporting data to explain the detailed molecular mechanism of inhibition of these histone chaperones by the MMR system, at least, the involvement of a trans-acting factor is probably excluded. This is because nucleosome exclusion specifically occurs around a mispaired base, and co-

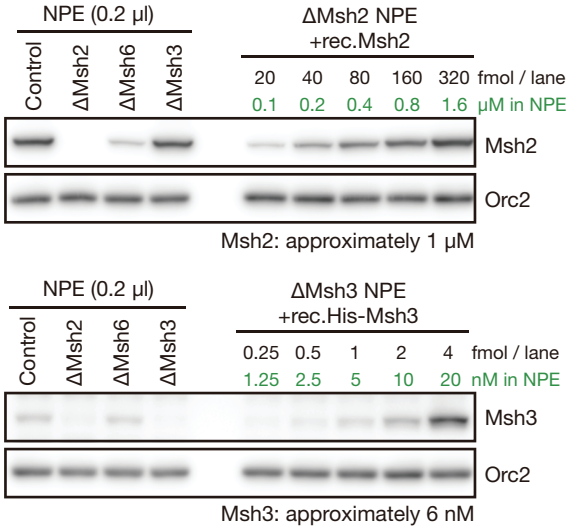

Figure 11. Quantification of Msh2 and Msh3 in NPE (performed by Dr. Takahashi)
NPE was treated with indicated antibodies and the indicated amount of either recombinant MutSα (top) or His-Msh3 (bottom) was supplemented to the extract. 0.2 µl each of NPE was separated by SDS-PAGE and probed with the indicated antibodies. The concentration of Msh2 was estimated to be approximately 1 µM, and that of Msh3 was estimated to be approximately 6 nM. This experiment was performed by Dr. Takahashi.

incubation of mismatch-carrying DNA with homoduplex DNA did not affect the chromatin assembly on homoduplex DNA (Figs. 4–6). Thus, nucleosome exclusion probably involves a cis-acting factor. For example, if DNA was covered by MutSα molecules, these physical barriers may inhibit the deposition of histones.

Figure 8 showed that nucleosome exclusion disassembles preassembled nucleosomes. It has been reported that human MutSα has chromatin remodeling activity (Javaid et al. 2009). In contrast, it has also been reported that MutSα can't handle nucleosome arrays (Gorman et al. 2010). Nucleosome exclusion handles nucleosome arrays under circumstances where nucleosome assembly occurs, implying that the chromatin remodeling activity of nucleosome exclusion is stronger than that of human MutSα *in vitro*. Thus, although it is possible that the chromatin remodeling activity of MutSα is used in nucleosome exclusion, the possibility that additional other factors assist MutSα to promote nucleosome exclusion is high. I'll examine this possibility in the next part.

The recombinant MutSα used here did not restore nucleosome exclusion of Msh2-depleted NPE. By contrast, the recombinant MutSα restores gap-directed MMR of Msh2-depleted NPE (Kawasoe et al. 2016). These results don't necessarily suggest that nucleosome exclusion doesn't contribute to eukaryotic MMR. Since the gap-directed MMR assay uses naked DNA as a substrate, part of MMR steps probably precedes nucleosome assembly. If the MMR steps that are sensitive to nucleosomes are accomplished before nucleosome assembly, nucleosomes may not inhibit gap-directed MMR. Thus, whether the gap-directed MMR assay is appropriate to a model system for MMR on chromatin is doubtful. Additionally, the supercoiling assay performed here does not separate the plasmids having the relative linking number of less than -7. Thus, it is possible that the recombinant MutSα has a nucleosome exclusion activity that is not detected by supercoiling assay, and this activity is sufficient to carry out gap-directed MMR.

Part II: Chromatin remodeler Smarcad1 facilitates nucleosome exclusion

II-1. Introduction

In the previous part, I demonstrated that nucleosomes are excluded around a mispaired base in an Msh2-dependent manner. MutSα is the only factor whose involvement in nucleosome exclusion is suggested. However, how MutSα performs nucleosome exclusion is unclear. As described in the discussion in *part I*, it is possible that MutSα itself disassembles nucleosomes or inhibits deposition of histones. Another plausible mechanism is MutS complexes recruit factors that handle nucleosomes such as chromatin remodelers or histone chaperones. In fact, a lot of functions on eukaryotic DNA, such as DNA replication, transcription, and recombination, evolve to utilize histone chaperones and chromatin remodelers to accommodate chromatin structure (reviewed in Ransom et al. 2010; Narlikar et al. 2013; Polo and Almouzni 2015).

In this part, I identified factors that were recruited onto mismatch-carrying DNA in NPE and gained chromatin remodeler Smarcad1 and histone chaperone FACT. Smarcad1 was recruited onto mismatch-carrying DNA in MutS complexes-dependent manner. Depletion of Smarcad1 from NPE weakened nucleosome exclusion. In contrast to Smarcad1, depletion of FACT did not have a detectable effect on nucleosome exclusion. However, double depletion of Smarcad1 and FACT weaken nucleosome exclusion further than Smarcad1 single depletion. These results suggest that Smarcad1 and FACT promote nucleosome exclusion.

II-2. Results

Identification of mismatch-carrying DNA binding factors

Since nucleosome exclusion involves displacement of nucleosomes, it is possible that chromatin binding factors bind to chromatin to displace pre-assembled nucleosomes. If it is the case, chromatin binding of them probably depends on a mispaired base because nucleosome exclusion is induced by a mispaired base. Thus, I compared chromatin binding factors on $pMM1^{homo}$ and $pMM1^{AC}$ in NPE.

To recover chromatin binding factors in NPE, $pMM1^{homo}$ or $pMM1^{AC}$ carrying a biotinylated thymine at position 1670 (see Fig. 1A) were prepared (Higashi et al. 2012; Kawasoe et al. 2016). $pMM1^{homo}$ or $pMM1^{AC}$ were immobilized on biotin Sepharose beads via streptavidin. The immobilized DNA was incubated in NPE for 30 min, and recovered (Fig. 12A). Supercoiling of $pMM1^{AC}$ was also inhibited in this condition (Fig. 12B). The recovered proteins were separated by SDS-PAGE and stained with silver nitrate (Fig. 12C). In addition to the bands detected in the $pMM1^{homo}$ pull-down sample, several additional bands appeared or became stronger in the $pMM1^{AC}$ pull-down sample (Fig. 12C, compare lanes 1 and 2). By using specific antibodies, Msh2, Msh6, and Mlh1 were detected (Fig. 12D). Msh2 and Msh6 were specifically detected in the $pMM1^{AC}$ pull-down sample, confirming that they bound to chromatin depending on a mispaired base. Although Mlh1 was detected in the $pMM1^{homo}$ sample, Mlh1 increased on $pMM1^{AC}$. It may be because Mlh1 non-specifically binds to immobilized $pMM1^{homo}$ in this condition.

I asked Dr. Obuse and Dr. Nagao to identify these chromatin-binding proteins by mass spectrometry and compared the abundance of chromatin-binding factors on $pMM1^{homo}$ to that of $pMM1^{AC}$ (Table 1). Spectral counts, which is defined as the number of spectra identified for a protein, is roughly correlated with the abundance of the protein (Liu et al. 2004). Consistent with the result of Western blotting (Fig. 12D), spectral counts of Msh2, Msh6, and Mlh1 significantly increased in the $pMM1^{AC}$-pulled down sample compared to these in the $pMM1^{homo}$-pulled down sample (Table 1), confirming that the $pMM1^{AC}$-pulled down collects mismatch-binding factors. The spectral counts of known chromatin-related factors such as HIRA and Smarca5 (ISWI) were reduced in the presence of a mismatch, probably because DNA was less chromatinized. In contrast, the spectral counts of Smarcad1 and the FACT subunits Spt16 and Ssrp1 were increased in the presence of a mismatch. This result implied that Smarcad1 and FACT preferentially bind to mismatch-carrying DNA.

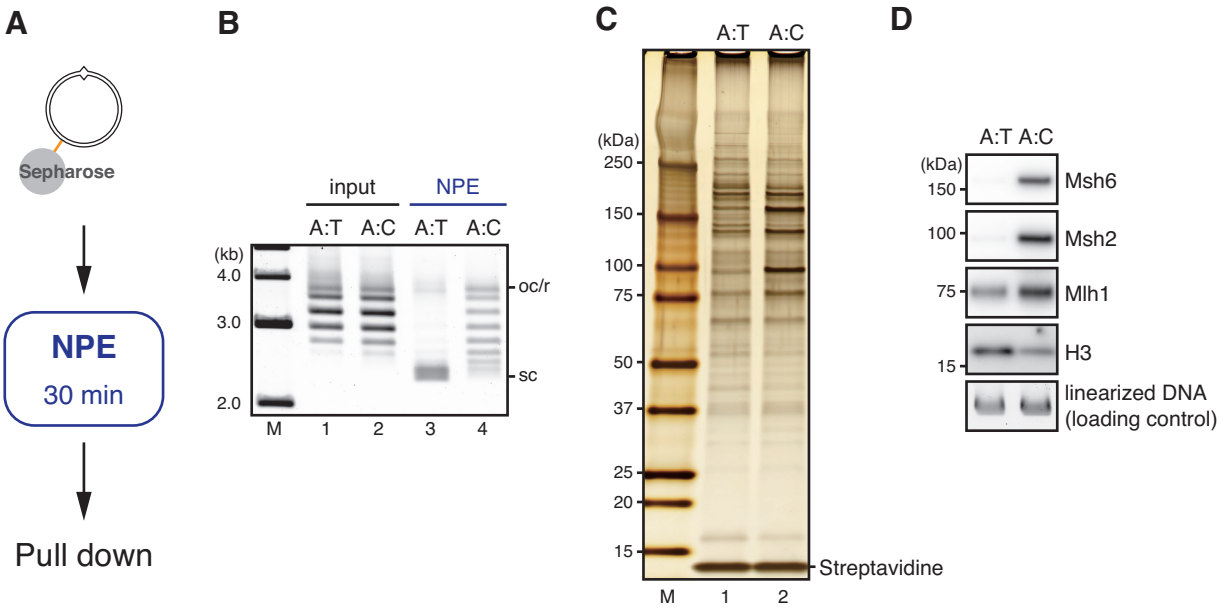

Figure 12. Identification of mismatch-carrying DNA binding factors
(A) Schematic diagram of the plasmid pull-down assay.
(B) Supercoiling state of plasmid in the pull-down assay. DNA was extracted from pull-down samples. The DNA samples were separated by agarose gel electrophoresis and stained with SYBR-Gold. A:T indicates pMM1^{homo}, and A:C indicates pMM1^{AC}. M indicates size markers.
(C) Silver staining of mismatch-DNA binding factors. Samples were separated by SDS-PAGE and stained with silver nitrate.
(D) Immunoblotting of mismatch-DNA binding factors. Samples were immunoblotted by indicated antibodies. DNA samples were linearized by XmnI, separated by agarose gel electrophoresis, and stained with SYBR-Gold. DNA samples were served as loading control.

Characterization of Xenopus laevis Smarcad1 and FACT in NPE

I decided to investigate the contribution of Smarcad1 and FACT on nucleosome exclusion. Although *Xenopus laevis* FACT had already been well characterized, full-length Smarcad1 gene of *Xenopus laevis* has not been identified. Thus, I first cloned the Smarcad1 cDNA and identified two isoforms of the Smarcad1 (Fig. 13A). Isoforms a and b shares approximately 90% identical amino acid sequences. They have the Snf2 family N-terminal domain and the Helicase conserved C-terminal domain, both of which are core domain of the SNF2 family chromatin remodeler and their sequence are well conserved from Fun30 (yeast counterpart of Smarcad1) to human Smarcad1.

To investigate contributions of Smarcad1 and FACT on nucleosome exclusion, antisera against these proteins were raised. The Spt16 or Ssrp1 antiserum was raised against full-length Spt16 or Ssrp1. Since Smarcad1 isoforms a and b share the same sequences in the C-terminus, Smarcad1 antisera was raised against the C-terminus of Smarcad1 to analyze both isoforms of Smarcad1. When NPE was separated by SDS-PAGE and probed with each antiserum, nearly a single band was detected, and the major band showed almost the same mobility as a recombinant protein, which was expressed in Sf9 insect cells and purified (Fig. 13B, compare lanes 5 to 6, 9 to 10, and 13 to 14). Each band was specifically immunoprecipitated by the corresponding antibody (see below). These data indicate that these antisera preferentially detect each antigen.

Smarcad1 specifically binds to mismatch-carrying DNA in an Msh2-dependent manner

Since nucleosome exclusion depends on Msh2 but not on Mlh1, Smarcad1 and FACT are possibly recruited to a mismatch site by MutS complexes to contribute to nucleosome exclusion. To test this possibility, the effects of Msh2 or Mlh1 depletion on DNA-bound Smarcad1 and FACT were examined by the plasmid pull-down assay (Figs. 14A and B).

Immunodepletion of Msh2 co-depleted Msh6 and Msh3 from NPE, but it didn't detectably deplete Smarcad1, FACT, and histones (Fig. 14A, compare lanes 1 and 2). Similarly, immunodepletion of Mlh1 specifically depleted Mlh1 from NPE, but it didn't detectably deplete Smarcad1, FACT, and histones (Fig. 14A, compare lanes 1 and 3). These results indicate that these immunodepletion treatments don't affect concentrations of Smarcad1, FACT, and histones in NPE.

In mock-treated NPE, Smarcad1 was detected in the pMM1^{AC} pull-down

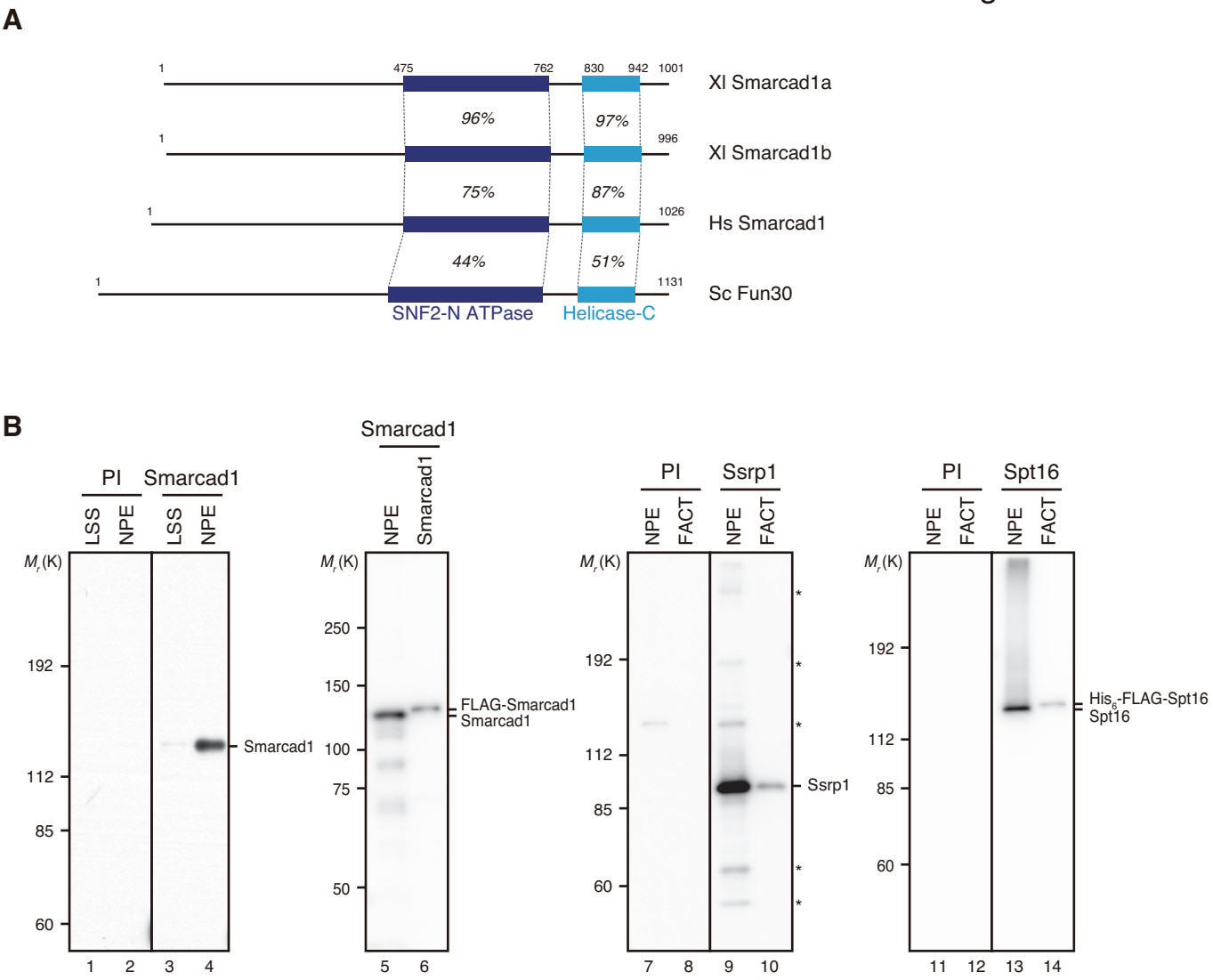

Figure 13. Characterization of Smarcad1 and FACT antisera.
(A) The domain architecture of Xenopus laevis (Xl) Smarcad1 isoforms (Smarcad1a and Smarcad1b) and Homo sapiens (Hs) Smarcad1 and Saccharomyces cerevisiae (Sc) Fun30. The positions and sequence-identities of the SNF2 family N-terminal domain (SNF2-N ATPase) and helicase C-terminal domain (Helicase-C) are indicated.
(B) Low-speed supernatant (LSS), NPE, or recombinant proteins were separated by SDS-PAGE and transferred onto PVDF membranes. Each membrane strip was probed with either the indicated antiserum or the pre-immune serum (PI) from the same rabbit. The same exposure sets are presented for each pair of PI and antiserum. Either Smarcad1 (lane 4), Ssrp1 (lane 9), or Spt16 (lane 13) was detected as nearly a single band in NPE. Becaue recombinant Smarcad1 or Spt16 has N-terminal tag, it migrated slightly slower than Smarcad1 or Spt16 in NPE. (*) Cross-reacting band.

sample while it wasn't detected in the pMM1^{homo} pull-down sample (Fig. 14B, compare lane 1 and 2), indicating that Smarcad1 specifically binds to mismatch-carrying DNA. The amount of Smarcad1 on the plasmid was quantified by comparing the band intensity of the pull-down sample to that of a dilution series of recombinant Smarcad1 (Fig. 14C). The number of Smarcad1 on pMM1^{AC} was estimated to be approximately 20 molecules per a plasmid. Although immunodepletion of Msh2 didn't reduce the concentration of Smarcad1 in NPE (Fig. 14A, compare lanes 1 and 2), it significantly reduced the Smarcad1 signal in the pMM1^{AC} pull-down sample (Fig. 14B, lane 4 and Fig. 14C). On the other hand, immunodepletion of Mlh1 didn't reduce the Smarcad1 signal in the pMM1^{AC} pull-down sample (Fig. 14B, lane 6, and Fig. 13C). These results indicate that Smarcad1 is recruited onto mismatch-carrying DNA depending on Msh2, but not on Mlh1. Spt16 and Ssrp1 were detected in both pMM1^{homo} and pMM1^{AC} samples, indicating that FACT binds to the immobilized DNA regardless of the existence of a mismatch, consistent with the mass spec data. Although I reproducibly detected more intensive Spt16 and Ssrp1 signals in the pMM1^{AC} sample than those in the pMM1^{homo} sample, the differences were not statistically significant with my sample number (n = 4) (Fig. 14C). Thus, I avoid concluding that FACT is preferentially recruited to the mismatch-carrying DNA. However, considering that other chromatin-binding factors decreased on the mismatch-carrying DNA, it is possible that loading of FACT on mismatch-carrying DNA was compensated by mismatch-dependent loading.

I also compared the relative amounts of histones H2B, H3, and H4 on immobilized DNA to confirm that nucleosomes are excluded from mismatch-carrying DNA in an Msh2-dependent manner (Fig. 14C). The relative amounts of histones H2B, H3, and H4 on immobilized DNA were significantly reduced in the presence of a mismatch in mock-treated NPE, and the reduction of histones was detected in Mlh1-depleted NPE, but not in the Msh2-depleted NPE (Fig. 14C).

Smarcad1 physically interacts with Msh2-containing complexes in NPE

Since recruitment of Smarcad1 to mismatch-carrying DNA depends on Msh2, a possible scenario is Msh2 interacts with Smarcad1 and/or FACT. To estimate the Svedberg units of each factor in NPE, NPE was fractionated by sucrose gradient sedimentation (Fig. 15A). Msh2, Smarcad1, and FACT were eluted into different fractions. The Svedberg unit of Msh2 (MutSα and MutSβ) is 11.3 (corresponding to M_r of ~2.3×10^5), Smarcad1 is

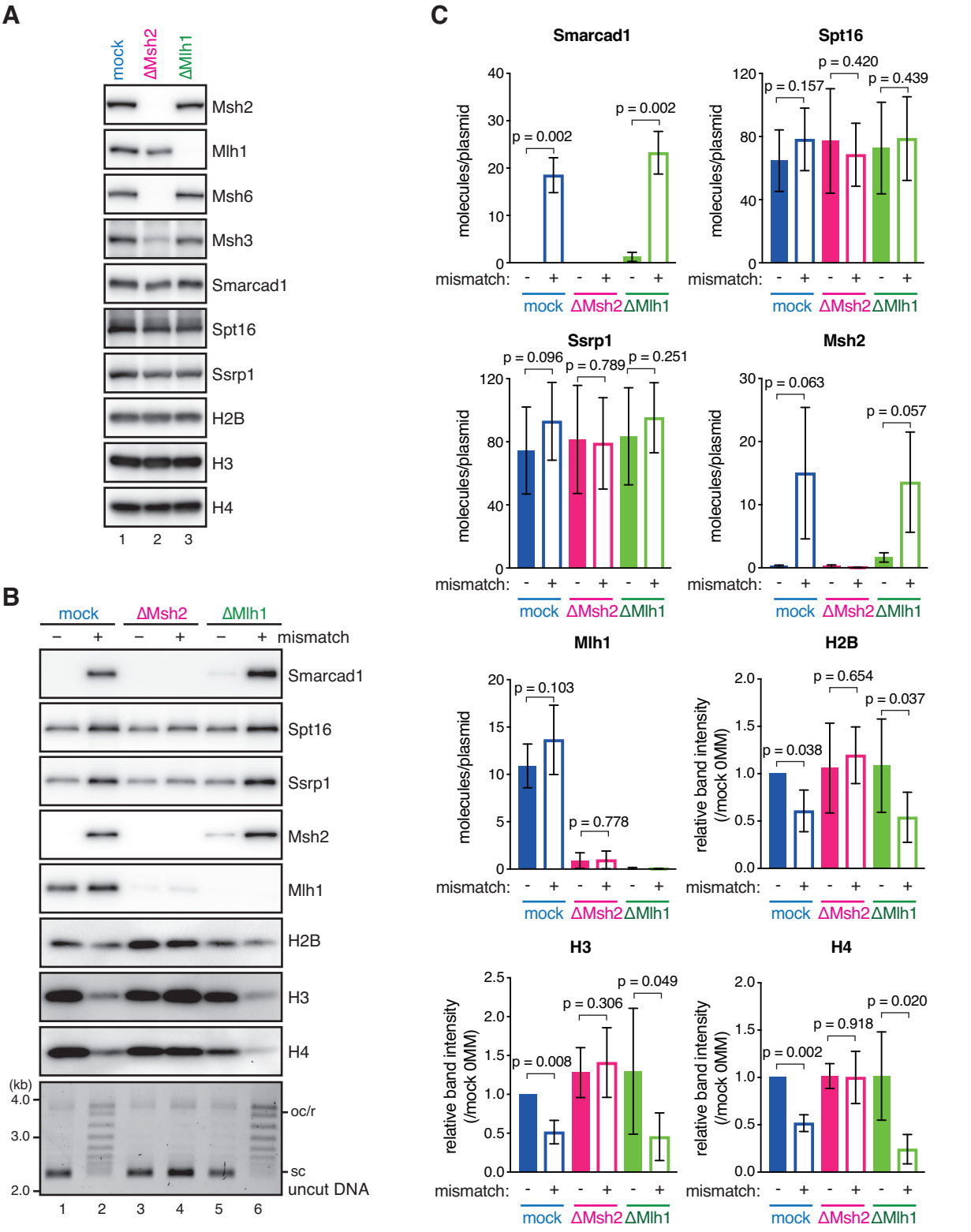

Figure 14. Smarcad1 specifically binds to mismatch-carrying DNA in an Msh2-dependent manner
(A) The immunodepletion of Msh2 or Mlh1. NPE was depleted using pre-immune antibodies (lane 1, mock), a mixture of Msh2 and Msh6 antibodies (lane 2, ΔMsh2), or Mlh1 antibodies (lane 3, ΔMlh1). 0.25-μL NPE was separated on SDS-PAGE and probed with the indicated antibodies.
(B) Immobilized pMM1^{homo} (lanes 1, 3 and 5) or pMM1^{AC} (lanes 2, 4 and 6) was incubated in NPE described in (A) and recovered. Immunoblotting of indicated antibodies and uncut DNA stained with SYBR-Gold are presented.
(C) Quantification of chromatin-binding factors. Band intensities were normalized to the amount of DNA quantified by qPCR. For Smarcad1, Msh2, Mlh1, Spt16, and Ssrp1, the number of molecules on a plasmid was estimated by using recombinant proteins as standards. Histones were normalized to the amount on no mismatch DNA in the mock sample. Mean ± 1SD (n = 4). p-values were calculated by the paired t-test (two-tailed).

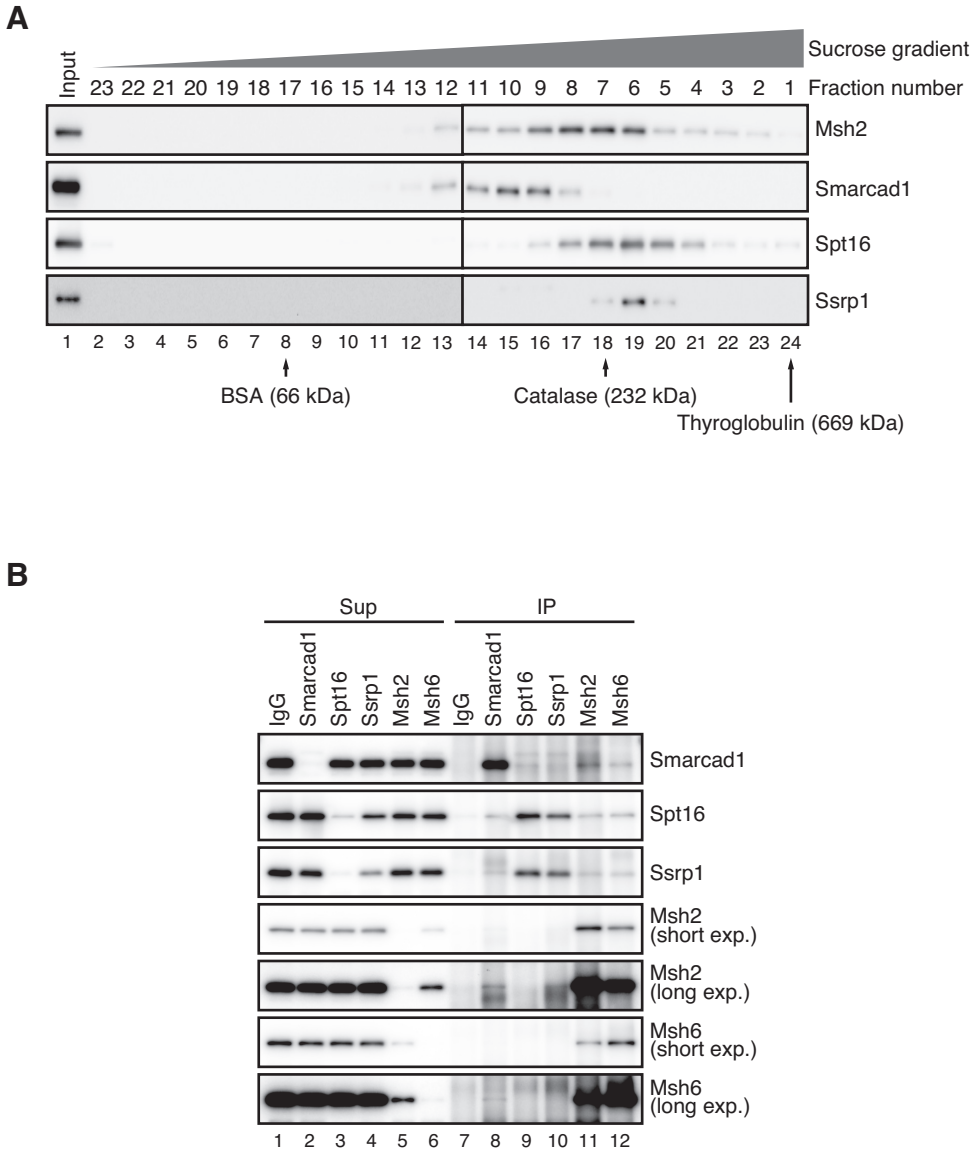

Figure 15. Smarcad1 physically interacts with Msh2-containing complexes in NPE
(A) Sucrose gradient sedimentation of NPE. NPE was separated by 5–20% sucrose gradient centrifugation and corrected as 24 fractions. 0.8 μL each of fractions 1–23 were separated by SDS-PAGE and probed with the indicated antibodies. The Svedberg units ($S_{20,w}$) estimated using catalase as a standard are as follows: Msh2, 11.3 (corresponding to Mr of ~2.3×10^5); Smarcad1, 9.3 (corresponding to Mr of ~1.7×10^5); FACT, 12.0 (corresponding to Mr of ~2.5×10^5).
(B) Co-immunoprecipitation of Smarcad1, FACT and MutSα. 25 μL each of the indicated antiserum was bound to 5 μL PAS, and the PAS beads were incubated in 3 μL NPE diluted with 12 μL ELB (total 15 μL) at 4°C for 1 h. The supernatant (Sup) and the bead (IP) samples corresponding to 0.04 μL of NPE were separated on SDS-PAGE and probed with the indicated antibodies.

9.3 (corresponding to M_r of ~1.7×10^5), and Spt16 and Ssrp1 are 12.0 (corresponding to M_r of ~2.5×10^5). This result suggests that most of the Msh2-containing complexes, Smarcad1, and FACT did not form a complex with each other in NPE. Consistent with this result, the immunoprecipitation assay also showed that major fractions of them were not co-precipitated with each other (Fig. 15B). However, a small amount of Smarcad1 was co-precipitated with Msh2 and Msh6, and a small amount of Msh2 and Msh6 were co-precipitated with Smarcad1, suggesting that Smarcad1 has potential to interact with Msh2-containing complexes, as reported in human cells (Okazaki et al. 2008; Rowbotham et al. 2011; Chen et al. 2016b). By contrast, I was not able to obtain evidence that FACT co-precipitates with MMR proteins.

Depletion of Smarcad1 from NPE weakens inhibition of supercoiling of mismatch-carrying DNA

Since Smarcad1 was recruited onto mismatch-carrying DNA in an Msh2-dependent manner, Smarcad1 is a good candidate that contributes to nucleosome exclusion. To examine this possibility, the supercoiling assay was performed using Smarcad1-depleted NPE (Figs. 16A–C). Using Smarcad1 specific antisera, approximately 98% of Smarcad1 was depleted from NPE. Immunodepletion of Smarcad1 did not detectably decrease Msh2 concentration in NPE (Fig. 16A). Smarcad1-depletion did not affect the supercoiling of $pMM1^{homo}$, suggesting that Smarcad1 does not play a major role in nucleosome assembly in this system (Fig. 16B, top panel, lanes 2–7). In the presence of a mismatch, however, plasmids having relative linking numbers of less than -6 were increased by Smarcad1 depletion, suggesting that inhibition of supercoiling is weakened by Smarcad1 depletion (Fig. 16B, bottom, compare lanes 2–4 to 5–7, and Fig. 16C).

Smarcad1 depletion possibly depletes not only Smarcad1 but also other factors from NPE. If depletion of these factors relieves inhibition of supercoiling of mismatch-carrying DNA, the addition of purified recombinant Smarcad1 to Smarcad1-depleted NPE could not rescue inhibition of supercoiling of mismatch-carrying DNA. N-terminally FLAG-tagged Smarcad1 was purified from Sf9 cells. FLAG-tagged Smarcad1 was fractionated by gel filtration, and it was eluted in fractions corresponding to the molecular mass of $2.5–5.0 \times 10^5$. The estimated molecular mass is slightly larger than the molecular mass of endogenous Smarcad1 in NPE estimated by Sucrose gradient sedimentation (Fig. 15A). The difference is probably derived from the difference of

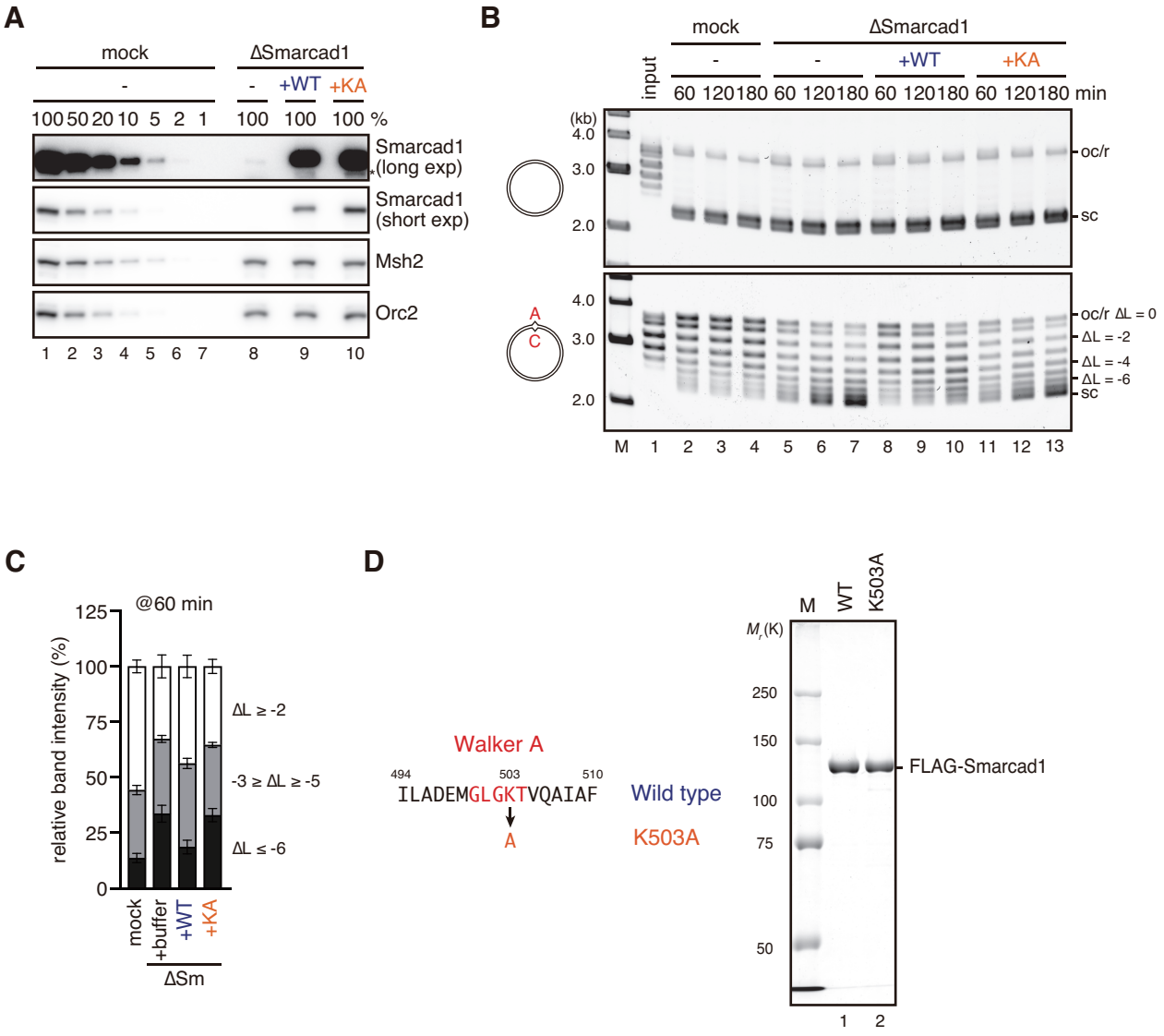

Figure 16. Depletion of Smarcad1 relieved the inhibition of supercoiling on mismatch-carrying DNA.
(A) The immunodepletion eficiency of Smarcad1. The indicated amount of mock-treated (lanes 1–7) or Smarcad1-depleted NPE (lanes 8–10) supplemented with either buffer (lane 8), 650 nM recombinant Smarcad1WT (lane 9), or Smarcad1K503A (lane 10) was separated by SDS-PAGE and probed with the indicated antibodies. 100% corresponds to 0.25-μL NPE. Orc2 served as a loading control. The depletion efficiency was estimated as 98%. Long exp: long exposure, short exp: short exposure. (*) cross-reacting band.
(B) Supercoiling assay in Smarcad1-depleted NPE described in (A). The linking number of each band relative to the oc/r position (ΔL) is indicated.
(C) The statistical analysis of the supercoiling assay in Smarcad1-depleted NPE. The ratio of the plasmids of indicated ΔL is quantified and presented as a graph. Mean ± 1SD (n = 3).
(D) Recombinant Smarcad1 used for the rescue experiments. 1 μg of wild-type (lane 1, WT) or the K503A mutant (lane 2, K503A) of recombinant Smarcad1 purified from baculovirus-infected Sf9 cells were separated by SDS-PAGE and stained with Coomassie brilliant blue R-250. The amino acid sequence of the Walker A motif, and the lysine residue which was substituted by alanine in K503A mutant is presented.

approach, and the FLAG tag that was conjugated to the N-terminus of the recombinant Smarcad1. It is unlikely that Smarcad1 forms a huge complex in NPE because the estimated molecular mass was not significantly different from recombinant Smarcad1.

Addition of the recombinant Smarcad1 to the Smarcad1-depleted NPE decreased pMM1^{AC} having relative linking numbers of less than -6 (Fig. 16B, compare lanes 5–7 to 8–10, and Fig. 16C for quantification), strongly suggesting that the presence of Smarcad1 promotes inhibition of supercoiling of mismatch-carrying DNA. Functional rescue of Smarcad1-depletion with recombinant Smarcad1 indicates that no essential subunit was co-depleted with Smarcad1. Since Smarcad1 is an ATP-dependent chromatin remodeling enzyme, a plausible mechanism of nucleosome exclusion is Smarcad1 excludes nucleosomes using its ATPase activity. Smarcad1 has a highly conserved lysine at the position 503 in a Walker A motif. This lysine residue was substituted with alanine and to construct ATPase mutant of Smarcad1 (referred to as Smarcda1^{K503A}). In contrast to wild-type Smarcad1, the addition of Smarcad1^{K503A} to the Smarcad1-depleted NPE did not alter the pattern of supercoiling of mismatch-carrying DNA (Fig. 16B, compare lanes 5–7 to 11–13, and Fig. 16C for quantification). These results suggest that ATPase activity of Smarcad1 promotes inhibition of supercoiling of mismatch-carrying DNA.

Smarcad1 enhances the sensitivity to MNase digestion of mismatch-carrying DNA

To test whether Smarcad1 decreases nucleosome density of mismatch-carrying DNA, the MNase sensitivity of mismatch-carrying DNA in the Smarcad1 depleted NPE was also examined (Figs. 17A–C). MNase digestion of mismatch-carrying DNA in NPE and quantification of undigested DNA fragments were carried out as Figures 4B–C. The supercoiling state of the plasmids before MNase digestion was analyzed by agarose gel electrophoresis. All of the three biological replicates showed that Smarcad1 depletion relieves the inhibition of supercoiling of pMM1^{AC}, and recombinant Smarcad1 reversed this effect (Figs. 17A and B). In mock-treated NPE, the amount of undigested DNA fragments of pMM1^{AC} was markedly decreased compared to that of pMM1^{homo} at the mismatch site-spanning region (Fig. 17C; P1). In the experiment #3, the amount of undigested DNA of pMM1^{AC} was larger than that in the experiments #1 and #2. This tendency was also observed in the supercoiling assay (Fig. 17B). It is probably because the activity of nucleosome exclusion varies depending on the preparation of NPE. The relative amount of undigested DNA fragments at P1 and P3 of pMM1^{AC} was increased

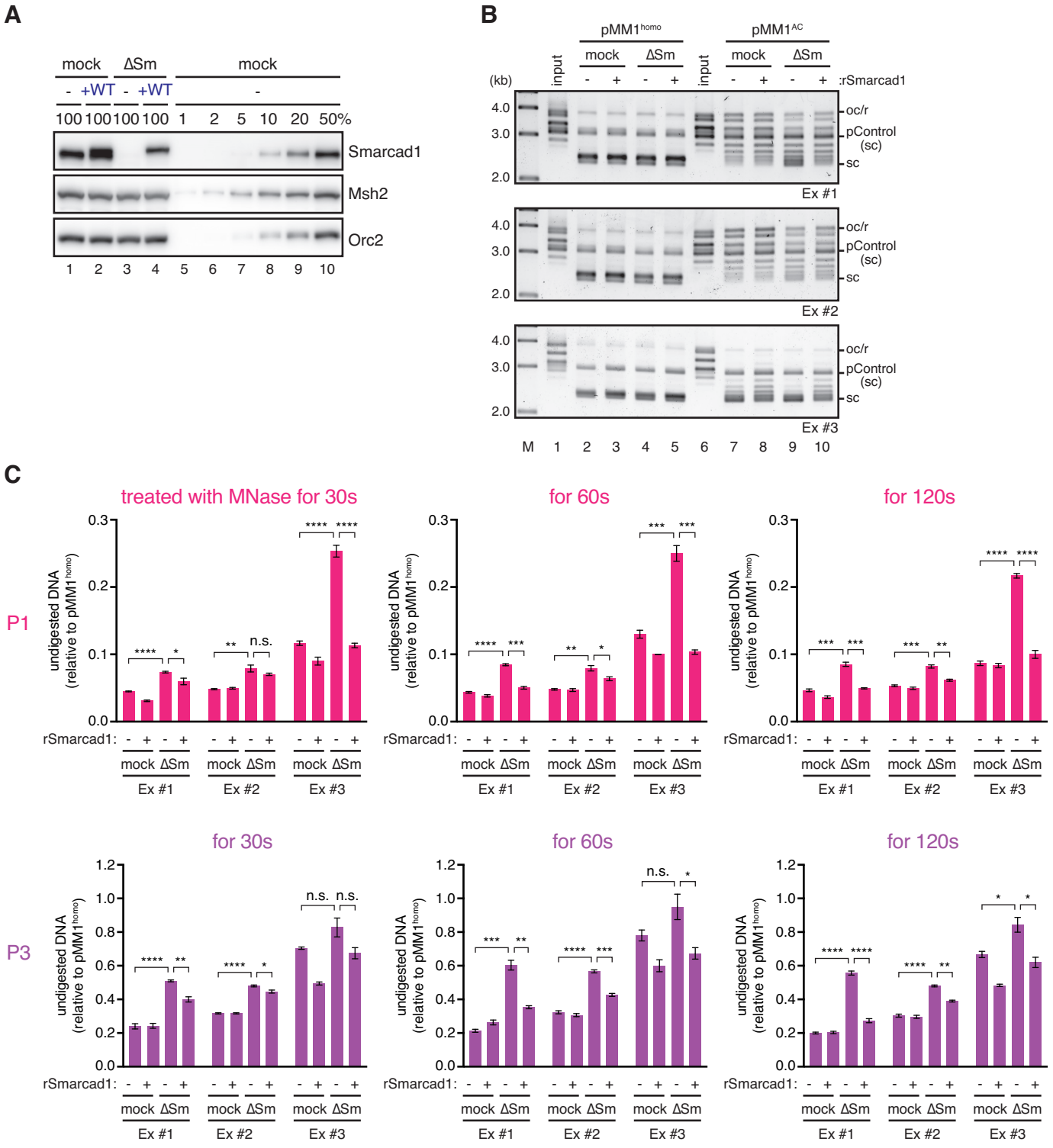

Figure 17. Smarcad1 enhance the sensitivity to MNase digestion of mismatch-carrying DNA
(A) The representative immunodepletion eficiency of Smarcad1 in the MNase digestion assay. The indicated amount of mock-treated (lanes 1–2, and 5–10) or Smarcad1-depleted NPE (lanes 3–4) supplemented with either buffer (lanes 1, 3, 5–10), or 650 nM recombinant Smarcad1WT (lanes 2 and 4) was separated by SDS-PAGE and probed with the indicated antibodies. 100% corresponds to 0.25-µL NPE. Orc2 served as a loading control. The depletion efficiency was estimated as 98%. The Smarcad1-depletion efficiency was confirmed to be >98% also for all MNase digestion assays.
(B) Supercoiling assay in Smarcad1-depleted NPE. The small aliquot of the reaction was sampled immediately before addition of MNase, and the DNA samples were purified and separated by agarose gel electrophoresis. Ex #1, #2, and #3 represent independent experiments.
(C) The MNase assay was performed as described in Fig. 1D using Smarcad1-depleted NPE. The experiment numbers (Ex #1–#3) corresonds to (B). The amount of undigested DNA relative to pMM1^{homo} is plotted as a graph. Mean ± 1SD (n = 3, technical replicates). p-values were calculated by the unpaired t-test (two-tailed). * $p < 0.05$, ** $p < 0.01$, *** $p < 0.001$, **** $p < 0.0001$

by depletion of Smarcad1 and the effect is reversed by addition of recombinant Smarcad1 in experiments #1 to #3, suggesting that the presence of Smarcad1 decreases the density of nucleosomes on pMM1^{AC} (Fig. 17C). The supercoiling assay and the MNase assay strongly suggest that Smarcad1 facilitates nucleosome exclusion.

FACT assists inhibition of supercoiling of mismatch-carrying DNA

The effect of Smarcad1 depletion on nucleosome exclusion was partial compared to Msh2-depletion, suggesting that there are other mechanisms for promoting nucleosome exclusion. FACT is one of the plausible candidates because it was identified as a mismatch-binding factor by the mismatch-carrying DNA pull-down assay (Table 1). I examined the effect of FACT depletion from NPE on supercoiling (Figs. 18A and B). Approximately 95% of FACT (both Spt16 and Ssrp1) was immunodepleted by specific antibodies. FACT-depletion did not detectably decrease the amount of Smarcad1 and Msh2. Although single depletion of FACT had no detectable effect on supercoiling, simultaneous depletion of Smarcad1 and FACT further enhanced supercoiling of pMM1^{AC} than single depletion of Smarcad1, suggesting that FACT also promotes, albeit to a lesser extent, nucleosome exclusion (Fig. 18B).

I next examined whether Smarcad1 and FACT are required for the removal of pre-assembled nucleosomes. A plasmid carrying three mismatches was first chromatinized in a MutS-depleted NPE similarly to Figure 8E. The DNA was then transferred to Smarcad1- and/or FACT-depleted NPE (Figs. 19A and B). Depletion of either Smarcad1 or FACT from the second NPE weakened the relaxation of mismatch-carrying DNA, suggesting that these factors assist with the displacement of nucleosomes (Fig. 19B, compare lanes 10 and 11, or 12). Importantly, simultaneous depletion of Smarcad1 and FACT strongly inhibited the relaxation of mismatch-carrying DNA, suggesting that Smarcad1 and FACT are critical for the disassembly of nucleosomes from mismatch-carrying DNA (Fig. 19B, lane 13).

Smarcad1 facilitates inhibition of supercoiling of mismatch-carrying DNA in the primer-extension system

Whether Smarcad1 promotes nucleosome exclusion in the presence of the CAF-1-mediated chromatin assembly is important to understand the contribution of Smarcad1 to eukaryotic MMR because MMR cooperates with DNA replication. Thus, the relationship

Figure 18

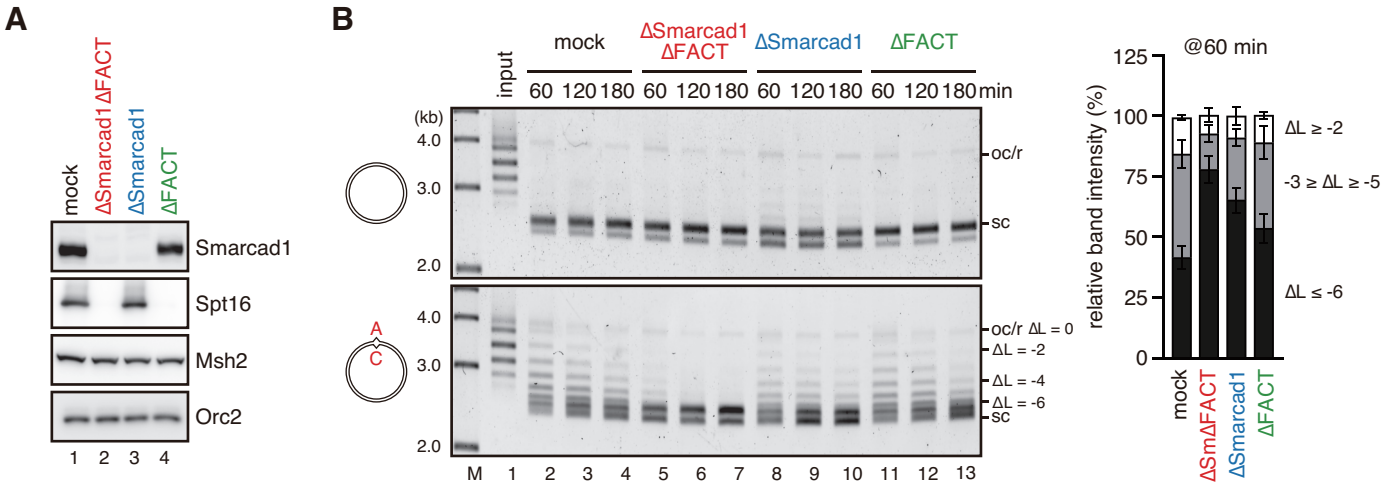

Figure 18. FACT assists inhibition of supercoiling of mismatch-carrying DNA.
(A) The immunodepletion efficiencies of Smarcad1 and FACT. Mock-treated (lane 1), FACT- and Smarcad1- (lane 2), Smarcad1- (lane 3), or FACT-depleted NPE (lane 4) was separated by SDS-PAGE and probed with the indicated antibodies. 0.25 µL each of NPE was loaded. The depletion efficiencies for Smarcad1 and Spt16 were estimated as 98% and 95%, respectively.
(B) Supercoiling assay in NPE described in (A). The ratio of the plasmids of indicated ΔL is quantified and presented as a graph. Mean ± 1SD (n = 3).

Figure 19

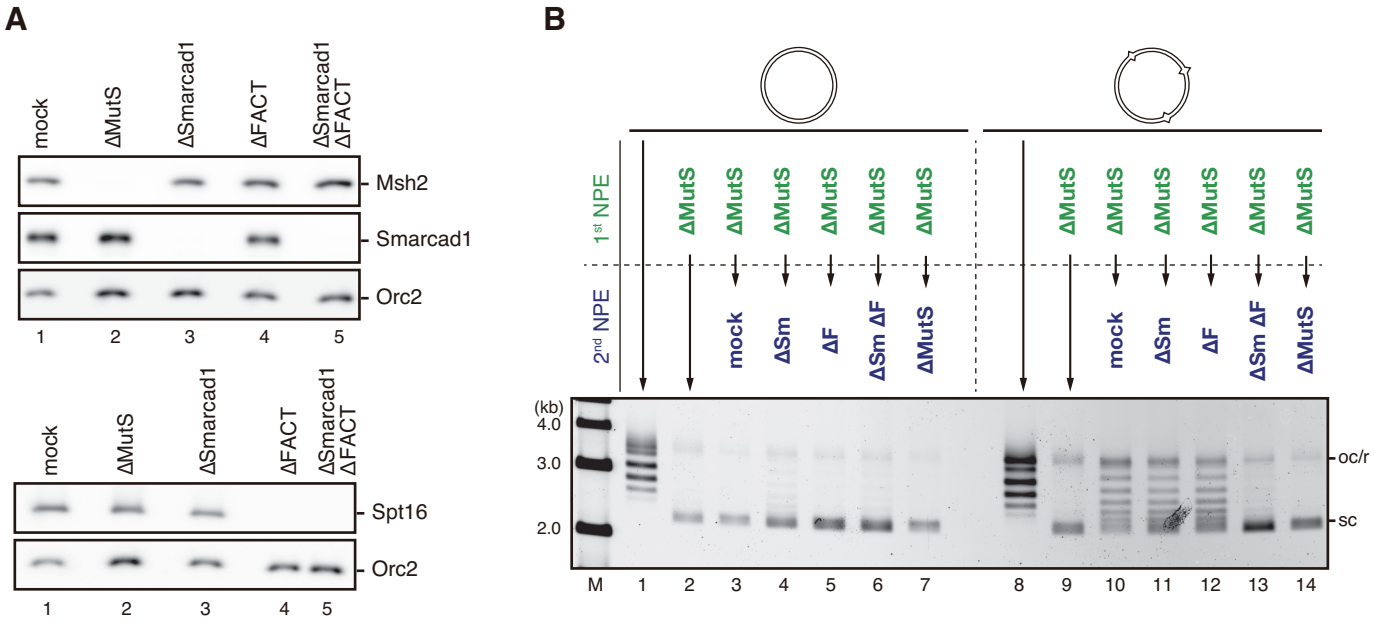

Figure 19. Smarcad1 and FACT promotes disassembly of pre-assembled nucleosomes on the mismatch-carrying DNA.
(A) Immunodepletion efficiencies of Msh2, Smarcad1, and Spt16 (FACT). 0.25 µL of NPE was separated by SDS-PAGE and probed with indicated antibodies. Depletion efficiencies for Msh2, Smarcad1, and Spt16 were estimated as 98%, 98%, and 95%, respectively. Orc2 served as a loading control.
(B) Nucleosome displacement assay. pMM1^{homo} (lanes 1—7) or pMM1^{3MM} (lanes 8—14) was sequentially incubated in the indicated extracts. (mock) indicates mock-treated NPE, (ΔMutS) indicates Msh2-depleted NPE, (ΔSm) indicates Smarcad1-depleted NPE, (ΔF) indicates FACT-depleted NPE. Double depletion of Smarcad1 and FACT significantly impaired disassembly of pre-assembled nucleosomes similarly to Msh2-depletion.

between Smarcad1 depletion and supercoiling of primer-extension products was examined (Figs. 20A and B). To see the supercoiling state of mismatch-retaining primer-extension products, Mlh1 was depleted from NPE in this assay (Fig 20A). The primer-extension reaction produces not only mismatch-carrying DNA but also single-stranded DNA containing intermediates and homoduplex DNA. To detect the specific signal derived from mismatch-carrying DNA, these intermediates and homoduplex DNA were digested by a single-stranded DNA specific endonuclease, an exonuclease (Fig. 20B, middle), and XhoI (Fig. 20B, bottom). Supercoiling products were increased in Mlh1- and Smarcad1-doubly-depleted NPE compared to Mlh1-depleted NPE, and the effect of Smarcad1 depletion was countered by the addition of recombinant Smarcad1 (Figs. 20A and B, bottom, compare lanes 3–4, 5–6, and 7–8. See Fig. 20F for quantification). This result suggests that Smarcad1 facilitates the inhibition of supercoiling of mismatch-carrying DNA in the primer-extension system.

As shown in Figure 9C, supercoiling of primer-extension products depends on CAF-1 in the HIRA-depleted NPE. To examine whether Smarcad1 promotes inhibition of CAF-1-dependent supercoiling of mismatch-carrying DNA, the primer-extension assay in Smarcad1/Mlh1/HIRA-triply-depleted NPE was performed. Although more than 20% of HIRA was retained in NPE, HIRA depletion impaired supercoiling of closed circular double-stranded pMM1^{homo} in NPE (Figs. 20C and D). Even in the HIRA-depleted NPE, Smarcad1-depletion increased the supercoiling of mismatch-carrying DNA in the primer-extension assay, and the addition of recombinant Smarcad1 rescued the inhibition of supercoiling of mismatch-carrying DNA (Figs. 20C–F). These results suggest that Smarcad1 facilitates the inhibition of CAF-1-dependent supercoiling of mismatch-carrying DNA.

Smarcad1- and FACT-depletion did not have any detectable effect on gap-directed MMR in NPE

I next tried to examine whether Smarcad1 and FACT promote MMR on chromatin. Although MMR corrects errors that are generated during the replication of chromosomal DNA, there is no assay that recapitulates the correction of replicational errors in *Xenopus* egg extracts. Thus, I examined the effect of Smarcad1- and FACT-depletion on gap-directed MMR in NPE. Although the gap-directed MMR assay in NPE did not couple with replication, at least, nucleosome assembly coincides with gap-directed MMR. If

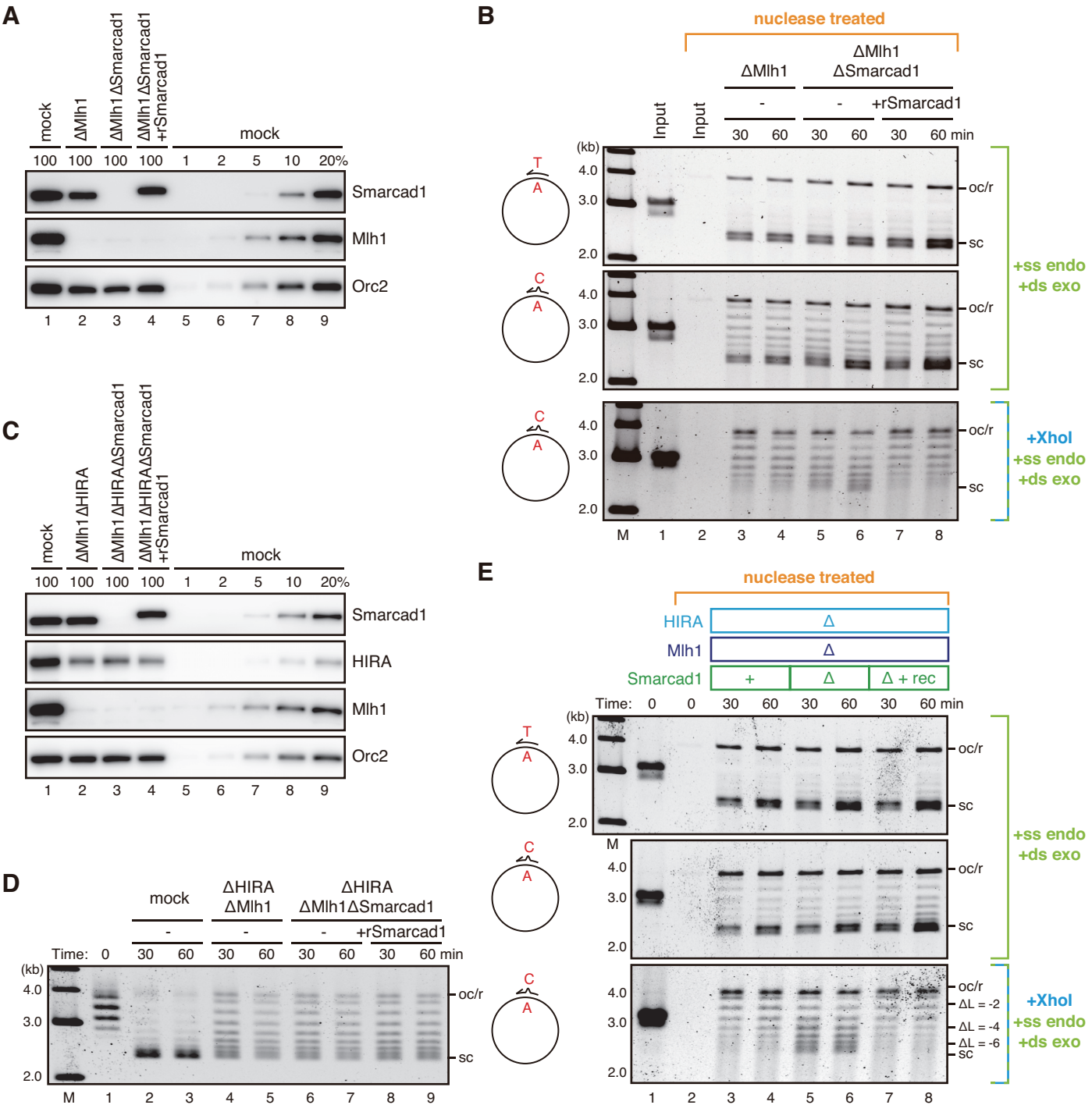

Figure 20. Smarcad1 facilitates inhibition of supercoiling of mismatch-carrying DNA in the primer-extension assay.

(A) Immunodepletion efficiency of Mlh1 and Smarcad1. The indicated amount of mock-treated (lanes 1 and 5–9), Mlh1- (lane 2), or Mlh1/Smarcad1-depleted NPE (lanes 3 and 4) supplemented with buffer (lanes 1–3) or 650 nM recombinant Smarcad1 (lane 4) was separated by SDS-PAGE and probed with the indicated antibodies. 100% corresponds to 0.25-μL NPE.

(B) Primer-extension assay in Mlh1/Smarcad1-depleted NPE. The assay presented in Fig. 9C was repeated in NPE described in (A). The linking number of each band relative to the oc/r position (ΔL) is indicated on the right of the gel.

(C) Immunodepletion efficiency of Mlh1, HIRA, and Smarcad1. The indicated amount of mock-treated (lanes 1 and 5–9), Mlh1/HIRA- (lane 2), or Mlh1/HIRA/Smarcad1-depleted NPE (lanes 3 and 4) supplemented with buffer (lanes 1–3) or 650 nM recombinant Smarcad1 (lane 4) was separated by SDS-PAGE and probed with the indicated antibodies. 100% corresponds to 0.25-μL NPE.

(D) Supercoiling assay in Mlh1/HIRA/Smarcad1-depleted NPE. Closed circular pMM1^{homo} was incubated in NPE described in (C), and sampled at indicated times. Mlh1/HIRA-depletion and Mlh1/HIRA/Smarcad1-depletion significantly attenuated supercoiling of pMM1^{homo}.

(E) The assay presented in (B) was repeated in NPE described in (C). The linking number of each band relative to the oc/r position (ΔL) is indicated on the right of the gel.

(F) The ratio of the plasmids of indicated ΔL in (B) and (E) was quantified and presented as a graph. Mean ± 1SD (n = 3).

nucleosomes are formed between a mispaired base and strand-discrimination signals before the strand-discrimination step, nucleosome exclusion might promote gap-directed MMR.

As shown in Figure 21, for a substrate carrying a 15-nt gap at a position 340-nt away from an A:C mismatch, no reproducible reduction in the MMR efficiencies was detected by depletion of Smarcad1, FACT, or both. Since 340 bp of DNA forms only one nucleosome at most, the gap is possibly too close to the mispaired base to mimic MMR on chromatin. Thus, I next used the substrate in which the mismatch-gap distance was extended to 1.9 kb to increase the probability of nucleosome deposition between a mispaired base and the gap. However, the depletion of Smarcad1, FACT, or both did not reduce the gap-directed MMR efficiencies (Figs. 21A and B). Since it is possible that MMR steps that is sensitive to nucleosomes is finished before assembly of nucleosomes in the gap-directed MMR assay, establishment of a replication-coupled MMR assay in *Xenopus* egg extracts is essential to examine the intrinsic contribution of Smarcad1 and FACT on eukaryotic MMR.

Smarcad1 promotes the repair of mispaired bases on chromatinized DNA

Since Smarcad1 and FACT contribute to disassembly of pre-assembled nucleosomes around mispaired bases (Figs. 19A and B), a possible scenario is Smarcad1 and FACT promote the repair of mispaired bases on chromatinized DNA. Dr. Kawasoe in our lab established an assay for gap-directed MMR on chromatinized DNA and examined whether Smarcad1 promotes gap-directed MMR in the presence of pre-assembled nucleosomes as an in-house collaboration. Since it seems necessary to explain his results for productive discussion of how MMR functions on chromatin with the aid of Smarcad1, with his kind permission, I describe his results below.

To prepare the chromatinized substrate, Dr. Kawasoe performed a stepwise-incubation experiment (Fig. 22A). He incubated gap-carrying pMM1^{AC} in Msh2-depleted NPE to assemble nucleosomes on the mismatch-carrying DNA. Since the gap needs to be present on pMM1^{AC} to induce gap-directed MMR in the 2nd NPE, gap filling in the first NPE was suppressed by inhibiting the PCNA function with a PCNA binding peptide derived from p21 (Mattock et al. 2001). He showed that closed circular pMM1^{AC} was supercoiled in the Msh2-depleted NPE containing p21 peptides (Fig. 22B, lane 4) but supercoiling of the gap-carrying pMM1^{AC} was inhibited by p21 peptides (Fig. 22B,

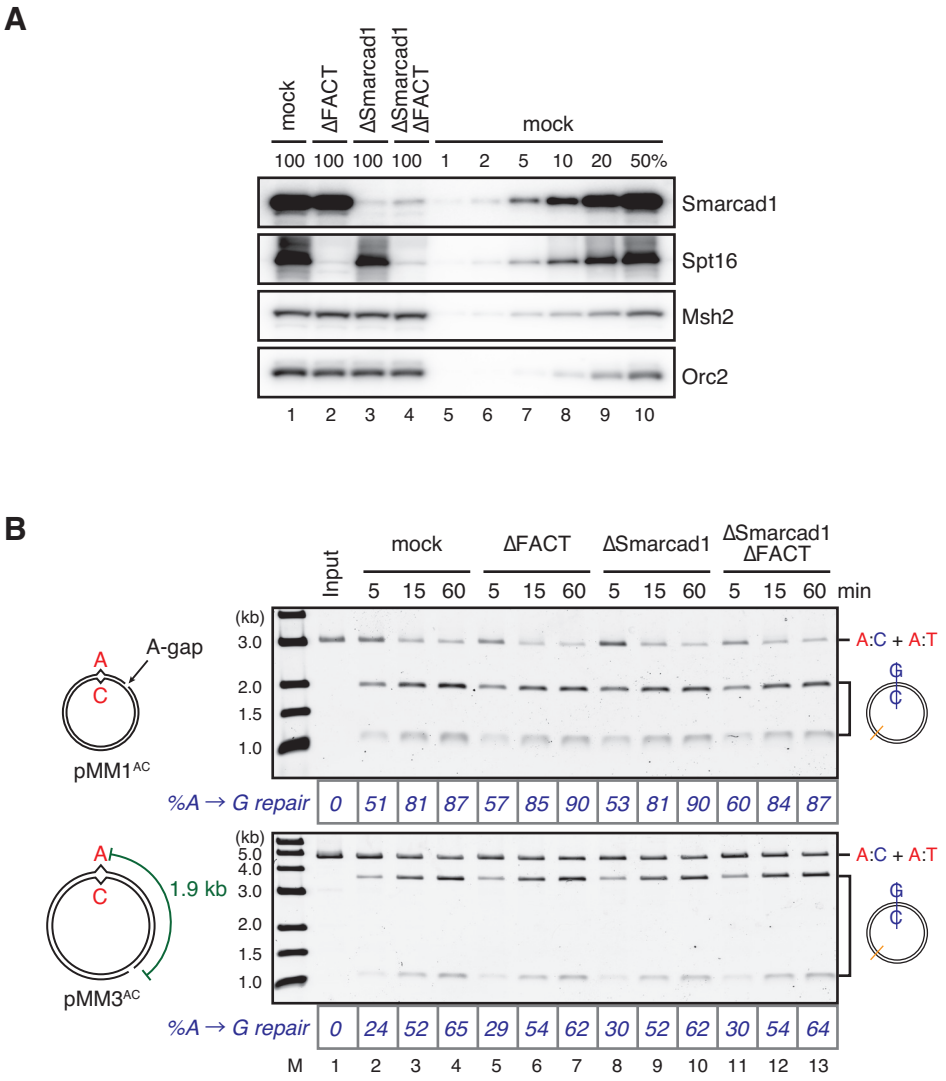

Figure 21. Depletion of Smarcad1 and FACT did not have detectable effect on gap-directed MMR in NPE.
(A) Immunodepletion efficiencies of Smarcad1 and FACT. NPE was depleted using pre-immune (lanes 1, 5–10, mock), Spt16 (lane 2, ΔFACT), Smarcad1 (lane 3, ΔSmarcad1), or a mixture of Smarcda1 and Spt16 antibodies (lane 4, ΔSmarcad1 ΔFACT). The indicated amount of NPE was separated by SDS-PAGE and probed with the indicated antibodies. 100% corresponds to 0.25 μL of NPE. Depletion efficiencies for Spt16 and Smarcda1are estimated as 98%.
(B) Gap-directed MMR in NPE described in A. pMM1^{AC} (Top) or pMM3^{AC} (bottom) carrying a 15-nt gap on the A-strand was incubated in indicated NPE and sampled at the indicated times. %repair was calculated based on the percentage of BamHI sensitive DNA molecules.

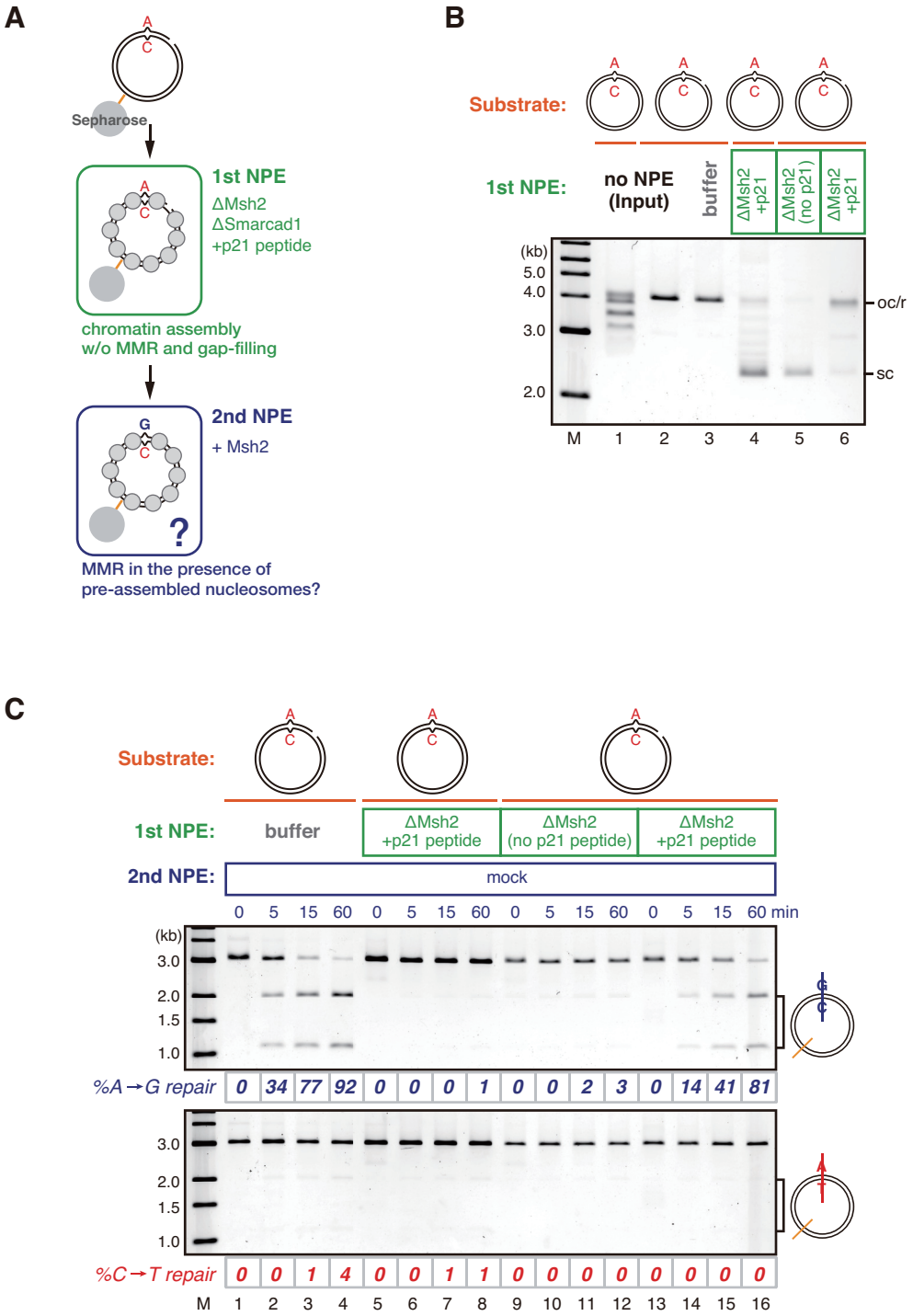

Figure 22. A mispaired base on chromatinized DNA is repaired in NPE (performed by Dr. Kawasoe)
(A) Schematic diagram of the stepwise incubation assay. pMM1^{AC} carrying a 15-nt gap on the A strand was immobilized on Sepharose beads and incubated in an Msh2-depleted NPE (1st NPE) containing 1 mg/mL p21 PCNA-binding peptide (NH2-KRRQTSMTDFYHSKRRLIFS-COOH) for 30 min. The plasmid was then transferred into the second NPE (2nd NPE) containing Msh2 and incubated for the indicated times.
(B) Supercoiling assay in the first NPE. Closed circular pMM1^{AC} (lanes 1 and 4) or pMM1^{AC} carrying 15-nt gap on the A-strand (lanes 2, 3, 5, and 6) was incubated in buffer (lane 3) or Msh2-depleted NPE (lanes 4–6) containing 1 mg/mL p21 PCNA-binding peptide (lanes 4 and 6) for 30 min. Closed circular pMM1^{AC} became mostly supercoiled after incubation in the first NPE (lane 4), suggesting that pMM1^{AC} was chromatinized by this treatment. After incubation in the first NPE containing the p21 peptide, a majority of pMM1^{AC} carrying 15-nt gap remained in the open circular or relaxed form (lane 6), suggesting that the p21 peptide suppressed gap filling.
(C) MMR efficiencies after the incubation in the second NPE. DNA was digested with XmnI and either BamHI (top, A to G repair) or XhoI (bottom, C to T repair). %repair was calculated based on the percentage of XhoI or BamHI sensitive DNA molecules. When gap filling was suppressed by the p21 peptide in the first NPE, the A:C mismatch was efficiently corrected in the second NPE (lanes 14–16).

compare lanes 5 and 6). This result suggests that the NPE has a chromatin assembly activity even if it contains p21 peptides and the gap is retained on the $pMM1^{AC}$ in the presence of p21 peptides. Transferring the chromatinized gap-carrying $pMM1^{AC}$ into the 2nd NPE, he demonstrated that the mispaired base on gap-containing strand was corrected (Fig. 22C, lanes 13–16). He also showed that the mispaired base was not corrected in the 2nd NPE when the gap-carrying DNA was pre-incubated in the Msh2-depleted NPE without p21 peptides (Fig. 22C, lanes 5–12), suggesting that the repair requires the gap. These results suggest that mispaired bases are efficiently corrected in NPE even after nucleosome assembly.

Using this stepwise incubation assay, Dr. Kawasoe examined the contribution of Smarcad1 on MMR on chromatinized DNA (Figs. 23A–D). He found that the repair efficiency of the 2nd NPE was slightly decreased by Smarcad1-depletion, and this effect was rescued by addition of recombinant Smarcad1 (Figs. 23C and D). These results suggest that Smarcad1 promotes gap-directed MMR on the chromatinized DNA.

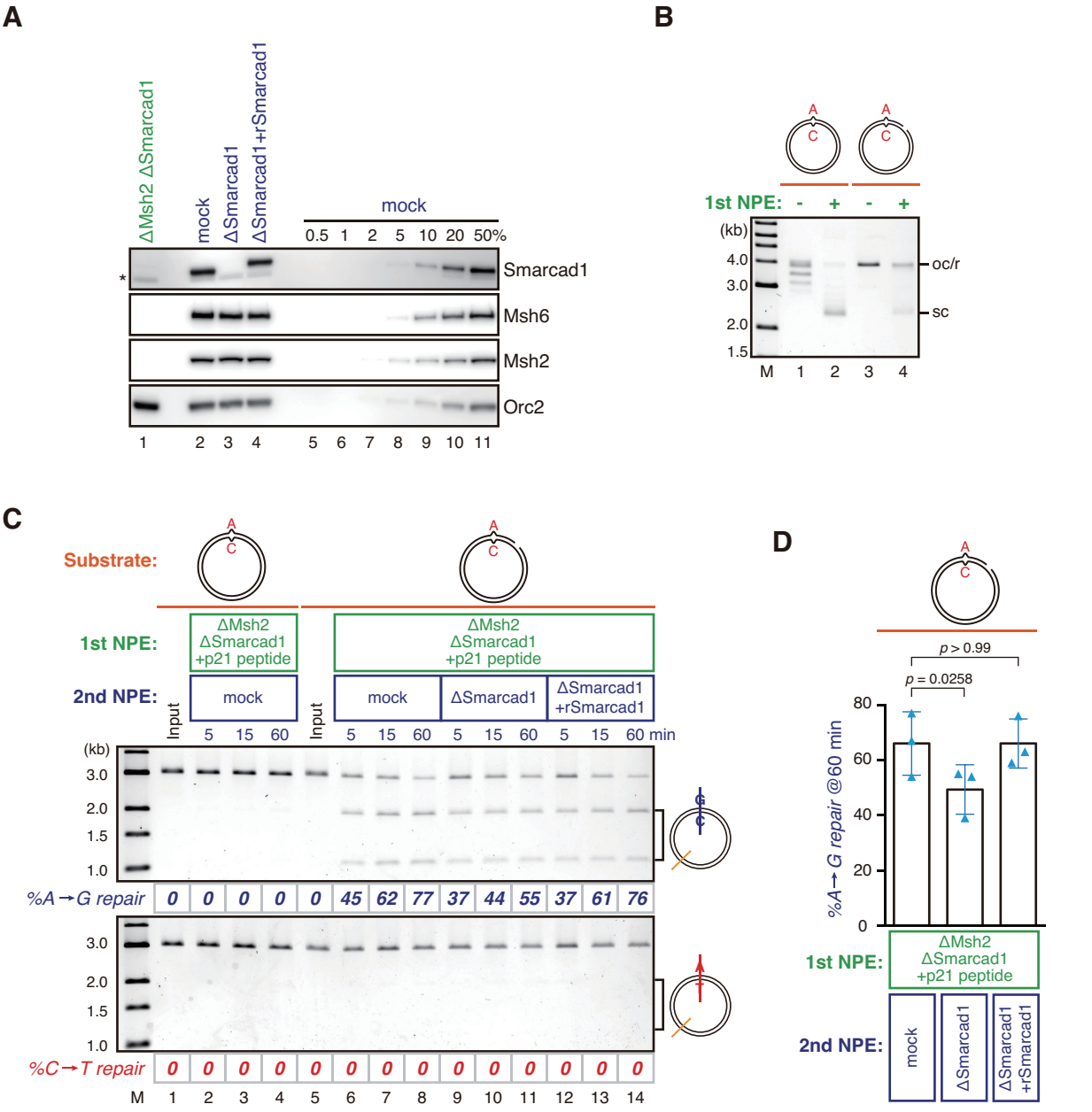

Figure 23. Smarcad1 promotes the gap-directed MMR on the chromatinized DNA (performed by Dr. Kawasoe)
(A) Immunodepletion efficiencies of MutSα and Smarcad1. (*) cross-reacting band.
(B) Supercoiling assay in the first NPE.
(C) MMR efficiencies after the incubation in the second NPE. DNA was digested with XmnI and either BamHI (top, A to G repair) or XhoI (bottom, C to T repair). %repair was calculated based on the percentage of XhoI or BamHI sensitive DNA molecules.
(D) Statistical analysis of the effect of Smarcad1 on mismatch repair in the stepwise incubation assay. The A to G repair efficiencies are plotted in a graph. Mean ± 1SD (n = 3). p-values were calculated by the paired t-test (two-tailed). Blue triangles indicate individual values.

II-3. Discussion

Here, I demonstrated that FACT and Smarcad1 promote nucleosome exclusion. It has been reported that histone chaperone FACT shows the removal of nucleosomes that inhibit progression of the machinery of transcription or replication *in vitro* (Orphanides et al. 1998; Tan et al. 2006), and in fact, FACT promotes both transcription and replication *in vivo* (for review, see Formosa 2012). Additionally, FACT also has an activity to exchange histone H2A-H2B dimers at DSB sites (Heo et al. 2008), suggesting that FACT promotes turnover of histones. Thus, FACT promotes temporal dissociation of histones and this activity probably helps motors to pass through nucleosomes. Since the MMR reaction involves sliding of MutS complexes along DNA, the MMR reaction on chromatin is, in some way, similar to transcription and replication, both of which are carried out by a progression of proteins along DNA. Thus it is possible that MMR also utilize FACT to assist sliding of MutS complexes along DNA.

It has been reported that chromatin remodeler Smarcad1 and its counterpart in yeast Fun30 accumulate at DSB sites and promote long-range resection of DSB ends (Chen et al. 2012; Costelloe et al. 2012; Eapen et al. 2012; Densham et al. 2016). It has also been reported that Fun30 has an ATP-dependent histone exchange activity *in vitro* (Awad et al. 2010). Smarcad1/Fun30 travels along DNA from DSB ends to 30-kb away, and this localization corresponds to that of resection machinery, accumulation of RPA, and decreases of histones around the DSB sites (Chen et al. 2012; Costelloe et al. 2012; Eapen et al. 2012). Based on these observations, it has been proposed that Smarcad1/Fun30 evict nucleosomes around DSB sites to promote progression of the resection machinery along the DSB ends. Considering that the MMR reaction involves resection of DNA from a strand-discrimination signal to a mispaired base by ExoI, the MMR reaction has similarity to the resection of DSB ends. Thus, the idea that Smarcad1 was used to promote MMR on chromatin is reasonable.

How does Smarcad1 promote nucleosome exclusion?

Figures 14B and C showed that chromatin remodeler Smarcad1 is recruited to the mismatch-carrying DNA. Smarcad1 was not detected on homoduplex DNA, indicating that recruitment of Smarcad1 is not mediated by nucleosomes (Figs. 14B–C). Recruitment of Smarcad1 onto DNA depends on a mispaired base and Msh2. Moreover, the number of Smarcad1 on mismatch-carrying DNA is comparable with that of Msh2

(Fig. 14C). Thus, I assume that the DNA-bound MutS complexes interact with Smarcad1 and function as a scaffold for Smarcad1. Consistent with this idea, it has been suggested that Smarcad1 interacts with MutS complexes in human cells (Okazaki et al. 2008; Rowbotham et al. 2011; Chen et al. 2016b), and Kolodner and his colleagues recently found that Fun30, the counterpart of Smarcad1 in yeast, interacts with Msh2 via its Msh2-interacting motif (Goellner et al. 2018). Human and *Xenopus* Smarcad1 also have the Msh2-interacting motif. Although immunoprecipitation experiment in NPE showed that a few fractions of Smarcad1 and MutSα interact with each other, it is possible that conformational change of MutSα after binding to a mispaired base enables it to interact with Smarcad1 similarly to the loading of MutLα.

Depletion of Smarcad1 relieved the inhibition of supercoiling of the mismatch-carrying DNA and the sensitivity of the mispaired base surrounding DNA to MNase (Figs. 16–20). Moreover, the ATPase mutant of Smarcad1 did not rescue the nucleosome exclusion activity of Smarcad1-depleted NPE, suggesting that the ATPase activity of Smarcad1 is required to promote nucleosome exclusion (Figs. 16B–C). The ATPase activities of Smarcad1 and Fun30 are required for its chromatin remodeling activity and other chromatin-related functions *in vivo* (Neves-Costa et al. 2009; Awad et al. 2010; Rowbotham et al. 2011; Chen et al. 2012; Costelloe et al. 2012; Durand-Dubief et al. 2012; Eapen et al. 2012). These data are consistent with the idea that Smarcad1 evicts nucleosomes to promote nucleosome exclusion. I assume that Smarcad1 binds to MutS complexes and slides along DNA, and the Smarcad1-MutS complex proceeds along DNA by evicting nucleosomes that inhibit the sliding of MutS complexes. Reconstitution of nucleosome exclusion by using a mismatch-carrying nucleosome array, MutS complexes, and Smarcad1 is attractive. If the reconstitution system works well, single molecule analysis of Smarcad1 and MutS complexes on a nucleosome array may reveal the detailed molecular mechanism of nucleosome exclusion.

How is FACT involved with nucleosome exclusion?

Since FACT is the histone chaperone, it has high affinity to histones. Consistent with this capacity, FACT was detected on DNA even in the absence of a mismatch (Figs. 14B and C). If the accumulation of FACT on the DNA is mediated by only binding to nucleosomes, the accumulation of FACT on mismatch-carrying DNA should decrease due to nucleosome exclusion. However, the accumulation of FACT on the mismatch-carrying

DNA was not decreased as compared to homoduplex DNA (Fig. 14C), implying that there is a specific mechanism which recruits FACT onto the mismatch-carrying DNA. Although I did not detect a clear interaction between the MutS complexes and FACT by co-immunoprecipitation, the possibility that MutSα and MutSβ directly recruit FACT onto mismatch-carrying DNA is not excluded. It is possible that DNA-bound MutS complexes bind to FACT.

A recent study suggests that the partial unwrapping of nucleosomes exposes the N-terminal domain of histone H2B and FACT invades this destabilized nucleosome to disassemble H2A-H2B dimers (Tsunaka et al. 2016). On the mismatch-carrying DNA, MutSα, Smarcad1, (and likely MutSβ) destabilizes nucleosomes. Thus, it is possible that FACT interacts with these destabilized nucleosomes, and promotes eviction of nucleosomes. However, I have not excluded the possibility that the effect of FACT-depletion is derived from co-depletion of other factors yet because I didn't examine whether the addition of recombinant FACT to FACT-depleted NPE rescue the defect of nucleosome exclusion. This point must be examined to clarify whether FACT is involved in nucleosome exclusion.

Smarcad1 and FACT independent nucleosome exclusion

Even if Smarcad1 and FACT were depleted from NPE, the nucleosome exclusion activity was retained in the NPE, suggesting that nucleosome exclusion has a Smarcad1- and FACT-independent pathway. As discussed in *part I*, the MutS complexes itself possibly perform nucleosome exclusion. In the previous part, I found that the addition of recombinant MutSα to the Msh2-depleted NPE failed to rescue nucleosome exclusion. One of the plausible cause of this result is co-depletion of factors that are required for nucleosome exclusion by Msh2-depletion. I expected that identification of factors that bind to the mismatch-carrying DNA could find out this factor. However, Smarcad1 and FACT are unlikely to be this factor because they were not depleted by Msh2-depletion. It is possible that MutS complexes-interacting factors have important role in nucleosome exclusion.

Does Smarcad1 promote the MMR reaction?

Although depletion of Smarcad1 from NPE didn't have any detectable effect on gap-directed MMR on naked DNA (Figs. 21A and B), Smarcad1-depletion decreased the

efficiency of MMR on chromatinized DNA (Figs. 23A, C, and D). The chromatinized substrate may mimic the situation where a mispaired base is surrounded by nucleosomes before it is recognized by the MutS complexes. MMR of leading strand possibly faces this situation. Ribonucleotides embedded in a leading strand facilitate MMR depending on RNase H2 *in vivo* (Ghodgaonkar et al. 2013; Lujan et al. 2013). Ribonucleotides embedded in DNA are efficiently repaired by ribonucleotide excision repair (RER). RER is initiated when RNase H2 incises a ribonucleotide embedded DNA (Rydberg and Game 2002; Nick McElhinny et al. 2010; Sparks et al. 2012). Thus, intermediates of RER supply strand discontinuities *in vivo*, and they would be used by the MMR system to discriminate the newly-synthesized strand. Since these strand discontinuities are generated after access of RNase H2, these strand discontinuities are probably surrounded by nucleosomes. Smarcad1 possibly disassembles these nucleosomes to facilitate MMR.

Part III: Fun30, the yeast counterpart of Smarcad1, facilitates the suppression of mutations

III-1. Introduction

I demonstrated that Smarcad1 facilitates nucleosome exclusion in the previous part. The important question is whether Smarcad1 promotes the MMR reaction. Smarcad1-depletion did not affect gap-directed MMR in NPE when naked DNA was used as a substrate. On the other hand, when the chromatinized DNA was used as a substrate, Smarcad1 depletion decreased gap-directed MMR in NPE. The latter assay picks out the situation where nucleosomes are assembled before recognition of replication errors by the MutS complexes. Does the MMR system encounter such a situation while it corrects errors that are misincorporated by DNA polymerases during chromatin replication? In other words, does Smarcad1 indeed facilitate the MMR reaction *in vivo*?

To address this question, I switched the experimental system to budding yeast *Saccharomyces cerevisiae*. Budding yeast is a highly sophisticated model system to investigate MMR *in vivo*. There are a number of reporter genes that detect spontaneous mutations in budding yeast. Specifically, reporter genes that contain the hotspot sequence for MMR are mutated with 1,000 to 10,000-fold higher frequencies in MMR-deficient strains than MMR-proficient strains (Marsischky et al. 1996; Tran et al. 1997). Thus, budding yeast can monitor MMR activity within a 10^3 to 10^4 order. Moreover, in budding yeast, genetic interactions are easily examined because gene disruption techniques have been established. Genetics is useful for MMR analysis. For example, the involvement of Exo1 in MMR *in vivo* was unclear at first, because single-deletion of *EXO1* increase the mutation rates much less than *msh2* or *mlh1* (Tishkoff et al. 1997). However, the analysis of the genetic interactions between Exo1 and other MMR related factors revealed deep relations between MMR and Exo1 and strongly suggested that Exo1 functions in MMR *in vivo* (Amin et al. 2001).

The yeast counterpart of Smarcad1 is Fun30. Fun30 involves in promotion of long-range resection of DNA double-strand breaks (DSBs) on chromatin, gene silencing, and maintenance of centromere chromatin (Neves-Costa et al. 2009; Yu et al. 2011; Chen et al. 2012; Costelloe et al. 2012; Eapen et al. 2012; Byeon et al. 2013; Chen et al. 2016a; Bantele et al. 2017). Fun30 shows ATP-dependent chromatin remodeling activity *in vitro* (Awad et al. 2010; Byeon et al. 2013). However, its function in MMR has not been addressed.

In this part, I measured spontaneous mutation rates using three reporter genes in yeast. Although single deletion of *FUN30* did not have significant effects on mutation rates, deletion of *FUN30* markedly increased mutations in *msh3Δ* or *msh6Δ* strains, both of which partially impairs the activity of the MutS complexes. Moreover, this contribution of Fun30 on a suppression of mutations was suppressed by inactivation of CAF-1. These results suggest that Fun30 facilitates the MMR reaction by counteracting CAF-1.

III-2. Results

Yeast strain for measurement of spontaneous mutation rates

I chose the BY4741 strain because it is useful for genetics due to deletion of genes that are commonly used as the selectable marker to construct auxotrophic mutants. Moreover, BY4741 has the *CAN1* gene, which is commonly used as a reporter gene to detect forward mutations. *CAN1* encodes plasma membrane arginine permease, which takes up basic amino acids into cells. Since plasma membrane arginine permease also takes up canavanine, which is a non-proteinogenic arginine analog, yeast strains that have functional products of the *CAN1* gene are sensitive to canavanine. Thus, forward mutations that inactivate the products of the *CAN1* gene are detected by counting yeast strains that become resistant to canavanine. Since depletion of Smarcad1 and FACT did not completely impair nucleosome exclusion in NPE, the contributions of these factors on MMR are possibly partial. To detect the effect of these factors on MMR even if contributions are mild, two reporter genes, *hom3-10* and *lys2::insE-A14*, both of which are highly sensitive to the MMR defect, were introduced into the parent strain.

The *hom3-10* gene has the insertion of a single thymine in a run of 6 thymines in the *HOM3* gene (Marsischky et al. 1996), which encodes aspartate kinase that is essential for threonine biosynthesis. Since this +1 frameshift mutation impairs *HOM3*, the budding yeast strain which has *hom3-10* instead of *HOM3* don't survive in threonine deficient media. -1 frameshift in the region surrounding the A/T-runs of *hom3-10* reverts this gene to *HOM3*. The *lys2::insE-A14* gene has the insert sequence which contains a run of 14 adenines (Tran et al. 1997). This insert results in the +1 frameshift mutation. -1 frameshift mutation in the run of 14 adenines results in in-frame *lys2* allele. Thus, mutation rates at these two loci are easily estimated by counting the revertants.

Single deletion of FUN30 *increases the reversion rate at lys2*

msh2Δ increased the mutation rate by 3,300-fold at *hom3*, by 10,000-fold at *lys2*, and by 67-fold at *CAN1*, indicating that *hom3-10* or *lys2::insE-A14* detect mutation rates within a 10^3 to 10^4 order and *CAN1* detects mutation rates within a 10^1 order (Table 2). In budding yeast, since MutSα and MutSβ redundantly function to suppress -1 frameshift mutations, either *msh6Δ* (ΔMutSα) or *msh3Δ* (ΔMutSβ) causes only a partial increase of the frameshift mutations (Table 2 and Marsischky et al. 1996). Similarly, the increase of the mutation rates in *exo1Δ* is mild probably due to the existence of Exo1-independent

MMR (Table 2 and Amin et al. 2001).

The budding yeast genome encodes one Smarcad1 homolog, Fun30 (see Fig. 13A). Single deletion of *FUN30* increased the reversion rate by 2.1-fold at *hom3* and by 1.9-fold at *lys2*, and increased the mutation rate by 1.2-fold at *CAN1* compared to WT (Table 2). In the *lys2::insE-A14* reversion assay, the difference of the reversion rates was significant in Mann-Whitney tests ($P < 0.0001$) and the 95% confidence intervals were not overlapped (Table 2). This result suggests that *fun30Δ* increase the reversion rate at *lys2*. In contrast, in the *hom3-10* reversion assay and the *CAN1* mutation assay, although the differences of the mutation rates were significant in Mann-Whitney tests ($P = 0.0024$ in the *hom3-10* reversion assay or $P = 0.0217$ in the *CAN1* mutation assay), the 95% confidence intervals were overlapped. Thus, the effect is too weak to conclude *fun30Δ* is a mutator. Considering that Smarcad1-depletion mildly decreased the nucleosome exclusion activity of NPE compared to Msh2-depletion (Figs. 16A and B), it is possible that the effect of single deletion of *FUN30* on the mutation rate is mild due to the existence of Fun30-independent nucleosome exclusion.

<u>fun30Δ *synergistically increases reversion rates in* msh3Δ *or* msh6Δ *strains*</u>

Not only *fun30Δ*, but also *msh6Δ*, *msh3Δ*, and *exo1Δ* mildly increase the mutation rates compared to *msh2Δ*. The synergic interactions between MSH6 and MSH3, or EXO1 and other MMR related factors have strongly suggested that MSH6, MSH3, and EXO1 function in MMR *in vivo* (Marsischky et al. 1996; Amin et al. 2001). To test the possibility that Fun30 suppresses spontaneous mutations cooperating with the MMR system, genetic interactions between Fun30 and MMR factors were examined. Interestingly, in the *msh6Δ* background, *fun30Δ* synergistically increased the reversion rate by 12-fold at *hom3* and ~6-fold at *lys2*. In contrast, a synergistic increase of the mutation rate at *CAN1* was not observed by deletion of *FUN30* in the *msh6Δ* strain. Since even in *msh2Δ*, the mutation rate at *CAN1* were increased by only 67 fold (Table 2), indicating that *CAN1* is much less sensitive to the MMR defect than *hom3-10* and *lys2::insE-A14*. This is probably the reason why the mutation rates at *CAN1* was not synergistically increased by *fun30Δ* in the *msh6Δ* strain. As well as in the *msh6Δ* background, *fun30Δ* increased the reversion rates by ~2-fold in *msh3Δ* cells at both loci, and this increase was much higher than the sum of the reversion rates of each single mutants. These results suggest that Fun30 is closely related to the MutS-dependent

reactions. Consistent with this idea, in *msh2Δ* strain, which loses both MutSα and MutSβ, the synergistic increase of the reversion rates by *fun30Δ* did not appear, suggesting that the synergistic increase of the reversion rates depends on the MutS complexes.

fun30Δ did not increase the reversion rates with *exo1Δ*, which also partially impairs MMR (Tishkoff et al. 1997; Amin et al. 2001). Since the effect of *fun30Δ* is much weaker than that of *exo1Δ*, this result does not clarify whether *FUN30* is epistatic to *EXO1*. Importantly, *fun30Δ* still synergistically increased the reversion rates in the *exo1Δ msh6Δ* background (compare *exo1Δ msh6Δ and exo1Δ msh6Δ fun30Δ*), indicating that the synergistic interaction between *FUN30* and *MSH6* is kept in the *exo1Δ* background. These factor-specific genetic interactions suggest that the function of Fun30 in MMR is closely related to MutSα- and MutSβ-dependent steps.

The effect of fun30Δ *on spontaneous mutations is different from that of impairment of the homology-directed-repair activity*

Since Fun30 is involved in the repair of DSBs in the homology-directed-repair (HDR) pathway (Chen et al. 2012; Costelloe et al. 2012; Eapen et al. 2012; Densham et al. 2016), it is possible that the impairment of the HDR activity by *fun30Δ* increase the mutation rates. To exclude this possibility, the effect of *rad52Δ*, which impairs homologous recombination activity, on the mutation rates was tested (Table 3). *rad52Δ* partially increased mutation rates at *hom3*, *lys2*, and *CAN1*, suggesting that impairment of homologous recombination also increases mutation rates. However, the effects of *rad52Δ* are different from that of *fun30Δ*. First, although *fun30Δ* did not increase the mutations at *CAN1*, *rad52Δ* significantly increased the mutations at *CAN1*. Since the canavanine assay monitors the inactivation of the *CAN1* gene, aberrant recombination also increases the mutation rates at *CAN1*. Thus, the effect of *rad52Δ* on mutations at *CAN1* is probably due to the impairment of the homologous recombination. Secondly, *rad52Δ* did not synergistically increase the mutation rates in *msh6Δ* (compare *msh6Δ* and *msh6Δ rad52Δ*), suggesting that the impairment of homologous recombination and MMR did not synergistically increase the mutation rates. Finally, sequencing of *hom3* or *lys2* loci in the revertant strains showed that the frameshift mutations seen in *fun30Δ* cells were concentrated in the homopolymer 'hotspot' runs, as seen in MMR mutants (Figs. 24A and B). By contrast, mutations in *rad52Δ* cells were dispersed compared to mutations in MMR-deficient cells. These results collectively suggest that the effects of *fun30Δ* on

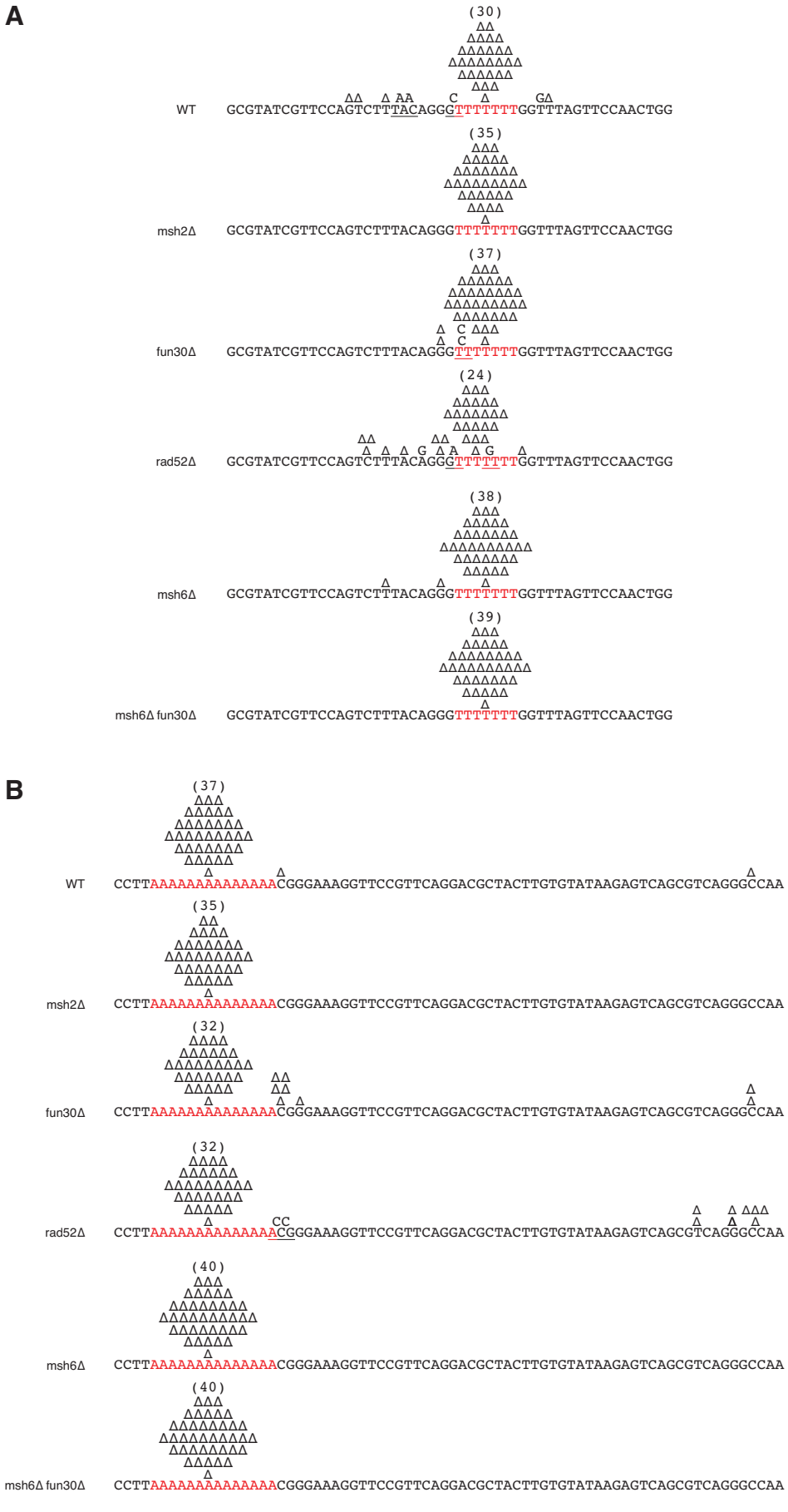

Figure 24. Spectra of reversion mutations of *hom3-10* and *lys2::insE-A14*.
(A) Spectrum of reversion mutations of *hom3-10*. Reversion mutants were sampled and sequenced, and each mutation was plotted on the sequence of the *hom3-10* gene fragment. The run of seven thymines is indicated in red. Underlines indicate simultaneous mutations of multiple bases. Δ indicates a deletion.
(B) Spectrum of reversion mutations of *lys2::insE-A14*.

spontaneous mutation rates are not derived from the impairment of homologous recombination. In fact, the synergistic effects of *fun30Δ* in *msh6Δ* still observed in the *rad52Δ* background (compare *rad52Δ msh6Δ* and *rad52Δ msh6Δ fun30Δ*), suggesting that Fun30 and MutS complexes cooperatively suppress the mutations in a Rad52-independent manner.

An ATPase mutant of Fun30 shows similar phenotype with fun30Δ

A plausible mechanism of suppression of mutations by Fun30 is that Fun30 promotes nucleosome exclusion by using its ATPase activity to facilitate the MMR reaction. Indeed, *fun30-K603A*, which is the Walker A mutant of Fun30, synergistically increased the reversion rates of *hom3-10* and *lys2::insE-A14* in the *msh6Δ* strain (Table 2), suggesting that the ATP-binding motif of Fun30 is important to suppress mutations.

Fun30 counteracts CAF-1 to suppress spontaneous mutations

Smarcad1 facilitates inhibition of CAF-1-dependent supercoiling of mismatch-carrying DNA in NPE (Figs. 20C–F). If Fun30 also inhibits CAF1-mediated chromatin assembly to facilitate MMR in yeast, impairment of the CAF1-mediated chromatin assembly should mitigate the mutator phenotype of *fun30Δ*. To test this possibility, the effects of the deletion of *CAC1*, the largest subunit of CAF-1 in yeast, on the mutation rates were examined. Single deletion of *CAC1* did not have a significant effect on the mutation rates of all loci that are examined here (Table 4). Deletion of *CAC1* in *fun30Δ* strain slightly decreased the reversion rate at *hom3*, but increased the reversion rate at *lys2* and the mutation rate at *CAN1*. Since deletion of *CAC1* could affect various reactions, including replication, transcription, and recombination, it possibly increases mutation rates like *rad52Δ*. These effects may complicate the effect of *cac1Δ* on MMR.

Since *fun30Δ* synergistically increased the mutation rates in the *msh3Δ* strain and *msh6Δ* strain, it is possible that MMR in the *msh3Δ* strains and *msh6Δ* strains are more sensitive to chromatin assembly. In fact, *cac1Δ* slightly reduced the reversion rates at *hom3* and *lys2* in both the *msh3Δ* and *msh6Δ* (compare *msh6Δ* and *msh6Δ cac1Δ*, and *msh3Δ* and *msh3Δ cac1Δ*), suggesting that CAF-1 is inhibitory for both MutSα- and MutSβ-dependent MMR. Importantly, in *msh6Δ fun30Δ* cells, *cac1Δ* decreased the reversion rates by more than 5-fold at *hom3* and 3-fold at *lys2*. This reduction suggests that the majority of the mutations that were generated by *fun30Δ* in *msh6Δ fun30Δ* cells

were suppressed by *cac1Δ*. *cac1Δ* also reduced mutation rates in *msh3Δ fun30Δ* cells. Importantly, *cac1Δ* did not significantly change the reversion rates in *msh2Δ* cells, indicating that the effect of *cac1Δ* is epistatic to *msh2Δ*. These results suggest that CAF-1 impedes Msh2-dependent MMR, and Fun30 counteracts the function of CAF-1 to suppress spontaneous mutations.

A temperature-sensitive mutant of FACT is not a mutator

Since FACT is essential, the effect of *factΔ* on spontaneous mutation rates is not available. Thus, I examined the effect of a temperature-sensitive mutant of FACT, *spt16-d922* (Evans et al. 1998), on spontaneous mutation rates. Even at 30˚C, which is semi-permissive temperature, *spt16-d922* did not show a significant mutator phenotype (Table 5). Even when *spt16-d922* was combined with *msh6Δ* or *fun30Δ*, it did not significantly increase the mutation rates. Thus, there is no evidence that supports the hypothesis that FACT facilitates the MMR reaction *in vivo*.

III-3. Discussion

Fun30 cooperates with the MutS complexes to suppress mutations

Partial impairment of either MutSα or MutSβ by deletion of *MSH6* or *MSH3* enhances the contribution of *FUN30* on the suppression of mutations. I assume that the synergistic increase of mutation rates by deletion of *FUN30* in *msh3Δ* or *msh6Δ* is explained by the relation between nucleosome exclusion activity and the amounts of the DNA-bound MutS complexes. When both Msh3 and Msh6 are expressed, the supply of MutSα and MutSβ is so enough to counteract the negative effect of nucleosomes without the assistance of Fun30. Thus, the increase of mutation rates by deletion of *FUN30* is mild. In contrast, when either Msh3 or Msh6 is absent, the decrease in the total amount of MutS complexes probably decreases the nucleosome exclusion activity. Thus, the contribution of Fun30 on nucleosome exclusion is relatively increased.

Curiously, deletion of *FUN30* in the *msh6Δ* strains increased the mutation rates larger extent than the *msh3Δ* strains, suggesting that Fun30 facilitates MutSβ-mediated MMR to a larger extent than MutSα-mediated MMR. It has been reported that human MutSα has chromatin remodeling activity, and interferes with CAF-1-mediated chromatin assembly (Javaid et al. 2009; Kadyrova et al. 2011; Schopf et al. 2012; Rodriges Blanko et al. 2016). Although it is unclear whether MutSβ has these activities, the difference of these activities between MutSα and MutSβ could account for the difference of dependency on Fun30 between MutSα- and MutSβ-mediated MMR in yeast. However, I measured the mutation rates by using only two genetic markers. Thus, it is possible that contribution of Fun30 on MutSα- or MutSβ-mediated MMR varies by genetic locus.

Functions of Smarcad1 and Fun30, such as enhancement of the long-range resection of DNA double-strand breaks, and heterochromatin structure maintenance, are conserved from yeast to human (Rowbotham et al. 2011; Stralfors et al. 2011; Yu et al. 2011; Chen et al. 2012; Costelloe et al. 2012; Eapen et al. 2012; Steglich et al. 2015). Regarding nucleosome exclusion, relationships between Smarcad1, MutS complexes, and CAF-1 in *Xenopus* egg extracts are parallel to those in yeast. First, Smarcad1 is recruited onto the mismatch-carrying DNA in an Msh2-dependent manner in NPE. The effect of *fun30Δ* on the mutation rates depends on *MSH2* in yeast. Secondly, Smacad1 inhibits the CAF-1-dependent supercoiling of mismatch-carrying DNA in NPE. The increase of the mutation rates by *fun30Δ* in *msh6Δ fun30Δ* and *msh3Δ fun30Δ* is significantly suppressed

by *cac1Δ*, suggesting that Fun30 also counteracts CAF-1 to facilitate MMR in yeast. Finally, the ATPase motif of Smarcad1 is important to promotes nucleosome exclusion in NPE, and the ATPase motif of Fun30 is also important to suppress mutations in yeast. Based on these findings, I assume that Smarcad1 and Fun30 function in nucleosome exclusion in the same manner.

CAF-1 counteracts the MMR reaction in vivo

Here, I demonstrated that deletion of *CAC1* suppresses mutation rates in yeast. Since CAF-1 deposits histones immediately after the replication forks, the result supports the idea that concomitant occurrence of nucleosome assembly counteracts the MMR reaction *in vivo*. Although deletion of *CAC1* in wild-type background does not have any detectable effect on mutation rates, *cac1Δ* decreased the mutation rates in the *msh3Δ* or *msh6Δ* strains. A plausible interpretation of this result is that when both Msh3 and Msh6 are expressed, supplies of MutSα and MutSβ are so enough to counteract the negative effect of CAF-1. In contrast, when either Msh3 or Msh6 is absent, the decrease of DNA-bound MutS complexes probably decreases the nucleosome exclusion activity, so that the MMR reaction is counteracted by CAF-1.

Does FACT contribute to MMR?

Since FACT is essential for budding yeast, I have not examined whether FACT contributes to suppression of spontaneous mutations in yeast. Although the temperature-sensitive mutant, *spt16-d922* did not show mutator phenotype, whether this temperature-sensitive mutant impairs function of FACT on nucleosome exclusion is unclear. FACT functions in replication, transcription, and DNA damage responses, all of them indirectly affect the spontaneous mutation rates. Thus, it is difficult to demonstrate that FACT contributes to MMR *in vivo*. Further characterization of FACT function in nucleosome exclusion *in vitro* is required to understand the involvement of FACT in MMR.

Conclusions

In this thesis, I demonstrated that nucleosomes are excluded around mispaired bases in a MutS-dependent manner. I found that chromatin remodeler Smarcad1 and histone chaperone FACT promote nucleosome exclusion. Smarcad1 was recruited onto mismatch-carrying DNA in a MutS-dependent manner. Moreover, yeast genetics suggested that Fun30 cooperates with the MutS complexes to suppress mutations, and Fun30 counteracts CAF-1 to suppress mutations.

Based on these data, I propose a model for how MMR occurs at the site of chromatin replication. Yeast genetics suggested that CAF-1 counteracts MMR (Table 4). Since CAF-1 binds to PCNA (Shibahara and Stillman 1999), it is likely that CAF-1 mediates chromatin assembly just after DNA synthesis. MutS complexes that bind to a mispaired base recruit Smarcad1/Fun30 as well as MutLα onto chromatin to exclude these nucleosomes. Since the ATPase activity of Smarcad1/Fun30 is required to facilitate nucleosome exclusion and suppression of mutations, Smarcad1/Fun30 probably evicts nucleosomes by using its chromatin remodeling activity when it collides with nucleosomes. To demonstrate that this model is true, additional biochemical studies are apparently needed. Whether Smarcad1 binds to DNA-bound MutSα or MutSβ, and they translocate along DNA with each other in the purified system should be examined. To confirm whether Fun30, MutSα, and MutSβ operate nucleosome exclusion, reconstitution of nucleosome exclusion by using purified yeast proteins is also needed.

There would be many pathways to promote MMR on chromatin. The model indicated above is one of these pathways. Chromatin remodeling by MutSα (Javaid et al. 2009), counteraction of CAF-1-mediated chromatin assembly by MutSα (Kadyrova et al. 2011; Schopf et al. 2012; Rodriges Blanko et al. 2016), and histone chaperon FACT probably functions in nucleosome exclusion. The existence of these pathways may render eukaryotic MMR resistant to nucleosomes. Further investigation of these nucleosome exclusion pathways are also needed to understand the relationship between MMR and chromatin.

Materials and methods

Preparation of nucleoplasmic extracts (NPE)

Xenopus laevis was purchased from Kato-S-kagaku (Chiba, Japan), and maintained and handled according to the animal care regulations in Osaka University and Kyushu University.

Preparation of NPE was carried out essentially as described previously (Lebofsky et al. 2009). Xenopus eggs were collected and dejellied with 2.2% (w/v) cysteine hydrochloride (pH7.7 with NaOH), washed three times with 0.5× modified MMR (50 mM NaCl, 1 mM KCl, 0.5 mM $MgSO_4$, 1 mM $CaCl_2$, 0.05 mM ethylenediaminetetraacetic acid [EDTA], 25 mM Hepes-NaOH, pH 7.8), and three times with 1× egg lysis buffer (ELB: 10 mM Hepes-KOH, 2.5 mM $MgCl_2$, 50 mM KCl, pH 7.7) containing 250 mM sucrose, 1 mM dithiothreitol (DTT), and 50 μg/mL cycloheximide. Eggs were then packed in 50-mL polycarbonate tubes (Thermo Fisher Scientific, Waltham, MA, USA, Cat#3117-0500) and crushed by centrifugation at 10,000 rpm for 20 min in Tomy NS-1 (TOMY Seiko, Tokyo, Japan) after removing excess buffers and adding 2.5 μg/mL cytochalasin B, 5 μg/mL aprotinin, and 5 μg/mL leupeptin. Crude cytoplasmic extracts were recovered, supplemented with 5 μg/mL cytochalasin B, 10 μg/mL aprotinin, 10 μg/mL leupeptin, 50 μg/mL cycloheximide, 1 mM DTT, and 3.3 μg/mL nocodazole, and re-centrifuged at 30,000 rpm for 30 min in Beckman SW50.1 (Beckman Coulter, Brea, CA, USA). Cleared extracts were recovered, supplemented with 2 mM adenosine triphosphate (ATP), 20 mM phosphocreatine (PC), 5 μg/mL creatine phosphokinase (CPK), and 4,000 / μL demembraned sperm nuclei, incubated at 22°C for 100–120 min, and centrifuged at 9,000 rpm for 2 min in NS-1. A layer of nuclei floating on the top of the extract was collected and centrifuged at 46,000 rpm for 30 min in SW50.1. Nucleoplasmic extracts separated from lipids and chromatin were then collected, frozen in liquid nitrogen as 10–20 μL aliquots, and stored at -80°C.

Preparation of mismatch-carrying plasmids

In vitro synthesis of mismatch-carrying plasmids was performed essentially as described previously (Higashi et al. 2012; Kawasoe et al. 2016). Briefly, an oligonucleotide DNA was annealed on single-stranded DNA, prepared by using M13KO7 filamentous helper phage. To synthesize the complementary strand and ligate remaining nicks, the primed ssDNA was incubated in the solution containing 20 mM Tris-HCl (pH7.5), 10 mM $MgCl_2$,

1 mM DTT, 0.4 mM each deoxynucleotide triphosphates (dNTPs), 0.1 mg/ml bovine serum albumin (BSA), 0.04 unit/ μ l T7 DNA polymerase (New England Biolabs, Ipswich, MA, USA), and 0.25 unit/ μ l T4 DNA ligase (Nippongene, Tokyo, Japan). Covalently closed circular DNA was separated by cesium chloride/ethidium bromide density gradient centrifugation at 120,000 rpm for 3 hours at 20°C. Primers used in this study were listed in Table 5. To introduce mismatches, the following oligonucleotides were used: 721 for control homoduplex, 722 for an A:C mismatch, 411 for a ±1 insertion/deletion loop (IDL), 412 for a ±5 IDL, 413 for a C:C mismatch, 414 for a G:G mismatch, and 415 for a T:C mismatch. To introduce a site-specific biotin modification, 362 was also used. To introduce two additional mismatches, following oligonucleotides pairs were also used: 723 and 725 for control homoduplex, and 724 and 726 for an A:C and a T:C mismatch. A site-specific gap was introduced as described previously (Kawasoe et al. 2016). Mismatch-carrying DNA prepared by *in vitro* second-strand synthesis was doubly nicked with Nt.BbvCI (New England Biolabs) for 1 hour at 37°C, purified by phenol/chloroform extraction and ethanol precipitation, and dissolved in TE (10 mM Tris-HCl, 1 mM EDTA, pH7.4). The DNA was incubated for 20 min at 70°C to dissociate the 15-nt fragment flanked by two BbvCI sites from parental DNA. The DNA was then immediately chilled on ice, and loaded on a Microspin S-400HR column (GE Healthcare, Little Chalfont, UK) to remove the 15-nt fragment. The gap-carrying DNA was precipitated with ethanol and dissolved in TE.

Supercoiling and gap-directed MMR assay

The supercoiling assay and the gap-directed MMR assay was carried out essentially as described previously (Kawasoe et al. 2016). Briefly, supercoiling assay was carried out as blow. NPE was supplemented with 2 mM ATP, 20 mM PC, and 5 μ g/mL CPK, and pre-incubated at 22°C for 5 min. A typical reaction consisted of 17.4 μ L of NPE, 0.2 μ L of 200 mM ATP, 0.4 μ L of 1 M PC, 0.02 μ L of 5 mg/mL CPK, and 2 μ L of substrate DNA (200 ng/ μ L in TE). After adding DNA, reaction mixtures were incubated at 22°C, and aliquots (1.5–3 μ L for most experiments) were stopped by addition of 100 μ L of 1% sodium dodecyl sulfate (SDS) in 20 mM EDTA. DNA was purified by proteinase K treatment, phenol/chloroform extraction, and ethanol precipitation. The MMR assay was carried out essentially as described for the supercoiling assay, except that gap-carrying DNA was used as a substrate. To analyze the MMR efficiency, 10 ng

of DNA was digested with XmnI, and BamHI-HF or XhoI in a 10-μL reaction. After agarose gel electrophoresis, DNA was stained with SYBR Gold nucleic acid stain (Life Technologies, Carlsbad, CA, USA) and scanned with Typhoon FLA9000 (GE Healthcare). Signal intensities were quantified using ImageJ (National Institutes of Health, Bethesda, MD, USA).

Micrococcal nuclease digestion, Southern blotting, and quantitative PCR

A 17-μL supercoiling reaction including 850 ng pControl/pCDFDuet-1 (Merck Millipore, Billerica, MA, USA, Cat#71340-3CN) was set up and incubated at 22° C for 10 min. A 2-μL aliquot was sampled for supercoiling, and another 15-μL aliquot was quickly diluted with 1.5 mL MNase buffer (10 mM Tris-HCl, 50 mM NaCl, 2.5 mM $CaCl_2$, pH7.4) containing 20 U/mL micrococcal nuclease (Worthington, Lakewood, NJ, USA). The samples were incubated at 37°C, 350 μL each of aliquots were stopped by addition of 50 μL of C-stop buffer (160 mM EDTA, 6.8% SDS) at 15, 30, 60, and 120 sec, and DNA was purified. For Southern blotting, DNA was separated on 1.2% agarose gel in 0.5× TBE (Tris-borate-EDTA) buffer, stained with SYBR Gold, and scanned with Typhoon FLA9000. DNA was then transferred onto Hybond N+ nylon membrane (GE Healthcare) and hybridized with a ^{32}P-labelled probe prepared from the PvuII-PvuII 473-bp fragment of pMM1 using the Random Primer DNA Labeling kit (Takara, Kusatsu, Japan). The probe was stripped off after detection of ^{32}P, and the membrane was re-hybridized with another probe prepared from the DraI-DraI 692-bp fragment. Beta rays from ^{32}P were detected by Typhoon FLA9000 using a phosphor imaging plate. For qPCR, DNA samples were diluted in TE, and 10 μL reactions (5 μL qPCR master mix, 2 μL of 1 μM primer mix, and 3 μL diluted DNA sample) were run in a Mx3000P system (Stratagene, LA Jolla, CA) using KOD SYBR qPCR mix (TOYOBO, Osaka, Japan).

Plasmid pull-down and mass spectrometry identification of DNA-bound proteins

Singly-biotinylated plasmid DNA was immobilized on streptavidin-coated biotin-Sepharose beads as described previously (Higashi et al. 2012). For biotinylated sepharose bead preparation, EZ-Link Amine-PEG4-biotin (Thermo Fisher Scientific) was conjugated to NHS-activated sepharose HP (GE Healthcare) following manufacturer's protocol. 250 ng of site-specifically biotinylated plasmid DNA was incubated with 1 μ

g streptavidin (SA) protein in 25 μl of binding buffer (10 mM Tris-HCl (pH 7.4), 1 mM EDTA, 1 M NaCl, 0.1% Triton X-100) at 4°C overnight to assemble the DNA-SA complex, and 100 ng (with respect to DNA) of the complex was bound to 1 μl of the biotin-sepharose beads. Immobilized DNA was incubated in NPE at 20 ng/μL (600 ng DNA bound to 6 μL Sepharose in a 30-μL reaction) for 30 min at 22°C. The reaction mixture was diluted with 200 μL of 1×ELB containing 0.2% Triton X-100, layered over 300 μL of ELB containing 500 mM sucrose, and centrifuged at 12,700 × *g* for 2 min at 4°C in a horizontal centrifuge (TOMY Seiko). The beads were washed three times with ELB, and bound proteins were eluted with 12 μL of Laemmli's SDS sample buffer (62.5 mM Tris-HCl, 10% glycerol, 3% SDS, 0.005% bromophenol blue, 5% 2-mercaptoethanol, pH 6.8). To monitor DNA recovery, DNA was extracted with phenol/chloroform, precipitated with ethanol, and dissolved in TE. The amount of DNA was determined by qPCR with primers 1842 and 1843. Mass spectrometry analysis was carried out as described previously with minor modifications (Nozawa et al. 2010). The LC-MS/MS data were searched against a *X. laevis* subset database created from RefSeq (release 82). Identified proteins were semi-quantified by spectral counting (Liu et al. 2004) using Scaffold software version 4.8.3 (Proteome Software Inc., Portland, OR, USA).

Stepwise-incubation assay

Immobilized DNA was incubated in NPE as described in the method for plasmid pull-down. After a 30-min incubation, the DNA was recovered by centrifugation in a benchtop centrifuge, washed three times with ELB, and incubated in the second NPE at 20 ng/μL concentration (100 ng DNA bound to 1 μL Sepharose in a 5-μL reaction) at 22°C for 30 min unless otherwise stated. For the experiment shown in Fig. 2G, biotin-free DNA was used as a substrate, and an equal volume of the second NPE was directly added to the reaction. The reaction was stopped by addition of 100 μL of 1% SDS in 20 mM EDTA. DNA was purified by proteinase K treatment, phenol/chloroform extraction, and ethanol precipitation.

Sucrose gradient sedimentation

A Linear gradient of 20-40% sucrose was prepared in ELB containing 1 μg/ml aprotinin and 1 μg/ml leupeptin in a 5 ml thin wall tube (#344057, Beckman Coulter). 40 μl of

NPE diluted with 60 μl ELB was applied on the top of the gradient and the tube was spun in a SW50.1 rotor (Beckman Coulter) for 15 hours at 30,000 rpm at 4°C. A separate sucrose gradient with size marker proteins (100 μg BSA, 100 μg Catalase, and 130 μg Thyroglobulin) was spun at the same time for calibration. After centrifugation, 200 μl each of aliquots were collected from the bottom of the tubes.

Yeast strains

All *S. cerevisiae* strains used in this study were derived from BY4741 and are listed in Table 6. Transformation was performed using the standard lithium acetate method (Gietz and Woods 2002). The *hom3-10* and the *lys2::insE-A14* mutations were introduced as described below: Two fragments of the *hom3-10* gene were individually amplified by PCR from BY4741 genomic DNA with primers 1304 and 1315, and 1305 and 1318, respectively. The fragments were then fused by overlap-extension PCR with primers 1315 and 1318 and directly used for transformation of TTY15, in which the *HOM3* gene was disrupted by the *URA3* gene. Clones carrying the *hom3-10* mutation were selected on complete media (synthetic complete: SC) containing 5-fluoroorotic acid. The *lys2::insE-A14* allele was introduced into the resulting *hom3-10* strain (TTY20) by integration of the YIpURA3-*lys2::insE-A14* plasmid linearized by XhoI and excision of *URA3* and the wild-type *LYS2* gene. Further genetic manipulation was carried out using following plasmids or PCR fragments with following primers: *msh2*, 1347, 1348, 1349, and 1350; *msh6*, 1359, 1360, 1361, and 1362; *msh3*, 1365, 1366, 1367, and 1368; *fun30*, 1353, 1354, 1355, and 1356; *fun30-K603A*, YIpURA3-*fun30*-K603A (linearized with PstI); *cac1*, 1537, 1538, 1539, and 1540; *exo1*, 1481, 1482, 1483, and 1484; *rad52*, 1457, 1458, 1459, and 1460; *spt16-d922*, YIpURA3-*spt16-d922* (linearized with SalI). After each transformation step, gene integration was verified by colony-directed PCR. For integration of a point mutation, the sequence of the entire gene was confirmed after PCR amplification.

Yeast genetic analysis

Mutation rates were estimated by fluctuation analysis, using the Ma-Sandri-Sarkar (MSS) maximum likelihood method (Sarkar et al. 1992; Rosche and Foster 2000). 95% confidence intervals were estimated based on the mutation rates obtained by the MSS method. For each replicate in the fluctuation analysis, a yeast culture was started from a

single colony and grown to the stationary phase in 10 mL of yeast extract-peptone-dextrose medium plus adenine. Appropriate aliquots of cells were plated onto synthetic dextrose (SD) medium with amino acids lacking lysine or threonine to count Lys^+ or Thr^+ revertants, selective medium lacking arginine (SD-Arg) containing 60 mg/L L-Canavanine (Sigma Aldrich, MO, USA) for Can^r mutant count, and onto SC media or SD-Arg for viable cell count. For strains with very high mutation rates (strains carrying *msh2Δ*, *msh6Δ*, or *exo1Δ*), a single colony was directly suspended in 1 mL of distilled water and appropriate aliquots were plated on solid media.

Protein expression and purification

Purified *Xenopus laevis* MutSα protein was a kind gift from Yoshitaka Kawasoe. (Kawasoe et al. 2016).

Purification of *Xenopus laevis* Smarcad1 was performed as follows: Recombinant protein was expressed by infecting Sf9 insect cells with FLAG-Smarcad1 baculoviruses at 28°C in Sf-900II SFM (Life technologies) supplemented with 2% (v/v) fetal bovine serum. Cells were harvested, washed with phosphate buffered saline (PBS), and frozen in liquid nitrogen. Cells were suspended in buffer S (25 mM Tris-HCl, 10% glycerol, 300 mM NaCl, 5 mM 2-mercaptoethanol, 1 mM EDTA, pH 7.4) containing 1x cOmplete EDTA-free (Roche Life Science, Penzberg, Germany), and the lysates were centrifuged at 81,800 $\times g$ (30,000 rpm) for 30 min in Beckman 50.2Ti (Beckman Coulter). Cleared lysates were passed through FLAG-M2 agarose (Sigma Aldrich). The FLAG-Smarcad1 protein was eluted from the FLAG-M2 resin with 50 μg/mL FLAG-peptide (Sigma Aldrich) in buffer S containing 0.1x cOmplete EDTA-free. Peak fractions were pooled and three-fold diluted with buffer A (20 mM Tris-HCl, 5% glycerol, 5 mM 2-mercaptoethanol, 1 mM EDTA, pH 7.4) containing 0.1x cOmplete EDTA-free, loaded on a MonoQ 5/50 GL column (GE Healthcare), and the column was developed with a 0–1 M NaCl linear gradient in buffer A containing 0.1x cOmplete EDTA-free. Peak fractions were pooled and loaded on a Hi Load 16/60 Superdex 200 prep grade column (GE Healthcare), and the column was developed with buffer A containing 0.14 M NaCl. Fractions corresponding to the molecular mass of $2.5–5.0 \times 10^5$ (FLAG-Smarcad1: $M_r = 1.19 \times 10^5$) were pooled, concentrated using Amicon Ultra (Merck Millipore), and frozen in liquid nitrogen as small aliquots.

Purification of the N-terminally His_6-tagged, full-length *X. laevis* Msh3 protein

was performed as follows: Protein expression was induced in *E. coli* BL21(DE3) transformed with pET-HSD-MSH3 by addition of 0.4 mM isopropyl-β-D-thiogalactopyranoside (IPTG) for 1 hour at 37°C. Cells were harvested, lysed with 1 mg/mL lysozyme and sonicated in buffer SO (50 mM Na-phosphate, 500 mM NaCl, 1% Triton X-100, pH 8.0) containing 1 mM phenylmethylsulfonyl fluoride (PMSF) and 2 mM benzamidine and centrifuged at 10,000 rpm for 10 min in TA-24BH (TOMY Seiko). The inclusion bodies containing the Msh3 protein were resuspended in buffer SO, centrifuged again at 10,000 rpm for 10 min in TA-24BH, and these procedures were repeated three times. The Msh3 protein was dissolved in Laemmli's SDS sample buffer and purified by SDS-PAGE followed by electroelution.

Purification of the *X. laevis* FACT heterodimer was performed as follows: Recombinant proteins were expressed by co-infecting Sf9 insect cells with His_6-FLAG-Spt16 and Ssrp1 baculoviruses at 28°C in Sf-900II SFM supplemented with 2% (v/v) fetal bovine serum. Cells were harvested, washed with PBS and frozen in liquid nitrogen. Cells were suspended in buffer S containing 2 mM PMSF and 1 mM benzamidine and centrifuged at 81,800 $\times g$ (30,000 rpm) for 30 min in Beckman 50.2Ti. Cleared lysates were passed through a DEAE Sepharose Fast Flow column (GE Healthcare) and then a FLAG-M2 agarose column. The FACT heterodimer was eluted from the FLAG-M2 resin with 50 μg/mL FLAG-peptide in buffer S containing 0.2 mM PMSF and 0.1 mM benzamidine. Peak fractions were pooled and diluted three-fold with buffer A containing 0.2 mM PMSF and 0.1 mM benzamidine, loaded on a HiTrap Q-HP 1-mL column (GE Healthcare), and bound proteins were eluted with a 0–1 M NaCl linear gradient in buffer A. Peak fractions were pooled, dialyzed against buffer D (20 mM Tris-HCl, 100 mM KCl, 5% glycerol, pH 7.4), concentrated by Amicon Ultra, and frozen in liquid nitrogen as small aliquots.

Purification of the N-terminally His_6-tagged, full-length *X. laevis* Spt16 protein was performed as follows: Spt6-containing inclusion bodies were purified by the method essentially the same as that for Msh3, except that protein expression was induced for 2 hours. The inclusion bodies were resuspended in 0.5× buffer SO containing 0.5 mM PMSF, 1 mM benzamidine, 7 M urea, 2 M thiourea, 100 mM DTT. 4× Laemmli's SDS sample buffer was also added to final 1× concentration. The sample was incubated for 20 min at 37°C and centrifuged at 15,000 rpm for 20 min in TA-24BH to remove insoluble debris. The Spt16 protein was then purified by SDS-PAGE followed by electroelution.

Purification of the N-terminally His_6-tagged, full-length *X. laevis* Ssrp1 protein was performed as follows: The method for protein expression and preparation of bacterial lysate were essentially the same as that for Msh3, except that protein expression was induced at 20°C for 20 hours. The lysate was centrifuged at 81,800 ×*g* (30,000 rpm) for 30 min in Beckman 50.2Ti. The His-Ssrp1 protein in the cleared lysate was bound to the TALON metal affinity resin (Clontech, CA, USA) for 1 hour at 4°C and eluted with 100 mM imidazole in buffer W (20 mM Na-phosphate, 500 mM NaCl, 0.1% Triton X-100, pH 8.0) containing 0.1 mM PMSF and 0.2 mM benzamidine. The eluate was diluted four-fold with buffer B (50 mM Na-phosphate, 5% glycerol, pH 6.8), loaded on a HiTrap Q-HP 1-mL column, and the column was developed with a 0–1 M NaCl linear gradient in buffer B. Peak fractions were pooled, diluted four-fold with buffer B, loaded on a HiTrap SP-HP 1-mL column (GE Healthcare), and the column was developed with a 0–1 M NaCl linear gradient in buffer B.

The *E. coli* BL21 codon plus (DE3) cells carrying pET28c-xHIRA was a kind gift from Masato Kanemaki. The method for expression and purification of the *X. laevis* HIRA protein was essentially the same as that for Msh3, except that protein expression was induced for 7 hours at 37°C.

Purification of the N-terminally His_6-tagged, full-length *X. laevis* Mlh1 protein was performed as follows: The method for protein expression and preparation of bacterial lysate were essentially the same as that for Msh3, except that protein expression was induced for 5 hours. Inclusion bodies containing the Mlh1 protein were resuspended in wash buffer (50 mM Na-phosphate, 1 M NaCl, 0.1% Triton X-100, pH 8.0) and centrifuged at 13,000 rpm for 20 min in TA-24BH. The pellet was resuspended in wash buffer containing 1 M urea, centrifuged again at 13,000 rpm for 20 min in TA-24BH, and these procedures were repeated three times. The Mlh1 protein was dissolved in Laemmli's SDS sample buffer containing 4 M urea and purified by SDS-PAGE followed by electroelution.

Cloning and plasmids

pMM1 was constructed by Drs. Torahiko Higashi and Tatsuro Takahashi. A synthetic linker prepared by annealing of 5'-phosphorylated oligonucleotides 302, 303, 304, 305, 306, and 307, was inserted between the KpnI and SacI sites in pBluescript II KS (-) (Stratagene), resulting in pMM0. A synthetic linker carrying two BbvCI sites prepared

by the annealing of 5'-phosphorylated oligonucleotides 386 and 387 was inserted into the BspQI site in pMM0, resulting in pMM1.

Construction of pMM3 was performed as follows: A linker DNA fragment was amplified by PCR with primers 1079 and 1158 using fission yeast genomic DNA as a template. The DNA fragment was digested with PstI and BspQI and inserted between the same sites in pMM1, resulting in pMM3.

Cloning of *Xenopus laevis smarcad1* gene was performed as follows: A BLAST search using the *Xenopus tropicalis* Smarcad1 sequence identified two *Xenopus laevis* EST clones, TC422950 and TC460920. Based on these EST sequences, we designed two primers, 900 and 887, and amplified the *smarcad1* gene by PCR from *Xenopus* egg cDNA. The *smarcad1* gene fragment was digested with NdeI and BamHI-HF and cloned into pDE1a, a derivative of the pDONR201 vector (Life Technologies) carrying NdeI and BamHI sites between attL1 and L2 sites. Sequencing of cloned genes revealed that two distinct isoforms, which we named *smarcad1a* and *smarcad1b*, were present (Plasmids: pDE1a-SMARCAD1A and pDE1a-SMARCAD1B). Smarcad1a and Smarcad1b were 90% identical and 95% similar with respect to their amino acid sequences. The *smarcad1a* gene was used for all subsequent construction and experiments, and therefore the gene product was called simply Smarcad1, unless otherwise indicated.

To introduce the lysine 503 to alanine substitution in the Walker A motif, the gene fragment was amplified by PCR using primer pairs, 887 and 955, and 900 and 956, using pDE1a-SMARCAD1A as a template, and the two PCR fragments were fused by overlap-extension PCR with primers 887 and 900. The resulting *smarcad1a*^{K503A} fragment was digested with NdeI and EcoRI, and cloned into the same sites in pDE1a-SMARCAD1A, resulting in pDE1a-SMARCAD1A-K503A. To add two tandem FLAG tags to the N-terminus of Smarcad1, a synthetic linker prepared by annealing of 5′ -phosphorylated oligonucleotides 60 and 61 was inserted in the NdeI sites in pDE1a-SMARCAD1A and pDE1a-SMARCAD1A-K503A, resulting in pDE1a-FLAG-SMARCAD1A and pDE1a-FLAG-SMARCAD1A-K503A, respectively. Baculoviruses for expression of FLAG-Smarcad1 and FLAG-Smarcad1-K503A were prepared by transferring the FLAG-*smarcad1a* and FLAG-*smarcad1a*^{K503A} genes into BaculoDirect C-term Linear DNA (Life Technologies) using the Gateway LR reaction.

cDNAs of *Xenopus laevis spt16* and *ssrp1* genes were kind gifts from Haruhiko Takisawa,

Yumiko Kubota, and Masato Kanemaki. The *spt16* gene was amplified by two-step PCR using primers 798 and 799, and then primers 344 and 345, and cloned into the pDONR201 vector using the Gateway BP reaction, resulting in pDONR-SPT16. The *ssrp1* gene was amplified by PCR using primers 770 and 771, digested with NcoI and Sse8387I (Takara, Kusatsu, Japan), and cloned into the same sites in a modified pDE1a vector, resulting in pDONR-SSRP1. For protein expression in *Escherichia coli*, the gene fragments on the Gateway entry vectors were transferred into pET-HSD, a derivative of the pETDuet-1 vector (Merck Millipore, Cat#71146-3CN) carrying a Gateway recombination cassette and a His-tag for N-terminal fusion, by the Gateway LR reaction, resulting in pET-HSD-SPT16 and pET-HSD-SSRP1, respectively. The N-terminally His_6-FLAG-tagged *spt16* gene was amplified by two-step PCR using primers 799 and 827, and then primers 799 and 81, digested with NcoI, and cloned into pDONR-SPT16, resulting in pDONR-His_6-FLAG-SPT16. Baculoviruses for expression of His_6-FLAG-Spt16 and Ssrp1 were constructed by transferring the His_6-FLAG-*spt16* and *ssrp1* genes into BaculoDirect C-term Linear DNA by the Gateway LR reaction.

Cloning of the *Xenopus laevis msh3* gene was performed as follows: A BLAST search using the *Xenopus tropicalis* Msh3 sequence identified a partial *Xenopus laevis* EST clone, CA988114. The missing 5′ and 3′ portions of the *msh3* cDNA were cloned by 5′ and 3′ RACE using the SMARTer RACE cDNA Amplification kit (Clontech) with primers 784 and 780, respectively. The full-length *msh3* ORF was then PCR-amplified from *Xenopus laevis* egg cDNA by using primers 957 and 958, and then 344 and 355, and cloned into pDONR201 by the Gateway BP reaction, resulting in pDONR-MSH3. For protein expression in *E. coli*, the *msh3* gene was transferred into pET-HSD by the Gateway LR reaction, resulting in pET-HSD-MSH3.

The budding yeast *fun30-K603A* mutant gene in which lysine 603 in the Walker A motif was replaced with alanine was prepared by overlap-extension PCR with primers 1564, 1565, 1566, and 1567 using BY4741 genomic DNA as templates. The resulting fragment was digested with EcoRI and BamHI, and cloned into YIplac211, resulting in YIpURA3-fun30-K603A.

The *lys2::insE-A14* gene was constructed as follows: Two partially overlapping fragments of the *lys2::insE-A14* gene were separately prepared by two-step PCR with following primer pairs: the 5′ half of the fragment, 1296 and 1298, and 1296 and 1426; the 3′ half of the fragment, 1297 and 1301, and 1297 and 1300. Two fragments were

then simultaneously inserted into pBluescript II KS(-) linearised by PCR with primers 1294 and 1295 by the Gibson assembly reaction (New England Biolabs), resulting in pBS-lys2::insE-A14. The PvuII-PstI fragment of pBS-lys2::insE-A14 was subcloned between the PstI and SmaI sites in YIplac211, resulting in YIpURA3-lys2::insE-A14.

The *spt16-d922* mutant gene was prepared by two-step overlap-extension PCR with primers 1571, 1572, 1573, and 1574 using BY4741 genomic DNA as templates. The fragment was digested with BamHI and HindIII, and cloned into YIplac211, resulting in YIpURA3-spt16-d922.

Construction of pDONR-xMLH1 was described previously (Kawasoe et al. 2016). For protein expression in *E. coli*, the *mlh1* gene was transferred into pDEST17 (Life Technologies) by the Gateway LR reaction, resulting in pDEST17-MLH1.

Immunological methods

The rabbit Msh2R1, Msh6, and Mlh1 antisera (Kawasoe et al. 2016) were produced by Ms. Kanae Taki. The rabbit Msh2R1 antiserum was raised against N-terminally His-tagged and C-terminally Strep-II-tagged full-length *Xenopus* Msh2 expressed in *E. coli*. The rabbit Msh6 antiserum was raised against peptide NH_2-CNGSPEGLALHKRLKLLQ-COOH, corresponding to residues 1324–1340 of *Xenopus* Msh6. The rabbit Mlh1 antiserum was raised against N-terminally His-tagged, full-length *Xenopus* Mlh1 expressed in E. coli. The rabbit Cdc7 antisera (Takahashi and Walter 2005) was produced by Dr. Tatsuro Takahashi. The rabbit Cdc7 antiserum was raised against N-terminally His-tagged full-length *Xenopus* Cdc7 expressed in *E. coli*. The rabbit Msh2pep antiserum was raised against peptide NH_2-CLAKNNRFVSEVISRTKTGL-COOH, corresponding to residues 914–932 of Msh2. The rabbit Msh2R2 antiserum was raised against N-terminally His_6-tagged and C-terminally Strep-II-tagged full-length Msh2 expressed in *E. coli*. The rabbit Msh3 antiserum was raised against N-terminally His_6-tagged, full-length Msh3 expressed in *E. coli*. The rabbit HIRA antiserum was raised against N-terminally His_6-tagged, full-length HIRA expressed in *E. coli*. The rabbit Spt16 antiserum was raised against N-terminally His_6-tagged, full-length Spt16 expressed in *E. coli*. The rabbit Ssrp1 antiserum was raised against N-terminally His_6-tagged, full-length Ssrp1 expressed in *E. coli*. The rabbit H2B antiserum was raised against peptide NH_2-CAKHAVSEGTKAVTKYTSAK-COOH, corresponding to residues 108–126 of H2B. The rabbit H3 antiserum was raised against

peptide NH_2-ARTKQTARKSTGGKAC-COOH and NH_2-CPKDIQLARRIRGERA-COOH, corresponding to residues 1–15 and 121–135 of H3, respectively. The rabbit Smarcad1 antiserum was raised against peptide NH_2-CDEGTIPLDMATLLKTSLGL-COOH, corresponding to residues 983–1001 of Smarcad1a. This peptide is 100% conserved between Smarcad1a and Smarcad1b, and therefore the resulting antibodies should recognize both isoforms. The rabbit xCAF-1 antiserum was raised against peptide NH_2-CSSADKPSGSDQTNK-COOH and NH_2-CFDEIKKRKPRKMG-COOH, corresponding to residues 555–569 of xCAF-1 p60 and 450–452 of xCAF-1 p150, respectively. All antibodies except for Mlh1, Spt16, Ssrp1, and CAF-1 were affinity-purified using corresponding antigens. The rabbit Orc2 antiserum was a kind gift from Johannes Walter (Vashee et al. 2003). The mouse histone H4 monoclonal antibody was a kind gift from Hiroshi Kimura (Hayashi-Takanaka et al. 2015). The CAF-1 p150 and p60 antibodies were kind gifts from Ruibin Zhu, Mari Iwabuchi, and Keita Ohsumi (Zhu et al. 2017). For immunoblotting, Msh2, Msh6, Mlh1, Cdc7, Smarcad1, Spt16, Ssrp1, p150, p60, xH3, H4 and Orc2 antisera were used at a dilution of 1:5,000. For immunoblotting of HIRA, xH2B, and Msh3, affinity-purified antibodies were used at 0.5–1 μ g/ml. HRP-conjugated Goat Rabbit IgG (H+L) antibodies (Jackson ImmunoResearch, West Grove, PA, USA, Cat#111-035-003), or Goat Mousse IgG (H+L) antibodies (#115-035-146) were used at a dilution of 1:10,000 as the secondary antibody. The secondary antibodies were detected by enhanced chemiluminescence using the SuperSignal West Pico or West Femto Chemiluminescent Substrate (Thermo Fisher Scientific), and the signals were collected either by ImageQuant LAS500 (GE Healthcare) or ChemiDoc Touch (BioRad Laboratories, Hercules, CA, USA).

For immunoprecipitation, 3 vol of an antiserum was bound to 1 vol of recombinant protein A-Sepharose (PAS, GE Healthcare). NPE was diluted 5-fold with ELB, and centrifuged at 15,000 rpm for 10 min in a benchtop centrifuge to remove insoluble debris. For each immunoprecipitation reaction, 12 μL of diluted NPE was mixed with 4 μL of IgG-coupled PAS, incubated at 4°C for 2 hours with gentle rotation, and the supernatant and the beads were separated by centrifugation at 5,000 rpm for 30 sec in a benchtop centrifuge. The beads were washed three times with ELB containing 0.1% Triton X-100, and the bound proteins were eluted with 20 μL of Leammli's SDS sample buffer.

Immunodepletion was performed as follows: For Smarcad1, 5 vol of the

Smarcad1 serum was bound to 1 vol of PAS. For Spt16, Mlh1, Msh3, or CAF-1, 3 vol of the serum was bound to 1 vol of PAS. For Spt16/Smarcad1-double depletion, 13 μg of xSmarcad1 IgG and 3 μL of the Spt16 serum were bound to 1 μL of PAS. For Msh2/Smarcad1-double depletion, 13 μg of xSmarcad1 IgG was bound to 1 μL of PAS. For HIRA, 20 μg of xHIRA IgG was bound to 1 μL of PAS. For Msh6, 0.5 μg of Msh6 IgG and 3 μL of the Msh6 serum were bound to 1 μL of PAS. For MutSα/MutSβ depletion from NPE, 2 μg of Msh2R1 IgG, 0.5 μg of Msh6 IgG, and 3 μL of the Msh6 serum were bound to 1 μL of PAS. To deplete NPE, 0.2 vol of IgG-coupled PAS was mixed with 1 vol of NPE, incubated at 4°C for 1 hour with gentle rotation, and the procedure was repeated twice except for Mlh1-depletion, in which the procedure was repeated once. For depletion of Spt16 or double-depletion of Spt16/Smarcad1, 0.3 instead of 0.2 vol of IgG-coupled PAS was used. For depletion of HIRA, 0.1 vol of HIRA-IgG coupled PAS was used. For double-depletion of Msh2/Smarcad1, 0.15 vol of Msh2/Msh6-IgG coupled PAS and 0.15 vol of Smarcad1-IgG coupled PAS were used. In most cases, 20–60 μL of NPE was depleted for each experiment.

Determination of the mutation spectra

Mutation sites were determined by Sanger sequencing of target regions amplified by colony-directed PCR. The *hom3* locus was amplified with primers 1290 and 1293, and sequenced with 1290, and the *lys2* locus was amplified with primers 1311 and 1314, and sequenced with 1428 and 1429. To ensure that each of the reversion mutations had been independently arisen, only one reversion mutant was isolated from an independent culture for sequencing.

Statistical Testing

At least two biological replicates, in each of which 7–11 technical replicates were included, were performed for each strain to estimate reliably the reversion rates (Rosche and Foster 2000). The exact number of total replicates (*n*), including both biological and technical replicates, is as follows: wild-type, 30; *fun30Δ*, 30; *fun30-K603A*, 25; *msh2Δ*, 22; *msh2Δ fun30Δ*, 22; *msh6Δ*, 22; *msh6Δ fun30Δ*, 22; *msh6Δ fun30-K603A*, 30; *msh3Δ*, 22; *msh3Δ fun30Δ*, 22 for *hom3* and 21 for *lys2*; *exo1Δ*, 37; *exo1Δ fun30Δ*, 37; *exo1Δ msh6Δ*, 22; *exo1Δ msh6Δ fun30Δ*, 22; *rad52Δ*, 30; *rad52Δ fun30Δ*, 29; *rad52Δ msh6Δ*,

21 for *hom3* and 22 for *lys2*; *rad52Δ msh6Δ fun30Δ*, 22; *cac1Δ*, 22; *fun30Δ cac1Δ*, 35 for *hom3* and 20 for *lys2*; *msh6Δ cac1Δ*, 22; *msh6Δ fun30Δ cac1Δ*, 22; *msh3Δ cac1Δ* 22; *msh3Δ fun30Δ cac1Δ*, 22; *msh2Δ cac1Δ*, 34 for *hom3* and 33 for *lys2*; *spt16-d922*, 30; *spt16-d922 fun30Δ*, 30; *spt16-d922 msh6Δ*, 38; *spt16-d922 msh6Δ fun30Δ*, 24.
To obtain the *p*-values, the number of revertants obtained by the same procedure was normalized by using viable cell counts, and compared by Mann-Whitney's U-test. Calculation was performed using Graphpad Prism 6 (Graphpad Software, La Jolla, CA, USA).

Repeatability

For supercoiling assays, mismatch-DNA binding assays, immunoprecipitations, and micrococcal nuclease digestion experiments, representative results, out of at least three independent experiments using at least two different preparations of NPE, are shown. Immunoblots for evaluation of depletion efficiencies were carried out once for each single depletion experiment. Spectral counting by mass spectrometry was carried out three times using three independent samples. Because there was no reliable method to merge spectral counts obtained from different experiments, two representative data were presented.

Table 1. Spectral counts of proteins from the plasmid pull-down assay calculated using the X. laevis protein database.

Accession Number	Description	Spectral counts			
		Ex.1 A:T	Ex.1 A:C	Ex.2 A:T	Ex.2 A:C
NP_001089247.1	msh6.L, mutS homolog 6 L homeolog	0	202	7	157
NP_001082502.1	Cluster of top2a.L, DNA topoisomerase II alpha L homeolog (NP_001082502.1)	67	141	77	89
XP_018118021.1	msh2.L, PREDICTED: DNA mismatch repair protein Msh2	0	100	12	102
NP_001084166.1	Cluster of supt16h.S, FACT complex subunit SPT16 (NP_001084166.1)	44	78	35	68
XP_018106057.1	fanci.L, PREDICTED: Fanconi anemia complementation group I L homeolog isoform X1	9	44	28	18
XP_018084656.1	rfc1.L, PREDICTED: replication factor C subunit 1	13	44	5	17
NP_001085290.1	Cluster of brd4.S, bromodomain-containing protein 4A (NP_001085290.1)	13	13	43	24
NP_001091279.1	Cluster of actg1, actin, cytoplasmic 2 (NP_001091279.1)	26	43	1	3
NP_001081571.1	parp1.L, poly [ADP-ribose] polymerase 1	27	41	12	14
NP_001082183.1	lig3.L, ligase III, DNA, ATP-dependent L homeolog	32	40	1	11
NP_001083827.1	exo1.S, exonuclease 1	5	38	9	33
NP_001089160.1	Cluster of fancd2.L, Fanconi anemia complementation group D2 L homeolog (NP_001089160.1)	4	36	23	13
NP_001082049.1	Cluster of atr.L, serine/threonine-protein kinase atr (NP_001082049.1)	5	33	11	6
NP_001084164.1	ssrp1.S, FACT complex subunit SSRP1	20	27	13	30
NP_001081585.1	Cluster of rpa1.L, replication protein A 70 kDa DNA-binding subunit (NP_001081585.1)	5	18	30	28
XP_018096456.1	Cluster of pbrm1.L, PREDICTED: protein polybromo-1 (XP_018096456.1)	28	14	20	8
NP_001083868.1	Cluster of smarca5.S, SWI/SNF related, matrix associated, actin dependent regulator of chromatin, subfamily a, member 5 S homeolog (NP_001083868.1)	19	7	28	13
XP_018099607.1	Cluster of hira.S, PREDICTED: protein HIRA isoform X1 (XP_018099607.1)	28	14	8	3
XP_018088308.1	Cluster of LOC108699999, PREDICTED: filamin-A-like (XP_018088308.1)	10	27	0	0
NP_001080735.1	nono.L, non-POU domain containing, octamer binding L homeolog	26	17	2	6
XP_018104999.1	Cluster of LOC108709556, PREDICTED: splicing factor, proline- and glutamine-rich-like isoform X1 (XP_018104999.1)	25	19	12	16
NP_001090545.1	mlh1.S, mutL homolog 1 S homeolog	1	25	13	18
XP_018092658.1	Cluster of ubtf.S, PREDICTED: nucleolar transcription factor 1-B isoform X1 (XP_018092658.1)	24	10	9	5
NP_001086442.1	Cluster of hells.L, helicase, lymphoid specific L homeolog (NP_001086442.1)	13	7	22	10
NP_001081591.1	coil.L, coilin	22	18	6	6
NP_001089668.1	Cluster of smarcal1.L, SWI/SNF-related matrix-associated actin-dependent regulator of chromatin subfamily A-like protein 1 (NP_001089668.1)	0	21	14	15
XP_018094497.1	Cluster of nop58.S, PREDICTED: nucleolar protein 58 (XP_018094497.1)	20	15	12	3
NP_001080332.1	Cluster of smarcc1.L, SWI/SNF related, matrix associated, actin dependent regulator of chromatin, subfamily c, member 1 L homeolog (NP_001080332.1)	19	1	20	9
XP_018082245.1	pnkp.S, PREDICTED: polynucleotide kinase 3'-phosphatase isoform X1	19	18	1	8
NP_001082151.1	nop56.L, XNop56 protein	19	9	1	0
NP_001165424.1	smarca4.S, SWI/SNF related, matrix associated, actin dependent regulator of chromatin, subfamily a, member 4 S homeolog	17	12	10	11
XP_018116404.1	LOC108715603, PREDICTED: acetyl-CoA carboxylase 2-like isoform X1	2	16	5	5
NP_001081545.1	lmnb3.L, lamin-L(III)	16	5	0	0
XP_018106608.1	rad50.L, PREDICTED: RAD50 homolog, double strand break repair protein L homeolog isoform X1	14	15	14	5
XP_018095629.1	Cluster of LOC108703833, PREDICTED: uncharacterized protein LOC108703833 (XP_018095629.1)	15	15	2	3

XP_018090070.1	Cluster of wrn.L, PREDICTED: Werner syndrome ATP-dependent helicase homolog isoform X1 (XP_018090070.1)	0	15	3	9
XP_018114226.1	LOC108714465, PREDICTED: ubinuclein-2-like isoform X1	14	12	9	5
XP_018090503.1	LOC108700952, PREDICTED: regulator of telomere elongation helicase 1-like isoform X1	7	14	8	8
NP_001081806.1	orc1.L, origin recognition complex subunit 1 L homeolog	14	6	11	4
NP_001089159.1	fanca.L, Fanconi anemia complementation group A L homeolog	8	14	5	2
NP_001080810.1	Cluster of krt18.L, keratin, type I cytoskeletal 18-B (NP_001080810.1)	14	10	0	0
XP_018085136.1	dkc1.L, PREDICTED: H/ACA ribonucleoprotein complex subunit 4 isoform X1	13	10	3	0
XP_018093627.1	Cluster of LOC108702580, PREDICTED: exportin-2-like (XP_018093627.1)	13	3	2	2
NP_001081011.1	pcna.L, proliferating cell nuclear antigen	1	13	1	1
XP_018091049.1	LOC108701222, PREDICTED: ATPase family AAA domain-containing protein 5-like	6	3	12	12
NP_001083624.1	ddb1.S, DNA damage-binding protein 1	12	2	9	7
NP_001082568.1	topbp1.L, DNA topoisomerase II binding protein 1 L homeolog	2	12	7	1
NP_001080711.1	Cluster of xrcc1.L, X-ray repair complementing defective repair in Chinese hamster cells 1 L homeolog (NP_001080711.1)	9	12	0	1
XP_018091930.1	LOC108701593, PREDICTED: mismatch repair endonuclease PMS2-like	0	12	3	6
XP_018107625.1	Smarcad / Cluster of LOC108710927, PREDICTED: SWI/SNF-related matrix-associated actin-dependent regulator of chromatin subfamily A containing DEAD/H box 1-like isoform X1 (XP_018107625.1)	0	12	0	9
NP_001136258.1	Cluster of smarcd1.L, SWI/SNF related, matrix associated, actin dependent regulator of chromatin, subfamily d, member 1 L homeolog (NP_001136258.1)	12	0	4	1
NP_001082757.1	rfc4.L, replication factor C subunit 4 L homeolog	3	12	0	0
XP_018108852.1	Cluster of LOC108711520, PREDICTED: Bloom syndrome protein homolog (XP_018108852.1)	1	12	0	0
XP_018113609.1	LOC108714167, PREDICTED: actin-binding protein anillin-like isoform X3	10	11	0	0
NP_001171151.1	fancm.L, Fanconi anemia complementation group M L homeolog	3	11	4	0
NP_001090595.1	Cluster of brd3.S, bromodomain containing 3 S homeolog (NP_001090595.1)	5	0	7	10
NP_001081890.1	Cluster of incenp.L, inner centromere protein A (NP_001081890.1)	9	10	1	1
NP_001088399.1	Cluster of snu13.S, NHP2-like protein 1 (NP_001088399.1)	10	10	0	0
NP_001089570.1	rfc3.L, replication factor C subunit 3 L homeolog	4	10	2	1
XP_018089754.1	Cluster of krt19.L, PREDICTED: keratin 19, type I L homeolog isoform X1 (XP_018089754.1)	10	4	0	0
XP_018111396.1	Cluster of LOC100158273, PREDICTED: AT-rich interactive domain-containing protein 2 isoform X1 (XP_018111396.1)	9	6	5	3
NP_001083550.1	smc6.L, structural maintenance of chromosomes protein 6	4	9	3	2
XP_018091136.1	ercc3.L, PREDICTED: TFIIH basal transcription factor complex helicase XPB subunit isoform X1	9	8	0	1
NP_001080314.1	Cluster of kif2c.S, kinesin-like protein KIF2C (NP_001080314.1)	9	8	0	1
NP_001079703.1	Cluster of ddx5.S, DEAD-box helicase 5 S homeolog (NP_001079703.1)	9	7	1	0
NP_001079597.1	MGC53266, Protein regulator of cytokinesis 1-like	7	9	0	1
NP_001087810.1	Cluster of smarcd2.L, SWI/SNF related, matrix associated, actin dependent regulator of chromatin, subfamily d, member 2 L homeolog (NP_001087810.1)	9	0	2	0
NP_001083684.1	med23.L, mediator of RNA polymerase II transcription subunit 23	9	1	0	0
XP_018117354.1	LOC108716033, PREDICTED: calcineurin-binding protein cabin-1-like isoform X1	8	6	1	2
NP_001086065.1	rps27a.S, ribosomal protein S27a S homeolog	1	8	3	3
NP_001086090.1	Cluster of hist1h2aa.L, histone cluster 1, H2aa L homeolog (NP_001086090.1)	8	2	3	2
NP_001084837.1	rfc2.L, replication factor C subunit 2 L homeolog	3	8	1	1
XP_018109434.1	hnrnpm.L, PREDICTED: heterogeneous nuclear ribonucleoprotein M isoform X1	8	3	0	0

NP_001082182.1	polr1a.L, polymerase (RNA) I polypeptide A L homeolog	1	8	0	0
XP_018116614.1	LOC108715716, PREDICTED: ubinuclein-2-like isoform X1	7	6	7	1
NP_001081070.1	orc2.S, origin recognition complex subunit 2	6	7	2	3
NP_001084870.1	mtbp.S, mdm2-binding protein	5	0	2	7
NP_001087989.1	hcfc1.S, uncharacterized protein LOC494675	7	3	2	2
NP_001081557.1	ncl.S, nucleolin S homeolog	7	6	0	0
XP_018087559.1	Cluster of fancg.S, PREDICTED: Fanconi anemia complementation group G S homeolog isoform X1 (XP_018087559.1)	3	7	2	1
NP_001080253.1	prpf8.S, pre-mRNA processing factor 8 S homeolog	5	7	0	0
NP_001089437.1	mcm8.L, DNA helicase MCM8	0	4	0	7
NP_001084773.1	mcm9.L, DNA helicase MCM9	0	3	0	7
NP_001184204.1	LOC100505439, uncharacterized protein LOC100505439	7	0	2	1
NP_001085393.1	rpa2.L, replication protein A 32 kDa subunit-A	0	7	3	0
NP_001079536.1	eftud2.S, elongation factor Tu GTP binding domain containing 2 S homeolog	7	2	0	0
NP_001080400.1	ruvbl2, RuvB-like protein 2	7	0	0	0
NP_001080975.1	mre11.L, double-strand break repair protein MRE11	5	5	6	1
XP_018118032.1	LOC108716424, PREDICTED: S1 RNA-binding domain-containing protein 1-like	6	5	3	2
NP_001081555.1	nolc1.L, nucleolar and coiled-body phosphoprotein 1 L homeolog	4	4	6	2
XP_018089812.1	top3a.L, PREDICTED: topoisomerase (DNA) III alpha L homeolog isoform X1	4	6	3	2
XP_018101508.1	LOC108707919, PREDICTED: Fanconi anemia group B protein-like	3	6	3	3
XP_018093755.1	LOC108702660, PREDICTED: pre-mRNA-processing factor 6	6	6	1	0
XP_018119715.1	orc3.S, PREDICTED: origin recognition complex subunit 3 S homeolog isoform X1	6	4	1	2
XP_018120376.1	LOC108717656, PREDICTED: zinc finger protein 318-like isoform X1	5	6	0	1
XP_018082138.1	LOC108696940, PREDICTED: rRNA 2'-O-methyltransferase fibrillarin-like	5	6	0	0
XP_018113564.1	sf3b3.L, PREDICTED: splicing factor 3B subunit 3	6	2	1	0
NP_001088070.2	phf10.S, PHD finger protein 10	6	0	3	0
XP_018110645.1	LOC108712757, PREDICTED: U5 small nuclear ribonucleoprotein 200 kDa helicase	2	6	0	0
NP_001086459.1	daxx.L, death-associated protein 6 L homeolog	6	0	1	0
XP_018086539.1	LOC108699180, PREDICTED: ELM2 and SANT domain-containing protein 1-like isoform X1	6	0	0	0
NP_001079694.2	xnf7.S, nuclear factor 7, ovary	5	3	2	2
XP_018086639.1	Cluster of LOC108699215, PREDICTED: bromodomain adjacent to zinc finger domain protein 1A-like isoform X1 (XP_018086639.1)	3	1	5	2
NP_001079632.1	hspa8.L, heat shock protein family A (Hsp70) member 8 L homeolog	5	0	2	3
NP_001084508.1	MGC83104, uncharacterized protein LOC414454	2	5	2	1
NP_001080537.1	Cluster of cdk9.L, cyclin-dependent kinase 9-B (NP_001080537.1)	5	2	1	2
NP_001081742.1	kpna7.S, importin subunit alpha-5	2	5	0	2
NP_001080005.1	polr1b.L, polymerase (RNA) I polypeptide B L homeolog	5	4	0	0
XP_018118444.1	LOC108716657, PREDICTED: bifunctional lysine-specific demethylase and histidyl-hydroxylase NO66-like	3	5	0	1
XP_018115223.1	atrip.S, PREDICTED: ATR interacting protein S homeolog isoform X1	0	0	5	3
NP_001082592.1	brd7.L, bromodomain-containing protein 7	5	1	1	1
NP_001087469.1	ints4.L, integrator complex subunit 4	3	5	0	0
NP_001089444.1	orc5.L, origin recognition complex subunit 5 L homeolog	5	3	0	0
XP_018119169.1	Cluster of LOC108717002, PREDICTED: actin-like protein 6A (XP_018119169.1)	5	2	0	0

XP_018098562.1	LOC108706553, PREDICTED: pre-mRNA-splicing factor ATP-dependent RNA helicase DHX15 isoform X2	5	1	1	0
NP_001085526.1	rfc5.S, replication factor C subunit 5 S homeolog	1	5	1	0
NP_001089101.1	rts, RECQL4-helicase-like protein	2	5	0	0
XP_018090418.1	Cluster of LOC108700894, PREDICTED: activity-dependent neuroprotector homeobox protein-like (XP_018090418.1)	5	0	1	0
NP_001082047.1	mcm10.L, protein MCM10 homolog	1	5	0	0
NP_001087094.1	tdp1.L, tyrosyl-DNA phosphodiesterase 1 L homeolog	1	5	0	0
NP_001085608.1	MGC82602, MGC82602 protein	1	5	0	0
XP_018124559.1	Cluster of LOC108719847, PREDICTED: supervillin-like isoform X1 (XP_018124559.1)	0	5	0	0
XP_018104067.1	LOC108708921, PREDICTED: AT-rich interactive domain-containing protein 1A-like	0	0	5	0
XP_018117421.1	fbxo11.L, PREDICTED: F-box protein 11 L homeolog isoform X1	0	0	0	5
XP_018093441.1	LOC108702475, PREDICTED: SWI/SNF-related matrix-associated actin-dependent regulator of chromatin subfamily E member 1-like isoform X1	4	4	0	0
NP_001082418.1	aurkb.L, aurora kinase B-A	3	4	0	0
XP_018085278.1	LOC108698360, PREDICTED: cullin-4B-like	4	0	1	2
NP_001085825.1	rbbp8.L, DNA endonuclease RBBP8	4	0	2	1
NP_001165777.1	ticrr.L, treslin	0	2	1	4
XP_018115482.1	LOC108715140, PREDICTED: H/ACA ribonucleoprotein complex subunit 3-like	4	3	0	0
XP_018109320.1	LOC108711784, PREDICTED: zona pellucida sperm-binding protein 3-like	3	4	0	0
NP_001080205.1	rpl10a.S, 60S ribosomal protein L10a	2	4	0	0
NP_001086875.1	rmi1.L, recQ-mediated genome instability protein 1	2	4	0	0
NP_001079545.1	pms1.S, postmeiotic segregation increased 1	0	4	0	1
XP_018087204.1	ints3.L, PREDICTED: integrator complex subunit 3	4	1	0	0
NP_001085625.1	dynll1.L, dynein light chain LC8-type 1 L homeolog	4	1	0	0
XP_018115447.1	LOC108715122, PREDICTED: pyruvate carboxylase, mitochondrial	4	0	0	0
NP_001080796.1	rps19.S, ribosomal protein S19 S homeolog	0	4	0	0
NP_001086576.1	ercc4.L, excision repair cross-complementation group 4 L homeolog	0	4	0	0
NP_001089951.1	ints6.L, integrator complex subunit 6-A	4	0	0	0
NP_001080085.1	sumo2.L, small ubiquitin-related modifier 2-A precursor	0	0	4	0
NP_001122095.1	pdcd11.L, programmed cell death 11 L homeolog	0	4	0	0
XP_018112160.1	rad26, PREDICTED: RAD26 protein isoform X1	2	2	3	3
NP_001079759.1	sumo3.L, small ubiquitin-related modifier 3 precursor	1	3	1	1
XP_018089931.1	smc5.S, PREDICTED: structural maintenance of chromosomes protein 5 isoform X1	2	3	0	0
NP_001129236.1	uhrf1.S, E3 ubiquitin-protein ligase UHRF1	2	3	0	0
NP_001080504.1	chd4.L, chromodomain helicase DNA binding protein 4 L homeolog	2	3	0	0
XP_018079501.1	LOC108695482, PREDICTED: plectin-like isoform X1	2	3	0	0
XP_018107720.1	LOC108710973, PREDICTED: probable ATP-dependent RNA helicase DDX41	3	1	1	0
XP_018103054.1	LOC108708645, PREDICTED: cell division cycle-associated protein 7-like isoform X1	2	3	0	0
XP_018085308.1	LOC108698385, PREDICTED: THO complex subunit 2-like	2	3	0	0
XP_018089646.1	bard1.L, PREDICTED: BRCA1 associated RING domain 1 L homeolog isoform X1	3	2	0	0
NP_001080459.1	Cluster of kpna2.L, karyopherin alpha-2 subunit like L homeolog (NP_001080459.1)	2	3	0	0
NP_001081980.1	gatad2a.L, GATA zinc finger domain containing 2A L homeolog	0	0	2	3
XP_018091854.1	LOC108701560, PREDICTED: integrator complex subunit 1-like	1	3	0	0

NP_001085902.1	ppp1r3c.1.L, protein phosphatase 1, regulatory (inhibitor) subunit 3C, gene 1 L homeolog	0	0	1	3
NP_001085329.1	gtf2h2.S, general transcription factor IIH subunit 2 S homeolog	3	1	0	0
NP_001087316.1	rpl38.L, ribosomal protein L38 L homeolog	3	1	0	0
NP_001080730.1	rpsa.S, ribosomal protein SA S homeolog	1	3	0	0
XP_018087741.1	LOC108699737, PREDICTED: ELM2 and SANT domain-containing protein 1-like isoform X1	3	1	0	0
XP_018114076.1	LOC108714393, PREDICTED: DBIRD complex subunit ZNF326 isoform X1	3	0	0	0
XP_018114568.1	LOC108714663, PREDICTED: ruvB-like 1	3	0	0	0
NP_001089646.1	sltm.S, SAFB-like transcription modulator	3	0	0	0
NP_001088529.1	rpa3.L, replication protein A3 L homeolog	0	3	0	0
NP_001086192.1	ints13.S, integrator complex subunit 13	3	0	0	0
NP_001086215.1	alyref-b, THO complex subunit 4-B	0	3	0	0
NP_001089452.1	ints8.S, integrator complex subunit 8	3	0	0	0
XP_018102122.1	LOC108708189, PREDICTED: mediator of RNA polymerase II transcription subunit 14 isoform X1	3	0	0	0
NP_001088269.1	erlin2.L, erlin-2-A precursor	3	0	0	0
XP_018085253.1	atrx.L, PREDICTED: transcriptional regulator ATRX	3	0	0	0
NP_001084150.1	sf3b1.S, splicing factor 3B subunit 1	3	0	0	0
NP_001080545.1	rpl4.L, 60S ribosomal protein L4-A	0	3	0	0
XP_018120049.1	LOC108717364, PREDICTED: RNA polymerase II elongation factor ELL2-like isoform X1	3	0	0	0
NP_001081985.1	zpax.L, egg envelope component ZPAX L homeolog precursor	0	3	0	0
XP_018103680.1	ttf2.S, PREDICTED: transcription termination factor, RNA polymerase II S homeolog isoform X1	2	2	2	0
XP_018085550.1	LOC108698517, PREDICTED: TFIIH basal transcription factor complex helicase XPD subunit-like isoform X2	2	2	1	1
NP_001082751.1	pias4.S, protein inhibitor of activated STAT 4 S homeolog	2	1	2	0
XP_018085243.1	LOC108698338, PREDICTED: uncharacterized protein LOC108698338 isoform X1	2	2	0	0
NP_001081386.1	gp37, gp37 protein precursor	2	2	0	0
XP_018082853.1	LOC108697384, PREDICTED: PWWP domain-containing protein 2B-like	0	0	2	2
NP_001082504.1	rpn1.L, dolichyl-diphosphooligosaccharide--protein glycosyltransferase subunit 1 precursor	2	2	0	0
NP_001083839.1	mta2.L, metastasis associated 1 family member 2 L homeolog	2	0	2	0
NP_001086246.1	erlin2.S, erlin-2-B precursor	2	2	0	0
NP_001090142.1	myef2.L, myelin expression factor 2 L homeolog	2	2	0	0
NP_001080134.1	rplp0.S, ribosomal protein, large, P0 S homeolog	2	2	0	0
XP_018091174.1	LOC108701281, PREDICTED: cyclin-T2-like isoform X2	2	0	2	0
NP_001081657.1	xlzpc, zona pellucida C glycoprotein precursor	2	2	0	0
NP_001082532.1	srrt.L, serrate RNA effector molecule homolog B	1	2	0	0
NP_001284564.1	Cluster of slx4.L, uncharacterized protein LOC432277 (NP_001284564.1)	0	2	0	1
XP_018106519.1	ik.L, PREDICTED: IK cytokine, down-regulator of HLA II L homeolog isoform X1	1	2	0	0
XP_018118879.1	LOC108716873, PREDICTED: midasin-like	1	2	0	0
XP_018091901.1	LOC108701575, PREDICTED: transformation/transcription domain-associated protein	1	2	0	0
NP_001087615.1	ccnt2.S, cyclin T2 S homeolog	1	0	2	0
NP_001091302.1	npat.S, protein NPAT	1	2	0	0
NP_001080277.1	gtf2h1.L, general transcription factor IIH subunit 1 L homeolog	2	1	0	0

NP_001082552.1	LOC398563, serine/threonine-protein phosphatase 2A 65 kDa regulatory subunit A beta isoform-like	2	1	0	0
XP_018122930.1	LOC108718919, PREDICTED: transitional endoplasmic reticulum ATPase-like	2	0	1	0
XP_018108489.1	LOC108711349, PREDICTED: fanconi-associated nuclease 1-like	0	1	2	0
NP_001081643.1	polb.S, DNA polymerase beta	2	1	0	0
NP_001085623.1	mdn1.L, midasin AAA ATPase 1 L homeolog	1	2	0	0
NP_001081858.1	zp2.L, zzona pellucida glycoprotein 2 L homeolog precursor	2	1	0	0
NP_001083504.1	capza1.L, F-actin-capping protein subunit alpha-1	2	1	0	0
NP_001084822.1	exosc10.L, exosome component 10 L homeolog	2	1	0	0
NP_001079507.1	npm1.L, nucleophosmin	1	2	0	0
NP_001165149.1	rpl29.L, ribosomal protein L29 L homeolog	2	1	0	0
XP_018085385.1	LOC108698422, PREDICTED: SLIT and NTRK-like protein 2	2	0	0	0
XP_018085522.1	LOC108698498, PREDICTED: RNA-binding motif protein, X chromosome-like	2	0	0	0
NP_001089405.1	rcc2.L, protein RCC2 homolog	2	0	0	0
NP_001086415.1	cdca9.S, borealin-2	2	0	0	0
NP_001085315.1	rps3.S, 40S ribosomal protein S3-B	0	2	0	0
XP_018085441.1	LOC108698453, PREDICTED: bromodomain and WD repeat-containing protein 3-like isoform X2	2	0	0	0
NP_001084420.1	nbn.L, nibrin L homeolog	0	0	2	0
XP_018101855.1	LOC108708072, PREDICTED: thyroid hormone receptor-associated protein 3-like isoform X1	2	0	0	0
XP_018096714.1	LOC108704603, PREDICTED: dolichyl-diphosphooligosaccharide--protein glycosyltransferase subunit 2-like isoform X1	2	0	0	0
NP_001086446.1	ctr9.S, RNA polymerase-associated protein CTR9 homolog	0	2	0	0
NP_001080116.1	capzb.L, capping protein (actin filament) muscle Z-line, beta L homeolog	0	2	0	0
XP_018117845.1	LOC108716231, PREDICTED: E1A-binding protein p400-like isoform X1	2	0	0	0
NP_001080325.1	rps3a.S, 40S ribosomal protein S3a-A	0	2	0	0
XP_018085825.1	LOC108698672, PREDICTED: YLP motif-containing protein 1-like	0	2	0	0
NP_001131045.1	cdc5l.L, cell division cycle 5-like protein	2	0	0	0
NP_001079070.1	prkdc.L, DNA-dependent protein kinase catalytic subunit	0	2	0	0
NP_001080852.1	ldhb.S, L-lactate dehydrogenase B chain	0	2	0	0
NP_001080283.1	ddx3x.L, DEAD-box helicase 3, X-linked L homeolog	2	0	0	0
NP_001093376.1	med17.L, mediator complex subunit 17 L homeolog	2	0	0	0
NP_001079726.1	rpl37a.L, 60S ribosomal protein L37a	2	0	0	0
NP_001089734.1	krt18, keratin 18	2	0	0	0
NP_001089402.2	smtn.S, smoothelin	0	2	0	0
XP_018099006.1	LOC108706798, PREDICTED: elongation factor 2	2	0	0	0
NP_001087819.1	zpy1.S, zona pellucida protein Y1 S homeolog precursor	2	0	0	0
NP_001081752.1	igf2bp3.L, insulin-like growth factor 2 mRNA-binding protein 3-A	2	0	0	0
XP_018107503.1	jade2.L, PREDICTED: protein Jade-2 isoform X1	2	0	0	0
NP_001079585.1	nsmce2.L, E3 SUMO-protein ligase NSE2	0	2	0	0
NP_001085273.1	prpf3.S, U4/U6 small nuclear ribonucleoprotein Prp3	0	2	0	0
NP_001082490.1	thoc1.L, THO complex 1 protein L homeolog	2	0	0	0
NP_001080126.1	atp5f1b.S, mitochondrial ATP synthase beta subunit	2	0	0	0
NP_001081535.1	h1foo.S, protein B4	2	0	0	0
NP_001080392.1	actr3.S, ARP3 actin-related protein 3 homolog S homeolog	0	2	0	0
NP_001082094.1	pabpc1l.S, embryonic polyadenylate-binding protein A	2	0	0	0

NP_001081968.1	atm.L, ATM serine/threonine kinase L homeolog	0	2	0	0
XP_018095297.1	LOC100158394, PREDICTED: uncharacterized protein LOC100158394 isoform X1	0	0	2	0
NP_001090516.1	taf9b.L, TATA-box binding protein associated factor 9b L homeolog	2	0	0	0
XP_018117150.1	LOC414649, PREDICTED: eukaryotic translation initiation factor 4E transporter isoform X1	0	2	0	0
NP_001088907.1	dynll2.S, dynein light chain LC8-type 2 S homeolog	2	0	0	0

Table 2. Mutation rates at the *hom3-10*, *lys2::insE-A14*, and *CAN1* loci.

Genotype	*hom3-10*		*lys2-14A*		*CAN1*	
	Reversion Rate ($\times 10^{-9}$)	(Fold increase)	Reversion Rate ($\times 10^{-7}$)	(Fold increase)	Mutation Rate ($\times 10^{-8}$)	(Fold increase)
Wild-Type	1.6 [0.9 - 2.4]	(1.0)	0.37 [0.30 - 0.46]	(1.0)	5.4 [4.4 - 6.4]	(1.0)
fun30Δ	3.3 [2.2 - 4.7]	(2.1)	0.70 [0.58 - 0.82]	(1.9)	6.6 [5.5 - 7.8]	(1.2)
fun30-K603A	5.1 [3.3 - 7.2]	(3.3)	0.93 [0.77 - 1.1]	(2.5)	9.7 [8.0 - 11]	(1.8)
msh6Δ	10 [7.0 - 14]	(6.5)	69 [56 - 84]	(190)	120 [84 - 170]	(23)
msh6Δ fun30Δ	120 [100 - 150]	(79)	400 [350 - 450]	(1,100)	140 [97 - 200]	(27)
msh6Δ fun30-K603A	130 [110 - 150]	(81)	300 [270 - 330]	(790)	140 [100 - 170]	(25)
msh3Δ	21 [14 - 30]	(14)	4.2 [3.5 - 5.0]	(11)	9.6 [7.5 - 12]	(1.8)
msh3Δ fun30Δ	36 [26 - 48]	(23)	8.9 [7.7 - 10]	(24)	12 [9.2 - 14]	(2.1)
msh2Δ	5,100 [3,900 - 6,400]	(3,300)	3,800 [3,100 - 4,500]	(10,000)	360 [270 - 460]	(67)
msh2Δ fun30Δ	6,200 [4,900 - 7,700]	(3,900)	2,500 [2,000 - 3,100]	(6,800)	370 [280 - 470]	(69)
exo1Δ	6.8 [4.8 - 9.1]	(4.3)	18 [14 - 22]	(47)	86 [62 - 110]	(16)
exo1Δ fun30Δ	7.3 [5.2 - 9.6]	(4.6)	11 [8.3 - 14]	(30)	88 [65 - 110]	(16)
exo1Δ msh6Δ	33 [25 - 41]	(21)	180 [150 - 200]	(470)	n.d.	
exo1Δ msh6Δ fun30Δ	230 [200 - 260]	(150)	460 [410 - 500]	(1,200)	n.d.	

The *hom3-10* (Thr^+) and *lys2::insE-A14* (Lys^+) reversion rates, and the *CAN1* mutation rate are presented with 95% confidence intervals in square brackets. Fold increase of reversion rates over that of wild-type cells is shown in parentheses.

Table 3. The effect of *rad52* deletion on mutation rates.

Genotype	*hom3-10*		*lys2-14A*		*CAN1*	
	Reversion Rate ($\times 10^{-9}$)	(Fold increase)	Reversion Rate ($\times 10^{-7}$)	(Fold increase)	Mutation Rate ($\times 10^{-8}$)	(Fold increase)
Wild-Type	1.6 [0.9 - 2.4]	(1.0)	0.37 [0.30 - 0.46]	(1.0)	5.4 [4.4 - 6.4]	(1.0)
fun30Δ	3.3 [2.2 - 4.7]	(2.1)	0.70 [0.58 - 0.82]	(1.9)	6.6 [5.5 - 7.8]	(1.2)
msh6Δ	10 [7.0 - 14]	(6.5)	69 [56 - 84]	(190)	120 [84 - 170]	(23)
msh6Δ fun30Δ	120 [100 - 150]	(79)	400 [350 - 450]	(1,100)	140 [97 - 200]	(27)
rad52Δ	15 [11 - 20]	(9.7)	1.3 [1.1 - 1.6]	(3.6)	170 [130 - 210]	(32)
rad52Δ fun30Δ	14 [10 - 18]	(8.8)	1.6 [1.3 - 1.8]	(4.2)	180 [140 - 230]	(34)
rad52Δ msh6Δ	44 [33 - 57]	(28)	120 [100 - 140]	(330)	n.d.	
rad52Δ msh6Δ fun30Δ	290 [250 - 340]	(190)	370 [320 - 430]	(1,000)	n.d.	

The *hom3-10* (Thr^+) and *lys2::insE-A14* (Lys^+) reversion rates, and the *CAN1* mutation rate are presented with 95% confidence intervals in square brackets. Fold increase of reversion rates over that of wild-type cells is shown in parentheses. The rates of *RAD52* cells were duplicated from Table 2.

Table 4. The effect of *cac1* deletion on mutation rates.

Genotype	*hom3-10*		*lys2-14A*		*CAN1*	
	Reversion Rate ($\times 10^{-9}$)	(Fold increase)	Reversion Rate ($\times 10^{-7}$)	(Fold increase)	Mutation Rate ($\times 10^{-8}$)	(Fold increase)
Wild-Type	1.6 [0.9 - 2.4]	(1.0)	0.37 [0.30 - 0.46]	(1.0)	5.4 [4.4 - 6.4]	(1.0)
cac1Δ	1.3 [0.7 - 2.0]	(0.8)	0.58 [0.45 - 0.72]	(1.6)	4.8 [3.7 - 6.1]	(0.9)
fun30Δ	3.3 [2.2 - 4.7]	(2.1)	0.70 [0.58 - 0.82]	(1.9)	6.6 [5.5 - 7.8]	(1.2)
fun30Δ cac1Δ	2.3 [1.5 - 3.2]	(1.4)	1.2 [1.0 - 1.5]	(3.3)	9.5 [7.5 - 12]	(1.8)
msh6Δ	10 [7.0 - 14]	(6.5)	69 [56 - 84]	(190)	120 [84 - 170]	(23)
msh6Δ cac1Δ	6.3 [3.9 - 9.2]	(4.0)	56 [43 - 70]	(150)	160 [110 - 220]	(29)
msh6Δ fun30Δ	120 [100 - 150]	(79)	400 [350 - 450]	(1,100)	140 [97 - 200]	(27)
msh6Δ fun30Δ cac1Δ	23 [17 - 29]	(15)	130 [110 - 150]	(340)	140 [90 - 190]	(27)
msh3Δ	21 [14 - 30]	(14)	4.2 [3.5 - 5.0]	(11)	9.6 [7.5 - 12]	(1.8)
msh3Δ cac1Δ	11 [6.8 - 16]	(7.0)	3.2 [2.7 - 3.8]	(8.6)	11 [8.3 - 15]	(2.1)
msh3Δ fun30Δ	36 [26 - 48]	(23)	8.9 [7.7 - 10]	(24)	12 [9.2 - 14]	(2.1)
msh3Δ fun30Δ cac1Δ	18 [12 - 24]	(11)	5.6 [4.9 - 6.4]	(15)	16 [12 - 20]	(3.0)
msh2Δ	5,100 [3,900 - 6,400]	(3,300)	3,800 [3,100 - 4,500]	(10,000)	360 [270 - 460]	(67)
msh2Δ cac1Δ	5,600 [4,700 - 6,600]	(3,500)	3,100 [2,700 - 3,600]	(8,300)	460 [380 - 540]	(85)

The *hom3-10* (Thr^+) and *lys2::insE-A14* (Lys^+) reversion rates, and *CAN1* mutation rate are presented with 95% confidence intervals in square brackets. Fold increase of reversion rates over that of wild-type cells is shown in parentheses. The rates of *CAC1* cells were duplicated from Table 2.

Table 5. Oligonucleotides used in this study.

No.	Sequence (5′ to 3′)
60	TATGGATTATAAAGATGATGACGATAAGGACTACAAGGATGACGACGATAAACTGGAAGTTCTGTTCCAGGGGCCCCT
61	TAAGGGGCCCCTGGAACAGAACTTCCAGTTTATCGTCGTCATCCTTGTAGTCCTTATCGTCATCATCTTTATAATCCA
81	GGAAAGCCATGGGCCACCACCACCATCACCATGATTATAAAGATGATGACGATAAGCTGG
302	GAATTCAAGCTTAGTCTGTTCCATGTCATGCAAGATATCTTCAGTC
303	ACTGGGTGACCGTACTGCATCTCGAGATCCATGTTACTGCGTCAGT
304	CGCTAACAGTCACGAACTGCTGCAGGAATTCGTAC
305	GAATTCCTGCAGCAGTTCGTGACTGTTAGCGACTGACGCAGTAACA
306	TGGATCTCGAGATGCAGTACGGTCACCCAGTGACTGAAGATATCTT
307	GCATGACATGGAACAGACTAAGCTTGAATTCAGCT
344	GGGGACAAGTTTGTACAAAAAAGCAGGCTCCAC
345	GGGGACCACTTTGTACAAGAAAGCTGGGTC
362	CGCCTTGATCGT[Bio-dT]GGGAACCGGAGCTGAATGAAGC
386	GCTCCTCAGCTTAATTAACCTCAGC
387	AGCGCTGAGGTTAATTAAGCTGAGG
406	GGGAACAAAAGCTGGGTACGAATTCCTGCAGCAGTTCGTGACTGTTAGCGACTGACGCAGTAACATGGATCTCGAGAT GCAGTACGGTCACC
407	GGGAACAAAAGCTGGGTACGAATTCCTGCAGCAGTTCGTGACTGTTAGCGACTGACGCAGTAACATGGATCCCGAGAT GCAGTACGGTCACC
411	CAGTAACATGGATCCGAGATGCAGTACGGTCACC
412	CAGTAACATGGATCCAACATCGAGATGCAGTACGGTCACC
413	CAGTAACATGGATCTCCAGATGCAGTACGGTCACC
414	CAGTAACATGGATCTGGAGATGCAGTACGGTCACC
415	CAGTAACATGGATCTCGCGATGCAGTACGGTCACC
721	CAGTAACATGGATCTCGAGATGCAGTACGGTCACC
722	CAGTAACATGGATCCCGAGATGCAGTACGGTCACC
723	GGTCGGGCTGAACGGGGGGTTCGTGCACACAGCCC
724	GGTCGGGCTGAACGAGGGGTTCGTGCACACAGCCC
725	GGTGGCACTTTTCGGGGAAATGTGCGCGGAACCC
726	GGTGGCACTTTTCGTGGAAATGTGCGCGGAACCC
770	GGAACCATGGCGGATACGTTGGAG
771	GGAACCTGCAGGTTAATCTGAACCCGATTCAGCTGAGC
780	CTGCTGCCAGTTTACGGGATGATGACCG
784	CTTGTCTCCAGCTCAGTGCGGGATTTGG
798	AAAGCAGGCTCCACCATGGCGGTCACACTTGACAAAGAAGC
799	ACAAGAAAGCTGGGTCCTCGAGTCACTTCTTCCTCTTTTTAGAAGGATTTGG
827	GATGATGACGATAAGCTGGAAGTTCTGTTCCAGGGGCCCGGGATGGCGGTCACACTTGAC
887	ACAAGAAAGCTGGGTCGGATCCTTAAAGACCCAGGGATGTTTTC
900	AAAGCAGGCTCCACATATGTCAGCATTTAATCTGGAACGCTTCC
955	GCAACTGTACAAGCCATAGC
956	GCTATGGCTTGTACAGTTGCTCCCAGACCCATTTCATCTGC
957	AAAGCAGGCTCCACTCGAGGGATGCGGCGGCAGAAGCAGG
958	ACAAGAAAGCTGGGTGGATCCTCACTCCGTTATCCGCAACCATTC
1079	GGAACCTGCAGGAGCTTATACAGCTATCTTGACTCCCG
1158	GAGGAGCGGAAGAGCGGTGGCTTCTAGTAGCGATGTCGGGTAGA
1290	GTTCCGCCCGTTCTTCATACACC
1293	CTGCATCTGGAATGGGCAAAGCC
1294	CTGCGGCCGCACTCCAATTCGCCCTATAGTGAGTCG
1295	CCACCTGCAGGAGGTCCAGCTTTTGTTCCCTTTAGTGAGG
1296	TGGAGTGCGGCCGCAGTTGGCTAGCTATGCTATGCCTTCC
1297	GGACCTCCTGCAGGTGGCGGAATTTTCGATATCTGGAATCTTACC
1298	TTTTTTTTCCAGGATCTGACGTGGGCAAACACTTTGAAACTGTAG
1300	ACGGGAAAGGTTCCGTTCAGGACGCTACTTGTGTATAAGAGTCAG
1301	CTACTTGTGTATAAGAGTCAGCGTCAGGGCCAAGGATGAAGAAGC
1304	CCAGTTGGAACTAAACCAAAAAAACCCTGTAAAGACTGGAACG
1305	CGTTCCAGTCTTTACAGGGTTTTTTTGGTTTAGTTCCAACTGG
1311	AAAAATGCCGACAATGAGCC
1314	CGCCTCCAATGATTTCTTCC
1315	TTCGGTGGTACATCTGTCGG
1318	ACATGGTACCAGCAATGCCG
1347	TCGGTTCTTACTGCCAAGTG
1348	CGTCAGGTGGCACTTTTCGGCTGAGGATTTTGATGTTAGGTCAGC
1349	CGTCTCGCGCGTTTCGGTGATTCATAATCCCTAAAAGTGTTCACG
1350	GCAACGTTATCATGCTTTGAACG
1353	TGGAGTGCGGCCGCAGTGCGCTCATCGTTGGAATTC
1354	CGTCAGGTGGCACTTTTCGGACGTTCCTTACTGTAGATAGTCGGG
1355	CGTCTCGCGCGTTTCGGTGATCTTCTGCGTGAACGCACCATGTGG
1356	GGACCTCCTGCAGGTGGGTACATGTTAGGCCTGTCGG
1359	AACCTAAATGCGGGTTTTCG
1360	CGTCAGGTGGCACTTTTCGGTTTGGAGTTCAAATTGGCTTTGTC

1361	CGTCTCGCGCGTTTCGGTGATGGTCGTTGAAAAAGGATTCAGAAC
1362	GCGCATTCTTCTAAGTTCGG
1365	AGGTCTGTGCTTTTCTTCGG
1366	CGTCAGGTGGCACTTTTCGGTCTATTTGCACTGCTTTTGGCTCTC
1367	CGTCTCGCGCGTTTCGGTGACGGATGGTACGTATGTTCTAAATGC
1368	GGTTCCAAATCAGGAGCTGC
1426	CCTGAACGGAACCTTTCCCGTTTTTTTTTTTTTTAAGGATCTGACGTGGGCAAACAC
1428	CCAAGCCAGCATCTGTATCACCAG
1429	CCACCAGTGAGCCCGCTTGCAG
1457	TGCCCATGCTATAGACTCCC
1458	CGTCAGGTGGCACTTTTCGGCAACAACACACCAAAGCCACC
1459	CGTCTCGCGCGTTTCGGTGAACGCTTCCTGGCCGAAAC
1460	GCATAGTTCAATTGCGTGACATC
1481	CATCACAGTTCATTGCTTCG
1482	CGTCAGGTGGCACTTTTCGGTCCTTTCTACGCCTTTCAG
1483	CGTCTCGCGCGTTTCGGTGATGCACGTTTCATATCGGAGG
1484	CAACGAGACGGTTCCGTTCC
1537	CCGGCGCCCAGTCAGCCTTTACG
1538	CGTCAGGTGGCACTTTTCGGCCATTTTCCCTTTTCCTTTCGATTCTC
1539	CGTCTCGCGCGTTTCGGTGACAACCCCGTCTTTGTAACTTGAACGG
1540	AGGCACAACGGGGGAGCTGGAG
1564	GGAAGAATTCGCACCAGCACCAGCACCAGTGG
1565	GACTTGACATGTAGCACCTAGACCCATGTCGTCTGCAAGG
1566	CATGGGTCTAGGTGCTACATGTCAAGTCATTTCATTTTTCGC
1567	GGAAGGATCCTTCCCAGATTGCATCCACTCGTC
1571	GGAAGGATCCCATTCCGAACCATGTGGTGCT
1572	GGCCATTTCTTCAGATGGATCGATATTCAGCTCTTCCATATTCACTTAAATACACG
1573	GTATTTAAGTGAATATGGAAGAGCTGAATATCGATCCATCTGAAGAAATGGCCAAC
1574	GGATTGACCTCGTCTTCCACCTCC
1840	GCTTAGTCTGTTCCATGTCATGC
1841	TGGGTACGAATTCCTGCAGC
1842	CGCAGAAGTGGTCCTGCAAC
1843	GACACCACGATGCCTGTAGC
1847	GTCGGGAAACCTGTCGTGCC
1848	CAGCGAGTCAGTGAGCGAGG
1862	TCATTGCGCTGCCATTCTCC
1864	GAAACTTCGGCTTCCCCTGG
1876	CATGTGAGCAAAAGGCCAGC
1877	GTTTCGCCACCTCTGACTTG
1878	CTCATAGCTCACGCTGTAGG
1879	ACCGGGTTGGACTCAAGACG
1916	TTTCCCCGAAAAGTGCCACC
1917	GGAAGGGAAGAAAGCGAAAGG
1918	GCCGGCTTTCCCCGTCAAGC
1919	CAGGGCGATGGCCCACTACG
1920	GCTGTATAAGCTCCTGCAGC
1921	CACTTATCTTCCCCGAAGCC
1922	AGATTTGTTTGGAGAGTGCAGG
1923	ATAGCAATCCCACTTGTGTCAAG
1924	ACTTTGCGCGTTAGGATGTAGC
1925	AACAAGAGCGCTTGGTTGTC
1926	CTTCATCCTATTCCGTTACGCG

Table 6. *S. cerevisiae* strains used in this study.

Name	Relevant genotype	Parental strain	Reference
BY4741	*MATa his3Δ1 leu2Δ0 met15Δ0 ura3Δ0*	S288C	Brachmann et al., 1998
TTY15	BY4741 *hom3Δ::URA3*	BY4741	This study
TTY20	BY4741 *hom3-10*	TTY15	This study
TTY49	BY4741 *hom3-10 lys2::(YIplac211-URA3-lys2::insE-A14)*	TTY20	This study
TTY53	BY4741 *hom3-10 lys2::insE-A14*	TTY49	This study
TTY57	TTY53 *fun30Δ::kanMX*	TTY53	This study
TTY61	TTY53 *msh2Δ::kanMX*	TTY53	This study
TTY65	TTY53 *msh6Δ::kanMX*	TTY53	This study
TTY69	TTY53 *msh3Δ::kanMX*	TTY53	This study
TTY78	TTY53 *rad52Δ::hphMX6*	TTY53	This study
TTY82	TTY53 *fun30Δ::kanMX rad52Δ::hphMX6*	TTY57	This study
TTY86	TTY53 *fun30Δ::kanMX msh2Δ::hphMX6*	TTY57	This study
TTY88	TTY53 *fun30Δ::kanMX msh3Δ::hphMX6*	TTY57	This study
TTY90	TTY53 *fun30Δ::kanMX msh6Δ::hphMX6*	TTY57	This study
TTY96	TTY53 *exo1Δ::hphMX6*	TTY53	This study
TTY98	TTY53 *fun30Δ::kanMX exo1Δ::hphMX6*	TTY57	This study
TTY117	TTY53 *cac1Δ::natMX6*	TTY53	This study
TTY119	TTY53 *msh6Δ::kanMX cac1Δ::natMX6*	TTY65	This study
TTY121	TTY53 *fun30Δ::kanMX msh6Δ::hphMX6 cac1Δ::natMX6*	TTY90	This study
TTY136	TTY53 *msh2Δ::hphMX6 cac1Δ::natMX6*	TTY117	This study
TTY154	TTY53 *fun30-K603A*	TTY53	This study
TTY156	TTY53 *msh6Δ::kanMX fun30-K603A*	TTY65	This study
TTY164	TTY53 *spt16-d922*	TTY53	This study
TTY166	TTY53 *msh6Δ::kanMX spt16-d922*	TTY65	This study
TTY186	TTY53 *spt16-d922 fun30Δ::hphMX6*	TTY164	This study
TTY188	TTY53 *msh6Δ::kanMX spt16-d922 fun30Δ::hphMX6*	TTY166	This study
TTY198	TTY53 *fun30Δ::kanMX cac1Δ::natMX6*	TTY57	This study
TTY262	TTY53 *msh3Δ::kanMX cac1Δ::natMX6*	TTY69	This study
TTY264	TTY53 *fun30Δ::kanMX msh3Δ::hphMX6 cac1Δ::natMX6*	TTY88	This study

TTY296	TTY53 *msh6Δ::kanMX rad52Δ::natMX6*	TTY90	This study
TTY298	TTY53 *fun30Δ::kanMX msh6Δ::hphMX6 rad52Δ::natMX6*	TTY90	This study
TTY306	TTY53 *msh6Δ::kanMX exo1Δ::natMX6*	TTY65	This study
TTY308	TTY53 *fun30Δ::kanMX msh6Δ::hphMX6 exo1Δ::natMX6*	TTY90	This study

All strains were derived from S288C (BY4741).

Acknowledgement

I would like to express my deepest appreciation to Dr. Tatsuro Takahashi, who gave me the opportunity to study these important questions in the field of MMR. His constructive suggestions and heartfelt comments have always helped and encouraged me. His logical way of thinking has been of great value to me. I also appreciate Prof. Hisao Masukata, Prof. Toshiki Tsurimoto, Dr. Takuro Nakagawa, and Dr. Eiji Ohashi for their comments and discussions, which was provided an enormous contribution to this work. I would also like to express my gratitude for Profs. Chikashi Obuse, Seiji Tanaka and Dr. Koji Nagao. Prof. Chikashi Obuse and Dr. Koji Nagao performed mass spectrometry analysis. Their help made me focus on Smarcad1. Prof. Seiji Tanaka gave me a lot of advises about yeast genetics and several yeast strains. Without his help, I could not have revealed deep relations between Fun30 and the MMR syste. I also appreciate Profs. Akira Shinohara, Chikashi Obuse, Haruhiko Takisawa, Tokuko Haraguchi for providing constructive comments on my job and this thesis. I would also like to thank all the Masukata lab and Tsurimoto lab members, for helpful suggestions and for encouraging me. I am especially grateful to Dr. Torahiko Higashi, Dr, Yoshitaka Kawasoe, Ms. Kanae Taki for helpful suggestions and constructions of experimental systems, Xenopus proteins, as well as Ms. Chikako Tokumura for helpful of protein expression. Owing to their contribution, I was able to concentrate all of my energy into my studies. This study was supported by a Grant-in-Aid from the Japan Society for the Promotion of Science Fellows.

November 2018

Riki Terui

References

Acharya S, Foster PL, Brooks P, Fishel R. 2003. The coordinated functions of the E. coli MutS and MutL proteins in mismatch repair. *Mol Cell* **12**: 233-246.

Acharya S, Wilson T, Gradia S, Kane MF, Guerrette S, Marsischky GT, Kolodner R, Fishel R. 1996. hMSH2 forms specific mispair-binding complexes with hMSH3 and hMSH6. *Proc Natl Acad Sci U S A* **93**: 13629-13634.

Adkins NL, Niu H, Sung P, Peterson CL. 2013. Nucleosome dynamics regulates DNA processing. *Nat Struct Mol Biol* **20**: 836-842.

Amin NS, Nguyen MN, Oh S, Kolodner RD. 2001. exo1-Dependent mutator mutations: model system for studying functional interactions in mismatch repair. *Mol Cell Biol* **21**: 5142-5155.

Au KG, Welsh K, Modrich P. 1992. Initiation of methyl-directed mismatch repair. *J Biol Chem* **267**: 12142-12148.

Awad S, Ryan D, Prochasson P, Owen-Hughes T, Hassan AH. 2010. The Snf2 homolog Fun30 acts as a homodimeric ATP-dependent chromatin-remodeling enzyme. *J Biol Chem* **285**: 9477-9484.

Bantele SC, Ferreira P, Gritenaite D, Boos D, Pfander B. 2017. Targeting of the Fun30 nucleosome remodeller by the Dpb11 scaffold facilitates cell cycle-regulated DNA end resection. *Elife* **6**.

Belotserkovskaya R, Oh S, Bondarenko VA, Orphanides G, Studitsky VM, Reinberg D. 2003. FACT facilitates transcription-dependent nucleosome alteration. *Science* **301**: 1090-1093.

Boehm EM, Gildenberg MS, Washington MT. 2016. The Many Roles of PCNA in Eukaryotic DNA Replication. *Enzymes* **39**: 231-254.

Brown MW, Kim Y, Williams GM, Huck JD, Surtees JA, Finkelstein IJ. 2016. Dynamic DNA binding licenses a repair factor to bypass roadblocks in search of DNA lesions. *Nat Commun* **7**: 10607.

Byeon B, Wang W, Barski A, Ranallo RT, Bao K, Schones DE, Zhao K, Wu C, Wu WH. 2013. The ATP-dependent chromatin remodeling enzyme Fun30 represses transcription by sliding promoter-proximal nucleosomes. *J Biol Chem* **288**: 23182-23193.

Chen X, Cui D, Papusha A, Zhang X, Chu CD, Tang J, Chen K, Pan X, Ira G. 2012. The Fun30 nucleosome remodeller promotes resection of DNA double-strand break ends. *Nature* **489**: 576-580.

Chen X, Niu H, Yu Y, Wang J, Zhu S, Zhou J, Papusha A, Cui D, Pan X, Kwon Y et al. 2016a. Enrichment of Cdk1-cyclins at DNA double-strand breaks stimulates Fun30 phosphorylation and DNA end resection. *Nucleic Acids Res* **44**: 2742-2753.

Chen Z, Tran M, Tang M, Wang W, Gong Z, Chen J. 2016b. Proteomic Analysis Reveals a Novel Mutator S (MutS) Partner Involved in Mismatch Repair Pathway. *Mol Cell Proteomics* **15**: 1299-1308.

Constantin N, Dzantiev L, Kadyrov FA, Modrich P. 2005. Human mismatch repair: reconstitution of a nick-directed bidirectional reaction. *J Biol Chem* **280**: 39752-39761.

Costelloe T, Louge R, Tomimatsu N, Mukherjee B, Martini E, Khadaroo B, Dubois K, Wiegant WW, Thierry A, Burma S et al. 2012. The yeast Fun30 and human SMARCAD1 chromatin remodellers promote DNA end resection. *Nature* **489**: 581-584.

Densham RM, Garvin AJ, Stone HR, Strachan J, Baldock RA, Daza-Martin M, Fletcher A, Blair-Reid S, Beesley J, Johal B et al. 2016. Human BRCA1-BARD1 ubiquitin ligase activity counteracts chromatin barriers to DNA resection. *Nat Struct Mol Biol* **23**: 647-655.

Drummond JT, Genschel J, Wolf E, Modrich P. 1997. DHFR/MSH3 amplification in methotrexate-resistant cells alters the hMutSalpha/hMutSbeta ratio and reduces the efficiency of base-base mismatch repair. *Proc Natl Acad Sci U S A* **94**: 10144-10149.

Drummond JT, Li GM, Longley MJ, Modrich P. 1995. Isolation of an hMSH2-p160 heterodimer that restores DNA mismatch repair to tumor cells. *Science* **268**: 1909-1912.

Durand-Dubief M, Will WR, Petrini E, Theodorou D, Harris RR, Crawford MR, Paszkiewicz K, Krueger F, Correra RM, Vetter AT et al. 2012. SWI/SNF-like chromatin remodeling factor Fun30 supports point centromere function in S. cerevisiae. *PLoS Genet* **8**: e1002974.

Dzantiev L, Constantin N, Genschel J, Iyer RR, Burgers PM, Modrich P. 2004. A defined human system that supports bidirectional mismatch-provoked excision. *Mol Cell* **15**: 31-41.

Eapen VV, Sugawara N, Tsabar M, Wu WH, Haber JE. 2012. The Saccharomyces cerevisiae chromatin remodeler Fun30 regulates DNA end resection and checkpoint deactivation. *Mol Cell Biol* **32**: 4727-4740.

Evans DR, Brewster NK, Xu Q, Rowley A, Altheim BA, Johnston GC, Singer RA. 1998. The yeast protein complex containing cdc68 and pob3 mediates core-promoter repression through the cdc68 N-terminal domain. *Genetics* **150**: 1393-1405.

Formosa T. 2012. The role of FACT in making and breaking nucleosomes. *Biochim Biophys Acta* **1819**: 247-255.

Gaillard PH, Martini EM, Kaufman PD, Stillman B, Moustacchi E, Almouzni G. 1996. Chromatin assembly coupled to DNA repair: a new role for chromatin assembly factor I. *Cell* **86**: 887-896.

Galio L, Bouquet C, Brooks P. 1999. ATP hydrolysis-dependent formation of a dynamic ternary nucleoprotein complex with MutS and MutL. *Nucleic Acids Res* **27**: 2325-2331.

Geier GE, Modrich P. 1979. Recognition sequence of the dam methylase of Escherichia coli K12 and mode of cleavage of Dpn I endonuclease. *J Biol Chem* **254**: 1408-1413.

Genschel J, Bazemore LR, Modrich P. 2002. Human exonuclease I is required for 5' and 3' mismatch repair. *J Biol Chem* **277**: 13302-13311.

Genschel J, Littman SJ, Drummond JT, Modrich P. 1998. Isolation of MutSbeta from human cells and comparison of the mismatch repair specificities of MutSbeta and MutSalpha. *J Biol Chem* **273**: 19895-19901.

Genschel J, Modrich P. 2003. Mechanism of 5'-directed excision in human mismatch repair. *Mol Cell* **12**: 1077-1086.

Ghodgaonkar MM, Lazzaro F, Olivera-Pimentel M, Artola-Boran M, Cejka P, Reijns MA, Jackson AP, Plevani P, Muzi-Falconi M, Jiricny J. 2013. Ribonucleotides misincorporated into DNA act as strand-discrimination signals in eukaryotic mismatch repair. *Mol Cell* **50**: 323-332.

Gietz RD, Woods RA. 2002. Transformation of yeast by lithium acetate/single-stranded carrier DNA/polyethylene glycol method. *Methods Enzymol* **350**: 87-96.

Goellner EM, Putnam CD, Graham WJt, Rahal CM, Li BZ, Kolodner RD. 2018. Identification of Exo1-Msh2 interaction motifs in DNA mismatch repair and new Msh2-binding partners. *Nat Struct Mol Biol* **25**: 650-659.

Goellner EM, Smith CE, Campbell CS, Hombauer H, Desai A, Putnam CD, Kolodner RD. 2014. PCNA and Msh2-Msh6 activate an Mlh1-Pms1 endonuclease pathway required for Exo1-independent mismatch repair. *Mol Cell* **55**: 291-304.

Gorman J, Plys AJ, Visnapuu ML, Alani E, Greene EC. 2010. Visualizing one-dimensional diffusion of eukaryotic DNA repair factors along a chromatin lattice. *Nat Struct Mol Biol* **17**: 932-938.

Gradia S, Acharya S, Fishel R. 1997. The human mismatch recognition complex hMSH2-hMSH6 functions as a novel molecular switch. *Cell* **91**: 995-1005.

Grilley M, Welsh KM, Su SS, Modrich P. 1989. Isolation and characterization of the Escherichia coli mutL gene product. *J Biol Chem* **264**: 1000-1004.

Groth A, Corpet A, Cook AJ, Roche D, Bartek J, Lukas J, Almouzni G. 2007. Regulation of replication fork progression through histone supply and demand. *Science* **318**: 1928-1931.

Gupta S, Gellert M, Yang W. 2012. Mechanism of mismatch recognition revealed by human MutSbeta bound to unpaired DNA loops. *Nat Struct Mol Biol* **19**: 72-78.

Habraken Y, Sung P, Prakash L, Prakash S. 1996. Binding of insertion/deletion DNA mismatches by the heterodimer of yeast mismatch repair proteins MSH2 and MSH3. *Curr Biol* **6**: 1185-1187.

Hayashi-Takanaka Y, Maehara K, Harada A, Umehara T, Yokoyama S, Obuse C, Ohkawa Y, Nozaki N, Kimura H. 2015. Distribution of histone H4 modifications as revealed by a panel of specific monoclonal antibodies. *Chromosome Res* **23**: 753-766.

Haye JE, Gammie AE. 2015. The Eukaryotic Mismatch Recognition Complexes Track with the Replisome during DNA Synthesis. *PLoS Genet* **11**:

e1005719.

Heinen CD, Cyr JL, Cook C, Punja N, Sakato M, Forties RA, Lopez JM, Hingorani MM, Fishel R. 2011. Human MSH2 (hMSH2) protein controls ATP processing by hMSH2-hMSH6. *J Biol Chem* **286**: 40287-40295.

Heo K, Kim H, Choi SH, Choi J, Kim K, Gu J, Lieber MR, Yang AS, An W. 2008. FACT-mediated exchange of histone variant H2AX regulated by phosphorylation of H2AX and ADP-ribosylation of Spt16. *Mol Cell* **30**: 86-97.

Herman GE, Modrich P. 1981. Escherichia coli K-12 clones that overproduce dam methylase are hypermutable. *J Bacteriol* **145**: 644-646.

Higashi TL, Ikeda M, Tanaka H, Nakagawa T, Bando M, Shirahige K, Kubota Y, Takisawa H, Masukata H, Takahashi TS. 2012. The prereplication complex recruits XEco2 to chromatin to promote cohesin acetylation in Xenopus egg extracts. *Curr Biol* **22**: 977-988.

Holmes J, Jr., Clark S, Modrich P. 1990. Strand-specific mismatch correction in nuclear extracts of human and Drosophila melanogaster cell lines. *Proc Natl Acad Sci U S A* **87**: 5837-5841.

Hombauer H, Campbell CS, Smith CE, Desai A, Kolodner RD. 2011. Visualization of eukaryotic DNA mismatch repair reveals distinct recognition and repair intermediates. *Cell* **147**: 1040-1053.

Hong F, Fang F, He X, Cao X, Chipperfield H, Xie D, Wong WH, Ng HH, Zhong S. 2009. Dissecting early differentially expressed genes in a mixture of differentiating embryonic stem cells. *PLoS Comput Biol* **5**: e1000607.

Hoogenboom WS, Klein Douwel D, Knipscheer P. 2017. Xenopus egg extract: A powerful tool to study genome maintenance mechanisms. *Dev Biol* **428**: 300-309.

Iyer RR, Pluciennik A, Burdett V, Modrich PL. 2006. DNA mismatch repair: functions and mechanisms. *Chem Rev* **106**: 302-323.

Javaid S, Manohar M, Punja N, Mooney A, Ottesen JJ, Poirier MG, Fishel R. 2009. Nucleosome remodeling by hMSH2-hMSH6. *Mol Cell* **36**: 1086-1094.

Jiricny J. 2013. Postreplicative mismatch repair. *Cold Spring Harb Perspect Biol* **5**: a012633.

Junop MS, Obmolova G, Rausch K, Hsieh P, Yang W. 2001. Composite active site of an ABC ATPase: MutS uses ATP to verify mismatch recognition and authorize DNA repair. *Mol Cell* **7**: 1-12.

Kadyrov FA, Dzantiev L, Constantin N, Modrich P. 2006. Endonucleolytic function of MutLalpha in human mismatch repair. *Cell* **126**: 297-308.

Kadyrov FA, Genschel J, Fang Y, Penland E, Edelmann W, Modrich P. 2009. A possible mechanism for exonuclease 1-independent eukaryotic mismatch repair. *Proc Natl Acad Sci U S A* **106**: 8495-8500.

Kadyrova LY, Blanko ER, Kadyrov FA. 2011. CAF-I-dependent control of degradation of the discontinuous strands during mismatch repair. *Proc Natl Acad Sci U S A* **108**: 2753-2758.

Kawasoe Y, Tsurimoto T, Nakagawa T, Masukata H, Takahashi TS. 2016. MutSalpha maintains the mismatch repair capability by inhibiting PCNA unloading. *Elife* **5**.

Kleczkowska HE, Marra G, Lettieri T, Jiricny J. 2001. hMSH3 and hMSH6 interact with PCNA and colocalize with it to replication foci. *Genes Dev* **15**: 724-736.

Kunkel TA, Erie DA. 2015. Eukaryotic Mismatch Repair in Relation to DNA Replication. *Annu Rev Genet* **49**: 291-313.

Kurat CF, Yeeles JTP, Patel H, Early A, Diffley JFX. 2017. Chromatin Controls DNA Replication Origin Selection, Lagging-Strand Synthesis, and Replication Fork Rates. *Mol Cell* **65**: 117-130.

Lacks S, Greenberg B. 1977. Complementary specificity of restriction endonucleases of Diplococcus pneumoniae with respect to DNA methylation. *J Mol Biol* **114**: 153-168.

Lahue RS, Au KG, Modrich P. 1989. DNA mismatch correction in a defined system. *Science* **245**: 160-164.

Lamers MH, Perrakis A, Enzlin JH, Winterwerp HH, de Wind N, Sixma TK. 2000. The crystal structure of DNA mismatch repair protein MutS binding to a G x T mismatch. *Nature* **407**: 711-717.

Langle-Rouault F, Maenhaut-Michel G, Radman M. 1987. GATC sequences, DNA nicks and the MutH function in Escherichia coli mismatch repair.

EMBO J **6**: 1121-1127.

Lau PJ, Flores-Rozas H, Kolodner RD. 2002. Isolation and characterization of new proliferating cell nuclear antigen (POL30) mutator mutants that are defective in DNA mismatch repair. *Mol Cell Biol* **22**: 6669-6680.

Lebofsky R, Takahashi T, Walter JC. 2009. DNA replication in nucleus-free Xenopus egg extracts. *Methods Mol Biol* **521**: 229-252.

Li F, Mao G, Tong D, Huang J, Gu L, Yang W, Li GM. 2013. The histone mark H3K36me3 regulates human DNA mismatch repair through its interaction with MutSalpha. *Cell* **153**: 590-600.

Li F, Tian L, Gu L, Li GM. 2009. Evidence that nucleosomes inhibit mismatch repair in eukaryotic cells. *J Biol Chem* **284**: 33056-33061.

Liu H, Sadygov RG, Yates JR, 3rd. 2004. A model for random sampling and estimation of relative protein abundance in shotgun proteomics. *Anal Chem* **76**: 4193-4201.

Liu J, Hanne J, Britton BM, Bennett J, Kim D, Lee JB, Fishel R. 2016. Cascading MutS and MutL sliding clamps control DNA diffusion to activate mismatch repair. *Nature* **539**: 583-587.

Lucchini R, Sogo JM. 1995. Replication of transcriptionally active chromatin. *Nature* **374**: 276-280.

Luger K, Mader AW, Richmond RK, Sargent DF, Richmond TJ. 1997. Crystal structure of the nucleosome core particle at 2.8 A resolution. *Nature* **389**: 251-260.

Lujan SA, Clausen AR, Clark AB, MacAlpine HK, MacAlpine DM, Malc EP, Mieczkowski PA, Burkholder AB, Fargo DC, Gordenin DA et al. 2014. Heterogeneous polymerase fidelity and mismatch repair bias genome variation and composition. *Genome Res* **24**: 1751-1764.

Lujan SA, Williams JS, Clausen AR, Clark AB, Kunkel TA. 2013. Ribonucleotides are signals for mismatch repair of leading-strand replication errors. *Mol Cell* **50**: 437-443.

Marinus MG, Morris NR. 1973. Isolation of deoxyribonucleic acid methylase mutants of Escherichia coli K-12. *J Bacteriol* **114**: 1143-1150.

-. 1974. Biological function for 6-methyladenine residues in the DNA of

Escherichia coli K12. *J Mol Biol* **85**: 309-322.

Marra G, Iaccarino I, Lettieri T, Roscilli G, Delmastro P, Jiricny J. 1998. Mismatch repair deficiency associated with overexpression of the MSH3 gene. *Proc Natl Acad Sci U S A* **95**: 8568-8573.

Marsischky GT, Filosi N, Kane MF, Kolodner R. 1996. Redundancy of Saccharomyces cerevisiae MSH3 and MSH6 in MSH2-dependent mismatch repair. *Genes & Development* **10**: 407-420.

Marsischky GT, Kolodner RD. 1999. Biochemical characterization of the interaction between the Saccharomyces cerevisiae MSH2-MSH6 complex and mispaired bases in DNA. *J Biol Chem* **274**: 26668-26682.

Mattock H, Jares P, Zheleva DI, Lane DP, Warbrick E, Blow JJ. 2001. Use of peptides from p21 (Waf1/Cip1) to investigate PCNA function in Xenopus egg extracts. *Exp Cell Res* **265**: 242-251.

Mazur DJ, Mendillo ML, Kolodner RD. 2006. Inhibition of Msh6 ATPase activity by mispaired DNA induces a Msh2(ATP)-Msh6(ATP) state capable of hydrolysis-independent movement along DNA. *Mol Cell* **22**: 39-49.

McKnight SL, Miller OL, Jr. 1977. Electron microscopic analysis of chromatin replication in the cellular blastoderm Drosophila melanogaster embryo. *Cell* **12**: 795-804.

Narlikar GJ, Sundaramoorthy R, Owen-Hughes T. 2013. Mechanisms and functions of ATP-dependent chromatin-remodeling enzymes. *Cell* **154**: 490-503.

Neves-Costa A, Will WR, Vetter AT, Miller JR, Varga-Weisz P. 2009. The SNF2-family member Fun30 promotes gene silencing in heterochromatic loci. *PLoS One* **4**: e8111.

Nick McElhinny SA, Kumar D, Clark AB, Watt DL, Watts BE, Lundstrom EB, Johansson E, Chabes A, Kunkel TA. 2010. Genome instability due to ribonucleotide incorporation into DNA. *Nat Chem Biol* **6**: 774-781.

Nozawa RS, Nagao K, Masuda HT, Iwasaki O, Hirota T, Nozaki N, Kimura H, Obuse C. 2010. Human POGZ modulates dissociation of HP1alpha from mitotic chromosome arms through Aurora B activation. *Nat Cell Biol* **12**: 719-727.

Obmolova G, Ban C, Hsieh P, Yang W. 2000. Crystal structures of mismatch repair protein MutS and its complex with a substrate DNA. *Nature* **407**: 703-710.

Okazaki N, Ikeda S, Ohara R, Shimada K, Yanagawa T, Nagase T, Ohara O, Koga H. 2008. The novel protein complex with SMARCAD1/KIAA1122 binds to the vicinity of TSS. *J Mol Biol* **382**: 257-265.

Olivera Harris M, Kallenberger L, Artola Boran M, Enoiu M, Costanzo V, Jiricny J. 2015. Mismatch repair-dependent metabolism of O6-methylguanine-containing DNA in Xenopus laevis egg extracts. *DNA Repair (Amst)* **28**: 1-7.

Orphanides G, LeRoy G, Chang CH, Luse DS, Reinberg D. 1998. FACT, a factor that facilitates transcript elongation through nucleosomes. *Cell* **92**: 105-116.

Orphanides G, Wu WH, Lane WS, Hampsey M, Reinberg D. 1999. The chromatin-specific transcription elongation factor FACT comprises human SPT16 and SSRP1 proteins. *Nature* **400**: 284-288.

Palombo F, Gallinari P, Iaccarino I, Lettieri T, Hughes M, D'Arrigo A, Truong O, Hsuan JJ, Jiricny J. 1995. GTBP, a 160-kilodalton protein essential for mismatch-binding activity in human cells. *Science* **268**: 1912-1914.

Palombo F, Iaccarino I, Nakajima E, Ikejima M, Shimada T, Jiricny J. 1996. hMutSbeta, a heterodimer of hMSH2 and hMSH3, binds to insertion/deletion loops in DNA. *Curr Biol* **6**: 1181-1184.

Pluciennik A, Burdett V, Baitinger C, Iyer RR, Shi K, Modrich P. 2013. Extrahelical (CAG)/(CTG) triplet repeat elements support proliferating cell nuclear antigen loading and MutLalpha endonuclease activation. *Proc Natl Acad Sci U S A* **110**: 12277-12282.

Pluciennik A, Dzantiev L, Iyer RR, Constantin N, Kadyrov FA, Modrich P. 2010. PCNA function in the activation and strand direction of MutLalpha endonuclease in mismatch repair. *Proc Natl Acad Sci U S A* **107**: 16066-16071.

Polo SE, Almouzni G. 2015. Chromatin dynamics after DNA damage: The legacy of the access-repair-restore model. *DNA Repair (Amst)* **36**: 114-121.

Pukkila PJ, Peterson J, Herman G, Modrich P, Meselson M. 1983. Effects of High-Levels of DNA Adenine Methylation on Methyl-Directed Mismatch Repair in Escherichia-Coli. *Genetics* **104**: 571-582.

Ransom M, Dennehey BK, Tyler JK. 2010. Chaperoning histones during DNA replication and repair. *Cell* **140**: 183-195.

Ray-Gallet D, Quivy JP, Scamps C, Martini EM, Lipinski M, Almouzni G. 2002. HIRA is critical for a nucleosome assembly pathway independent of DNA synthesis. *Mol Cell* **9**: 1091-1100.

Reijns MA, Kemp H, Ding J, de Proce SM, Jackson AP, Taylor MS. 2015. Lagging-strand replication shapes the mutational landscape of the genome. *Nature* **518**: 502-506.

Rodriges Blanko E, Kadyrova LY, Kadyrov FA. 2016. DNA Mismatch Repair Interacts with CAF-1- and ASF1A-H3-H4-dependent Histone (H3-H4)2 Tetramer Deposition. *J Biol Chem* **291**: 9203-9217.

Rosche WA, Foster PL. 2000. Determining mutation rates in bacterial populations. *Methods* **20**: 4-17.

Rowbotham SP, Barki L, Neves-Costa A, Santos F, Dean W, Hawkes N, Choudhary P, Will WR, Webster J, Oxley D et al. 2011. Maintenance of silent chromatin through replication requires SWI/SNF-like chromatin remodeler SMARCAD1. *Mol Cell* **42**: 285-296.

Rydberg B, Game J. 2002. Excision of misincorporated ribonucleotides in DNA by RNase H (type 2) and FEN-1 in cell-free extracts. *Proc Natl Acad Sci U S A* **99**: 16654-16659.

Sarkar S, Ma WT, Sandri GH. 1992. On fluctuation analysis: a new, simple and efficient method for computing the expected number of mutants. *Genetica* **85**: 173-179.

Schofield MJ, Nayak S, Scott TH, Du C, Hsieh P. 2001. Interaction of Escherichia coli MutS and MutL at a DNA mismatch. *J Biol Chem* **276**: 28291-28299.

Schoor M, Schuster-Gossler K, Gossler A. 1993. The Etl-1 gene encodes a nuclear protein differentially expressed during early mouse development. *Dev Dyn* **197**: 227-237.

Schoor M, Schuster-Gossler K, Roopenian D, Gossler A. 1999. Skeletal dysplasias,

growth retardation, reduced postnatal survival, and impaired fertility in mice lacking the SNF2/SWI2 family member ETL1. *Mech Dev* **85**: 73-83.

Schopf B, Bregenhorn S, Quivy JP, Kadyrov FA, Almouzni G, Jiricny J. 2012. Interplay between mismatch repair and chromatin assembly. *Proc Natl Acad Sci U S A* **109**: 1895-1900.

Selmane T, Schofield MJ, Nayak S, Du C, Hsieh P. 2003. Formation of a DNA mismatch repair complex mediated by ATP. *J Mol Biol* **334**: 949-965.

Shibahara K, Stillman B. 1999. Replication-dependent marking of DNA by PCNA facilitates CAF-1-coupled inheritance of chromatin. *Cell* **96**: 575-585.

Sirbu BM, McDonald WH, Dungrawala H, Badu-Nkansah A, Kavanaugh GM, Chen Y, Tabb DL, Cortez D. 2013. Identification of proteins at active, stalled, and collapsed replication forks using isolation of proteins on nascent DNA (iPOND) coupled with mass spectrometry. *J Biol Chem* **288**: 31458-31467.

Smith CE, Mendillo ML, Bowen N, Hombauer H, Campbell CS, Desai A, Putnam CD, Kolodner RD. 2013. Dominant mutations in S. cerevisiae PMS1 identify the Mlh1-Pms1 endonuclease active site and an exonuclease 1-independent mismatch repair pathway. *PLoS Genet* **9**: e1003869.

Smith S, Stillman B. 1989. Purification and characterization of CAF-I, a human cell factor required for chromatin assembly during DNA replication in vitro. *Cell* **58**: 15-25.

Sogo JM, Stahl H, Koller T, Knippers R. 1986. Structure of replicating simian virus 40 minichromosomes. The replication fork, core histone segregation and terminal structures. *J Mol Biol* **189**: 189-204.

Soininen R, Schoor M, Henseling U, Tepe C, Kisters-Woike B, Rossant J, Gossler A. 1992. The mouse Enhancer trap locus 1 (Etl-1): a novel mammalian gene related to Drosophila and yeast transcriptional regulator genes. *Mech Dev* **39**: 111-123.

Sparks JL, Chon H, Cerritelli SM, Kunkel TA, Johansson E, Crouch RJ, Burgers PM. 2012. RNase H2-initiated ribonucleotide excision repair. *Mol Cell* **47**: 980-986.

Steglich B, Stralfors A, Khorosjutina O, Persson J, Smialowska A, Javerzat JP,

Ekwall K. 2015. The Fun30 chromatin remodeler Fft3 controls nuclear organization and chromatin structure of insulators and subtelomeres in fission yeast. *PLoS Genet* **11**: e1005101.

Stralfors A, Walfridsson J, Bhuiyan H, Ekwall K. 2011. The FUN30 chromatin remodeler, Fft3, protects centromeric and subtelomeric domains from euchromatin formation. *PLoS Genet* **7**: e1001334.

Strand M, Prolla TA, Liskay RM, Petes TD. 1993. Destabilization of tracts of simple repetitive DNA in yeast by mutations affecting DNA mismatch repair. *Nature* **365**: 274-276.

Su SS, Lahue RS, Au KG, Modrich P. 1988. Mispair specificity of methyl-directed DNA mismatch correction in vitro. *J Biol Chem* **263**: 6829-6835.

Su SS, Modrich P. 1986. Escherichia coli mutS-encoded protein binds to mismatched DNA base pairs. *Proc Natl Acad Sci U S A* **83**: 5057-5061.

Szankasi P, Smith GR. 1992. A DNA exonuclease induced during meiosis of Schizosaccharomyces pombe. *J Biol Chem* **267**: 3014-3023.

Tagami H, Ray-Gallet D, Almouzni G, Nakatani Y. 2004. Histone H3.1 and H3.3 complexes mediate nucleosome assembly pathways dependent or independent of DNA synthesis. *Cell* **116**: 51-61.

Takahashi TS, Walter JC. 2005. Cdc7-Drf1 is a developmentally regulated protein kinase required for the initiation of vertebrate DNA replication. *Genes Dev* **19**: 2295-2300.

Tan BC, Chien CT, Hirose S, Lee SC. 2006. Functional cooperation between FACT and MCM helicase facilitates initiation of chromatin DNA replication. *EMBO J* **25**: 3975-3985.

Thomas DC, Roberts JD, Kunkel TA. 1991. Heteroduplex repair in extracts of human HeLa cells. *J Biol Chem* **266**: 3744-3751.

Tishkoff DX, Boerger AL, Bertrand P, Filosi N, Gaida GM, Kane MF, Kolodner RD. 1997. Identification and characterization of Saccharomyces cerevisiae EXO1, a gene encoding an exonuclease that interacts with MSH2. *Proc Natl Acad Sci U S A* **94**: 7487-7492.

Tran HT, Keen JD, Kricker M, Resnick MA, Gordenin DA. 1997. Hypermutability of homonucleotide runs in mismatch repair and DNA

polymerase proofreading yeast mutants. *Mol Cell Biol* **17**: 2859-2865.

Tsukuda T, Fleming AB, Nickoloff JA, Osley MA. 2005. Chromatin remodelling at a DNA double-strand break site in Saccharomyces cerevisiae. *Nature* **438**: 379-383.

Tsunaka Y, Fujiwara Y, Oyama T, Hirose S, Morikawa K. 2016. Integrated molecular mechanism directing nucleosome reorganization by human FACT. *Genes Dev* **30**: 673-686.

Vashee S, Cvetic C, Lu W, Simancek P, Kelly TJ, Walter JC. 2003. Sequence-independent DNA binding and replication initiation by the human origin recognition complex. *Genes Dev* **17**: 1894-1908.

Verreault A, Kaufman PD, Kobayashi R, Stillman B. 1996. Nucleosome assembly by a complex of CAF-1 and acetylated histones H3/H4. *Cell* **87**: 95-104.

Wagner R, Meselson M. 1976. Repair Tracts in Mismatched DNA Heteroduplexes. *P Natl Acad Sci USA* **73**: 4135-4139.

Walter J, Newport J. 2000. Initiation of eukaryotic DNA replication: origin unwinding and sequential chromatin association of Cdc45, RPA, and DNA polymerase alpha. *Mol Cell* **5**: 617-627.

Walter J, Sun L, Newport J. 1998. Regulated chromosomal DNA replication in the absence of a nucleus. *Mol Cell* **1**: 519-529.

Wang H, Hays JB. 2004. Signaling from DNA mispairs to mismatch-repair excision sites despite intervening blockades. *EMBO J* **23**: 2126-2133.

Warren JJ, Pohlhaus TJ, Changela A, Iyer RR, Modrich PL, Beese LS. 2007. Structure of the human MutSalpha DNA lesion recognition complex. *Mol Cell* **26**: 579-592.

Wei K, Clark AB, Wong E, Kane MF, Mazur DJ, Parris T, Kolas NK, Russell R, Hou H, Jr., Kneitz B et al. 2003. Inactivation of Exonuclease 1 in mice results in DNA mismatch repair defects, increased cancer susceptibility, and male and female sterility. *Genes Dev* **17**: 603-614.

Welsh KM, Lu AL, Clark S, Modrich P. 1987. Isolation and characterization of the Escherichia coli mutH gene product. *J Biol Chem* **262**: 15624-15629.

Yu Q, Zhang X, Bi X. 2011. Roles of chromatin remodeling factors in the formation and maintenance of heterochromatin structure. *J Biol Chem*

286: 14659-14669.

Zhang Y, Yuan F, Presnell SR, Tian K, Gao Y, Tomkinson AE, Gu L, Li GM. 2005. Reconstitution of 5'-directed human mismatch repair in a purified system. *Cell* **122**: 693-705.

Zhu R, Iwabuchi M, Ohsumi K. 2017. The WD40 Domain of HIRA Is Essential for RI-nucleosome Assembly in Xenopus Egg Extracts. *Cell Struct Funct* **42**: 37-48.